January 2010

The Role of Pax6 in Lens Placode Formation

Jie Huang
Washington University in St. Louis

WASHINGTON UNIVERSITY IN ST. LOUIS

Division of Biology and Biomedical Sciences

(Developmental Biology)

Dissertation Examination Committee:

David Beebe, Chair

John Cooper

David Ornitz

Robert Mecham

Jason Mills

Larry Taber

THE ROLE OF PAX6 IN LENS PLACODE FORMATION

by

Jie Huang

A dissertation presented to the
Graduate School of Arts and Sciences
of Washington University in
Partial fulfillment of the requirements for the degree
of Doctor of Philosophy

December 2010

Saint Louis, Missouri

Acknowledgements

It has been seven years since I came to the United States to pursuit my doctoral degree. At the beginning of these seven years, I encountered frustration, tears, and madness, because my research work was not sucessful at all. Then I switched the lab at the end of the third year. When I first had to decide which lab I want to join, I chose Dr. Beebe's lab, merely since I was told that Dr. Beebe is a nice guy. After a brief rotation in the Beebe lab, I realized that Dr. Beebe is not only a nice person, but also he will be a good mentor, because he is very inspirating. More importantly, the scientific research in his lab is very interesting due to his sharp insight and broad knowledge. Without a second rotaion, I decided to stay in Beebe lab to finish my thesis work without any hesitation.

Ever since I joined his lab, Dr. Beebe has been a constant source of inspiration, guidance, support and encouragement. On one hand, he always gave me a lot of independence to work on my thesis projects. One the other hand, he had made sure that I was on the right track. He is not the kind of person who is only caring about the research progress. He is also extremely dedicated to a student's progress and development. I would never obtain the opportunities for presenting my research work in the conventions

if I did not join his lab. In these four years of training in Dr. Beebe lab, I have attended three national conventions, one international convention and even more encouraged by Dr. Beebe, but for some reasons I did not go. Not only has he taught me how to think about the science, he has also taught me many other things, such as the scientific writing and up-to-date modern scientific techniques. I am extremely grateful to my mentor, David Beebe, for making my journey through graduate school such a rewarding, satisfying and joyful experience.

I would also like to thank the fundings coming from the NIH grant EY04853 to Dr. David Beebe, core grant NIH EY02687 to the Department of Ophthalmology and Visual Sciences (DOVS), and an unrestricted grant from Research to Prevent Blindness to the DOVS, to support our research works.

I am thankful to my thesis committee members, David Ornitz, Jason Mills, John Cooper, Larry Taber and Robert Mecham for their ideas and advice during the course of my work. I also want to thank all persons in DBBS, especially our student coordinator, Stacy Kiel and programme directors, Jim Skeath and Kerry Kornfeld. They have always been there for helping me and making sure that I am doing well.

My PhD experience wouldn’t have been as much fun and productive if not for the Beebe lab members. The Beebe lab is bunch of people who are extraordinarily helpful and caring each other. Every single member, past and present, has made a wonderful contribution to my research work. I want to express my special thanks to Ying Liu. Ying join our lab a year and half ago, she has helped me in many ways with my projects. Without her, I would not have finished the thesis project so rapidly. I also want to thank present member of Beebe lab, Ying-Bo Shui, Lisa Dattilo, Mary Feldmeier and Chenghua Wu for being so generous in helping me at all times. I also want to thank the past members Ramya Rajacopal, Luke Wiley, Ken Kompass and Mark Wilkins for their previous works, which made my research work much easier. I always consider myself to be very fortunate to have come to know all these amazing people.

I wish to thank Belinda McMahan and retired empolyee, Jean Jones, of the Histology Core Lab not only for their assistance with tissue sectioning and staining.

I am grateful to my family. First of all, I am indebted to my parents for bringing me into this world, giving me the physical supplies as much as they can, and tutoring me mentally. Without their early education for independence, I will not have been so

stress-free when I am alone studying abroad. I also want to thank my husband, Bo Ma, for entering my life and changing my life forever! From the time we met, Bo has been my best friend, brother, housekeeper, philosopher and guide. He has always been there for me, supporting, understanding and encouraging me in all my endeavors. I deeply appreciate him for taking care of all our household chores and business, so that I can spend more time on my research. I also thank Bo for criticizing me, which I can never get from my friends. His toughest criticism made me more reasonable and responsible and develope a better personality. Another family member that I cannot neglect is my little doggy, who has been my company when I first came alone. She has been such a source of joy and happiness, and always bringing a smile to my face with her funny movements and adorable faces.

I want to thank all my friends in St. Louis and other parts of United States and the world for all their support, friendship and love.

Table of Contents

Chapter1 The Mechanism of Lens Placode Formation and the Importance of Placode Formation in Lens Invagination

Abstract

Although placodes are ubiquitous precursors of tissue invagination, the mechanism of placode formation and its importance for invagination are unclear. We tested the "restricted expansion hypothesis" of lens placode formation by conditionally deleting the transcription factor, *Pax6*, or the matrix component, *Fibronectin1* (*Fn1*). Deletion of *Pax6* from the lens-forming ectoderm prevented placode formation without altering cell proliferation or volume. $Pax6^{CKO}$ ectoderm expanded, rather than being constrained to a constant area, as normally occurs during lens placode formation, and expressed lower levels of transcripts encoding several extracellular matrix components. Deletion of *Fn1*, which is required to organize the extracellular matrix, prevented lens placode formation. Consistent with the "restricted expansion hypothesis," $Fn1^{CKO}$ ectoderm expanded, rather than being constrained. Ectoderm cells of $Fn1^{CKO}$ embryos expressed markers of lens induction, reorganized their cytoskeleton as in wild type ectoderm, but did not invaginate. These results suggest that placode formation establishes the minimal mechanical

requirements for tissue invagination.

Introduction

The formation of epithelial placodes is a recurring theme in morphogenesis. Placode formation is the first step in the formation of ectodermally-derived sensory structures, including the vertebrate central nervous system and sensory ganglia, ectodermal appendages, like hairs, scales and feathers, mammary glands, the insect tracheal system, the eye lens, the inner ear and many others. Soon after their formation, placodes invaginate or involute, transforming surface epithelia into internal structures. Given their widespread participation in epithelial morphogenesis, it seems possible that placode formation is an essential precondition for these critical morphogenetic events. In spite of the ubiquity and potential importance of placodes in morphogenesis, the cellular mechanisms underlying their formation have rarely been explored and the requirement of placode formation for subsequent epithelial morphogenesis has not been tested.

Lens formation from surface ectoderm and the transformation of the optic vesicle into optic cup are the major morphogenetic events of eye formation. In mouse embryos, the morphogenesis of the eye commences on embryonic day 9 (E9), when the neural epithelium of the ventral forebrain evaginates to form the bilateral optic vesicles. The

optic vesicles soon contact and adhere to the head surface ectoderm on each side of the embryo (Fig. 1A). At the contact areas, the surface ectoderm thickens, forming the lens placodes (Fig. 1B). After a lens placode forms, it and the prospective retina invaginate, giving rise to the lens pit and optic cup. The lens pit subsequently separates from the surface ectoderm to form the lens vesicle, which differentiates into the lens. The optic cup differentiates into the retina, ciliary epithelium, iris and retinal pigment epithelium.

The cellular processes required for the formation of the lens placode have been studied most extensively in chicken embryos. Lens placode formation involves the transformation of the prospective lens ectoderm cells from a cuboidal to columnar shape; the cells do not multilayer (Zwaan and Hendrix 1973). At the time of lens placode thickening, cell density increases in the placodal ectoderm, compared to the surrounding non-placodal ectoderm (McKeehan 1951). In the chicken embryo, the mitotic index and the tritiated thymidine labeling index within and outside the forming placode is similar and the cell volume remains constant, suggesting that the placodal ectoderm does not thicken due to a local increase in cell proliferation or volume (McKeehan 1951; Zwaan and Pearce 1971). Zwaan and co-workers also noted that the contact area between the surface ectoderm and optic vesicle remained constant during placode formation and that

the extracellular matrix between the tissues increased after their contact (Zwaan and Pearce 1971; Zwaan and Hendrix 1973; Hendrix and Zwaan 1975). Based on these observations, they hypothesized that the adhesion between the optic vesicle and the overlying ectoderm, mediated by the extracellular matrix, prevented the expansion of the lens territory. With continued cell proliferation, the restriction in expansion mediated by the interfacial matrix led to cell crowding, resulting in cell elongation and placode formation (Hendrix and Zwaan 1975). We refer to this as the "restricted expansion" model of placode formation.

In agreement with the restricted expansion model, the insertion of a cellophane sheet into the space between the surface ectoderm and optic vesicle blocked their contact and prevented lens placode thickening (McKeehan 1951). In addition, the surface ectoderm thickened precociously or ectopically when the head ectoderm was ligatured with a fine hair prior to placode formation, even outside of the prospective lens-forming ectoderm, an observation that is consistent with the restricted expansion model (Wakely 1984). However, other studies found that insertion of agar sheets between the optic vesicle and surface ectoderm or culture of the ectoderm on a Millipore filter did not prevent lens

placode morphogenesis, suggesting that adhesion between these tissues may not be required for lens formation (McKeehan 1958; Muthukkaruppan 1965).

In the present study, we analyzed lens placode formation in the mouse embryo, where lens formation was prevented by conditional deletion of the transcription factor, *Pax6*. This permitted the genetic dissection of the events associated with lens placode formation and testing of the restricted expansion model of Zwaan and co-workers.

Materials & Methods

Genotyping and tamoxifen injection. All animals were treated in accordance with the ARVO Statement for the Use of Animals in Ophthalmic and Vision Research and with the approval of the Animal Studies Committee of the Washington University School of Medicine. Mice expressing Cre recombinase in the surface ectoderm (*Le-Cre*), or optic vesicle (*Rx-Cre*) and tamoxifen-inducible Cre (*CAGG-Cre*^{ERTM}) were described previously (Ashery-Padan, Marquardt et al. 2000; Hayashi and McMahon 2002; Swindell, Bailey et al. 2006). *Fn1*$^{fx/fx}$ mice were reported in previous studies (Sakai, Johnson et al. 2001). Noon of the day when the vaginal plug was detected was considered embryonic day (E) 0.5 of development. For animals carrying the Le-Cre transgene, matings between mice that were homozygous for the floxed allele in which the female was also Cre-positive, resulted in litters in which about half of the offspring were Cre-positive (conditional knockout; CKO), the others were Cre-negative (wild type; WT). For tamoxifen-inducible Cre, matings were between the *Fn1*$^{fx/+}$, *CAGG-Cre*^{ERTM} and *Fn1*$^{fx/fx}$ mice. The *Fn1*$^{fx/+}$, *CAGG-Cre*^{ERTM} was the control for potential tamoxifen toxicity, as described previously (Naiche and Papaioannou 2007). Total doses of 7.2mg/40kg tamoxifen were injected intraperitoneally into pregnant dams at E8.5 and E8.75. Embryos

were collected at the desired stages (*n*=3 to 5 for each genotype and stage).

Histology. Embryo heads were fixed in 4% paraformaldehyde/PBS overnight at 4°C, dehydrated through a series of ethanol concentrations, embedded in paraffin and sectioned at 4 μm. For morphological studies, sections were stained with hematoxylin and eosin (Surgipath, Richmond, IL, USA). Cell volume was determined by dividing the average cell area (μm^2) by the number of nuclei from sections of E9.5 embryo heads using the Spot camera software (Spot Diagnostic Instruments, Sterling Heights, MI). Cell density was determined by counting the number of nuclei per 50 μm length of the ectoderm. To analyze the thickness of the placode, 5 equidistant points were marked along the length of the placode and the height of the tissue was measured at those points. The extent of contact between the surface ectoderm and the optic vesicle was measured in serial sections through the area of contact.

TUNEL, EdU and BrdU labeling. Terminal deoxynucleotidyl transferase (TdT)-mediated deoxyuridine triphosphate nick end-labeling (TUNEL) was done with an Apoptag kit (Chemicon, Temecula, CA). The deparaffinized slides were treated with 3% H_2O_2 in methanol for 30 min, followed by proteinase K treatment (20 μg/ml) for 15 min.

Slides were incubated with TdT enzyme in equilibration buffer for 1 hr at 37° C. The reaction was terminated with wash buffer provided by the manufacturer for 10 min at RT and then incubated with anti-digoxigenin-peroxidase conjugate for 30 min at RT, followed by DAB + H_20_2 treatment. Slides were counterstained with hematoxylin.

For BrdU staining, pregnant females were injected with 50 mg/kg of body weight of 10 mM BrdU (Roche, Indianapolis, IN) and 1 mM 5-fluoro-5′-deoxyuridine (Sigma, St. Louis, MO) and sacrificed after 1 hr. A monoclonal anti-BrdU antibody (1:250) (Dako, Carpinteria, CA) was used with a Vectastain Elite Mouse IgG ABC kit as described above. Sections were counterstained with hematoxylin.

For EdU staining, pregnant females were injected intraperitoneally with 100 µg of 5-ethynyl-2'-deoxyuridine (EdU) (Invitrogen, Carlsbad, CA) one hr prior to death. Embryos were fixed and sectioned as above. EdU was detected with AlexaFluor 488-azide using a Click-iT™ Kit for one hr according to manufacturer's instructions (Invitrogen). Total nuclei were counterstained with DRAQ-5 (1:1,000; Biostatus Limited, Shepshed, Leicestershire, UK) for 30 min at RT in 1X PBS. Sections were rinsed in 1X

PBS and viewed using a Zeiss 510 confocal microscope (Carl Zeiss Microimaging, Inc., Thornwood, NY,).

Immunostaining on paraffin sections. Embryos were fixed as described above, embedded in 5 % agarose, processed and embedded in paraffin, sectioned at 4 μm, deparaffinized and rehydrated. Endogenous peroxidase activity was inactivated with 3% H_2O_2 in methanol for 30 min at RT for those samples that would be treated for horseradish peroxidase (HRP). Epitope retrieval was performed in 0.01 M citrate buffer (pH 6.0) by placing the slides in a pressure cooker for 3 min. Slides were then incubated in blocking solution containing 20% inactivated normal donkey serum for 30 min at RT followed by incubation in primary antibodies overnight at 4° C. Slides were then incubated for 1 hr at RT either with Alexa-Fluor-labeled secondary antibodies (Molecular Probes, Eugene, OR) or biotinylated secondary antibodies (Vector Laboratories, Burlingame, CA). Slides incubated with biotinylated secondary antibodies were treated with the ABC-peroxidase reagent from Vectastain Elite ABC Kit (Vector Laboratories, Burlingame, CA) followed by treatment with diaminobenzidine (DAB) (Sigma, St. Louis, MO) and H_20_2, washed with PBS and counterstained with hematoxylin (Surgipath, Richmond, IL).

Immunofluorescence on thick sections. Embryos were fixed as described above. After rinsing in PBS, heads were dissected in half, embedded in 4% agarose in PBS and allowed to set overnight at 4°C. Thick sections (120μm) were cut using a tissue slicer (Electron Microscopy Sciences, Hatfield, PA). Sections containing the lens placodes were blocked in 5% normal goat serum, 0.5% Triton-X 100 for permeabilization, and 0.03% sodium azide for 1 hr at RT and incubated with primary antibodies overnight at 4°C. After rinsing, sections were incubated with fluorescent labeled secondary antibodies for 1 hr at RT and counterstained with DRAQ-5 (1:1,000; Biostatus Limited, Shepshed, Leicestershire, UK), a vital, fluorescent DNA dye. Sections were mounted in Vectashield (Vector Laboratories, Burlingame, CA).

In situ hybridization on frozen sections. Frozen sections were fixed in 4% paraformaldehyde/PBS, treated with proteinase K (10 μg/ml), post-fixed in 4% paraformaldehyde/PBS and acetylated in triethanolamine-acetic anhydride solution. Samples were pre-hybridized in 50% formamide, 5×SSC, 5 mM EDTA, 1×Denhardt's, 100 μg/ml heparin, 0.3 mg/ml yeast tRNA and 0.1% Tween-20, incubated in the same solution with riboprobes overnight, washed with 0.2×SSC, blocked in 10% lamb serum and incubated with anti-digoxigenin antibody overnight. The color reaction was

developed using NBT and BCIP in the dark. After the reaction was completed, the slides were washed in PBS, fixed in 4% paraformaldehyde/PBS and mounted in 100% glycerol. Digoxigenin-labeled riboprobes were synthesized from cDNA generated from RNA isolated from wild-type E9.5 embryos using the following PCR primer pairs:

Fn1: 5'-gatcggcagggagaaaatgg-3'

5'-tggggtgtggattgaccttg-3'

Vcan: 5'- ctggcacaaattccaaggacag-3'

5'-cgctgaatgaaaccatctttgc-3'

TnC: 5'- ggcagatatggggacaataacc-3'

5'- gcaaggggtaacttccaatgac-3'

Antibodies and dye. The primary antibodies used were anti-phospho Histone H3 (Upstate Biotechnology, Lake Placid, NY) at 1:1000 dilution, anti-Fibronectin1 at 1:1000 dilution (Millipore Corporate, Billerica, MA) anti-αA crystallin at 1:1000 dilution (a gift from Dr. Usha Andley), anti-Pax6 at 1:500 dilution (Developmental Studies Hybridoma Bank, Iowa City, IA) and anti-pSmad 1/5/8 at 1:200 dilution (Cell Signaling Technology, Danvers, MA). Alexa-Fluor labeled phalloidin (Molecular Probes, Eugene, OR) were used at 1:1000 dilution.

PAS and Alcian Blue staining. The embryos were subsequently fixed for 16 hr in Gendre fluid fixative, as previously described (Webster, Silver et al. 1983), then washed in 80% ethanol twice and routinely prepared for paraffin sectioning.

For Periodic Acid Schiff (PAS) staining, sections were deparaffinized, hydrated to water, oxidized in periodic acid for 5 min, treated with Schiff's reagent for 15 min, washed and mounted in 100% glycerol (Sigma, St. Louis, MO).

For Alcian Blue staining, sections were deparaffinized, hydrated to water, and stained in Alcian Blue for 30 minutes, and then washed, counterstained with nuclear fast red,and mounted in 100% glycerol (Sigma, St. Louis, MO).

Imaging. All the brightfield images of lens sections were taken using an Olympus BX60 microscope (Olympus, Melville, NY) and Spot camera (Spot Diagnostic Instruments, Sterling Heights, MI). The fluorescent images were taken either using a Olympus BX51 with Spot camera or a Zeiss 510 confocal microscope (Carl Zeiss, Thornburgh, NY).

Laser microdissection and microarray analysis. E9.5 or E10.0 embryos were embedded in OCT and snap frozen on dry ice for 10-15min. 10 μm frozen sections were transferred to glass PEN foil slides (Leica Microsystems, #11505189). To avoid the

separation of the foil and slides, slides were dipped in 70% ethanol at 4°C for 1 min, washed in RNAase-free water twice for 30 Sec, rinsed in 95% ethanol, and stained in Eosin Y. Stained samples were washed in 95% ethanol and dehydrated in 100% ethanol and xylene. The slides were dried and the lens placode or prospective lens ectoderm was microdissected using a Leica LMD 6000 laser microdissection system. Approximately 50ng of total RNA was extracted from the tissue obtained from one embryo using a Qiagen RNeasy Microkit (Qiagen#74004). 15 ng of total RNA was amplified into 3-5µg of cDNA by using Nugen WT-Ovation™ Pico RNA Amplification System (NuGEN Technologies Inc, #3300-12). cDNA samples obtained from three embryos of each genotype (biological triplicates) were used to probe Illumina Mouse6 bead microarrays . Microarray data were analyzed using Illumina Beadstudio 3.0 software.

Explant culture. Pregnant dams were injected with 7.2mg/40kg total amount of tamoxifen at E8.5 and E8.75 and the embryos were collected at E9.5. Heads were dissected into halves; one half was cultured in medium supplemented with 10 µM 4-OH tamoxifen and the other in medium with vehicle (ethanol). Heads were cultured on a Micropore filter (Costar, #110414) floating on Dulbecco's Modified Eagle's Medium (DMEM) supplemented with 20% fetal bovine serum, 100 µM non-essential amino acids,

100 units penicillin and 100 μg/ml streptomycin. Tissues were harvested at E11.5, fixed for 30 min and then used for analysis.

Transmission electron microscopy. For ultrastructural analysis, developing embyo eyes were fixed in 2% paraformaldehyde/2.5% glutaraldehyde/ 1% Alcian blue in 100 mM phosphate buffer, pH 7.2 overnight at 4°C. Samples were washed in phosphate buffer and postfixed in 0.5% osmium tetroxide/0.8% potassium ferricyanide/100mM phosphate for 1 hr at room temperature. Samples were washed in phosphate buffer and placed in 1% tannic acid/100mM phosphate for 1hr. Samples were then rinsed extensively in dH_20 prior to en bloc staining with 1% aqueous uranyl acetate for 1 hr. Following several rinses in dH_20, samples were dehydrated in a graded series of ethanol and embedded in Eponate 12 resin (Ted Pella Inc.). Sections of 95 nm were cut with a Leica Ultracut UCT ultramicrotome (Leica Microsystems Inc., Bannockburn, IL), stained with uranyl acetate and lead citrate, and viewed on a JEOL 1200 EX transmission electron microscope (JEOL USA Inc., Peabody, MA).

Statistical tests. Unpaired Student's t-test was performed using GraphPad InStat, Version 3.05.

Results

Mouse lens placode formation is not associated with increased cell proliferation, decreased cell death, or increased cell volume. Previous studies showed that lens placode thickening in chicken embryos is accompanied by an increase in cell density, but the mitotic index, thymidine labeling index, and cell volume in the placode cells did not differ from the adjacent, non-placodal tissue (McKeehan 1951; Zwaan and Pearce 1971). We determined whether the same was true during mouse lens placode formation (Fig. 1A, B). We found that the cell density was almost twice as high in the lens placode as in the pre-placodal ectoderm of mouse embryos (Fig. 1C), but the average area per cell in tissue sections was not different in the pre-placode and placode, indicating that average cell volume remained constant during placode formation (Fig. 1D). To determine if the cell crowding that accompanies placode formation is driven by increased proliferation or decreased cell death, we performed BrdU labeling and TUNEL assays before and during placode formation. The percentage of BrdU-labeled nuclei was indistinguishable in the pre-placode ectoderm at E8.5 and the placode at E9.5 (Fig. 1E). The BrdU labeling index was also similar in the placodal and peri-placodal ectoderm at E9.5 (data not shown). Instead of a decrease in cell death, we found a greater than 2-fold increase in the TUNEL

labeling index in the lens placode compared to the pre-placode ectoderm (Fig. 1F), an observation confirmed using an antibody against activated caspase-3 (Fig. S2). Similarly, cell death was more than twice as high in the lens placode as in the adjacent peri-placodal ectoderm by TUNEL assay or antibody to activated caspase 3 (data not shown). Although it is not clear why cell death increased during lens placode formation, decreased cell death is not involved in the increase in cell density that accompanies placode formation.

Pax6 is required for lens placode formation. Conditional deletion of the transcription factor, *Pax6*, demonstrated that it is required in the surface ectoderm for lens formation (Ashery-Padan, Marquardt et al. 2000). However, the extent of placode thickening was not measured in this study. Therefore, we measured the thickness of the surface ectoderm in $Pax6^{LeCre-}$ (wild type*; WT*), $Pax6^{fx/+;\ LeCre+}$ (lens ectoderm-specific *Pax6* heterozygote) and $Pax6^{fx/fx;\ LeCre+}$ (lens ectoderm-specific *Pax6* conditional knockout; *CKO*) embryos (Fig 2A-C). At the lens placode stage, the $Pax6^{CKO}$ surface ectoderm was significantly thinner than wild type (Fig.2D) and indistinguishable from the pre-placodal ectoderm at E8.5 (data not shown). Heterozygosity for *Pax6* gave an intermediate phenotype, consistent with the haploinsufficiency seen in mice and humans heterozygous for *Pax6* mutations (Fig.2D). Cell volume, proliferation and apoptosis were not different in the

Pax6^{CKO} surface ectoderm before lens placode formation and at the time lens placode should have formed. However, cell density was decreased in the *Pax6*^{CKO} surface ectoderm compared to *WT* (Fig. 2E-H). In agreement with measurements in chicken embryos, the contact area between the optic vesicle and the surface ectoderm remained constant during placode formation in wild type embryos (Fig. 2I). However, contact area between these tissues increased in *Pax6*^{CKO} embryos.

Pax6 regulates transcripts encoding components of the ECM in the lens placode. We used microarray analysis to identify genes that are regulated by Pax6 in the lens placode. Wild type and *Pax6*^{CKO} surface ectoderm was collected at E9.5 or E10.0 by laser microdissection (Fig. 3A, B) and RNA was isolated and amplified for microarray analysis (Table 1). The >500 transcripts that were significantly decreased in *Pax6*^{CKO} embryos included well-known Pax6 targets and transcription factors required for normal lens development, including *Prox1*, *Sox2*, *Mab21l, Pitx3, Tcfap2a* and *Maf* (Table 1) (Reza, Ogino et al. 2002; Lang 2004; Cvekl and Duncan 2007). Several transcripts encoding components of the extracellular matrix (ECM) or involved assembly of the ECM, such as fibronectin1 (*Fn1*), versican (*Vcan*), tenascin-C (*Tnc*), hyaluronan synthase 2 (*Has2*), leprecan-like 1 (*Leprel1*; prolyl 3-hydroxylase 2), and α1-collagen type 13 (*Col13a1*)

were decreased in the *Pax6*^{CKO} placodes (Table 1). In situ hybridization confirmed that transcripts encoding *Fn1* (Fig. 3C, D), *Vcan* (Fig.3E, F) and *Tnc* (Fig. 3G, H) were decreased in the *Pax6*^{CKO} lens ectoderm. PAS and Alcian blue staining showed decreased ECM in *Pax6*^{CKO} embryos, compared to *WT* (Supplemental Figure 1), suggesting that Pax6 in the surface ectoderm is required for the accumulation of a normal level of ECM and that the lens placode is a major source of ECM deposited between the surface ectoderm and optic vesicle.

Fibronectin from multiple sources contributes to lens placode formation. To test the function of ECM in lens placode formation, we conditionally deleted *Fn1*. Fibronectin contains modules that can bind to a variety of extracellular and cell surface molecules, including collagens, glycosaminoglycans, fibrin, integrins and fibronectin itself, and is crucial for ECM assembly and for mediating adhesion between cells and their ECM (Oberley and Steinert 1983; Mattey and Garrod 1984; Akiyama, Yamada et al. 1989; Corbett, Lee et al. 1997; Wierzbicka-Patynowski and Schwarzbauer 2003; Huang, Liu et al. 2007; Leiss, Beckmann et al. 2008). Because of the lethality of the *Fn1* germline knockout (George, Georges-Labouesse et al. 1993), we conditionally deleted *Fn1* from surface ectoderm, optic vesicle, or both using *Le-Cre, Rx-Cre* or both transgenes,

respectively (Ashery-Padan, Marquardt et al. 2000; Swindell, Bailey et al. 2006). Deleting *Fn1* from the surface ectoderm, optic vesicle or both tissues did not prevent placode formation or lens invagination. However, in each of these conditional knockout embryos, residual Fn1 was present between the lens placode and optic vesicle (Fig. 4A-D).

Global deletion of Fn1 prevented placode formation and lens invagination. To globally delete *Fn1* while avoiding early lethality, tamoxifen was administered at E8.5 and E8.75 to $Fn1^{fx/+}$ or $Fn1^{fx/fx}$ pregnant dams carrying the $CAGG\text{-}Cre^{ERTM}$ transgene (Hayashi and McMahon 2002). We also introduced the *Le-Cre* transgene into this cross, since this construct expresses green fluorescent protein (GFP) from an internal ribosome entry site, thereby marking the prospective lens-forming ectoderm (Ashery-Padan, Marquardt et al. 2000). Global deletion of *Fn1* resulted in a pericardial edema at E10.5 (Fig. 5A, B), which is consistent with the function of fibronectin in cardiovascular development (George, Georges-Labouesse et al. 1993). Most of the $Fn1^{CKO}$ embryos died before E11.0. Distinct GFP fluorescence demarcated the lens pit cells in $CAGG\text{-}Cre^{ERTM}$; $Fn1^{fx/+}$ embryos at E10.5, but fluorescence was weaker and more broadly distributed in tamoxifen-treated $CAGG\text{-}Cre^{ERTM}$; $Fn1^{fx/fx}$ embryos with heart edema (Insets in Fig. 5A,

B). At E10.5, *CAGG-Cre*^{ERTM}; *Fn1*$^{fx/fx}$ embryos had not formed lens placode, while the *CAGG-Cre*^{ERTM}; *Fn1*$^{fx/+}$ littermates had an invaginating lens vesicle (Fig.5C, D). Staining for fibronectin in *CAGG-Cre*^{ERTM}; *Fn1*$^{fx/fx}$ embryos showed that deletion was fairly efficient (Fig.5D).

To address whether the inhibition of lens placode formation resulted from the deficiency in *Fn1* or from secondary effects, like the heart defect, we cultured bisected heads from embryos that had received tamoxifen at E8.5 and E8.75, beginning at E9.5, a day before the embryos developed pericardial edema. One half-head was cultured in 4-OH tamoxifen and the other half was cultured with vehicle (ethanol). Lens vesicles formed in the head explants from *CAGG-Cre*^{ERTM}; *Fn1*$^{fx/+}$ embryos, whether they were cultured in tamoxifen or not (Fig. 6A, B, E, F). In cultured heads of *CAGG-Cre*^{ERTM}; *Fn1*$^{fx/fx}$ embryos that received no supplemental tamoxifen, no lens vesicles formed, although small aggregates of lens cells ("lentoids") were sometimes seen (Fig. 6C, D). When tamoxifen was added to the culture medium, lens vesicles were absent from *CAGG-Cre*^{ERTM}; *Fn1*$^{fx/fx}$ embryos (Fig.6G, H).

We then examined placode formation in *Fn1* deficient head explants, and found that

the thickness of placode of *Fn1* deficient head explants was significantly decreased compared to *CAGG-Cre*^{ERTM}; *Fn1*$^{fx/+}$ head explants (Fig.7A), while the contact area between the surface ectoderm and optic vesicle increased (Fig.7B). Previous studies have shown that the ECM has the ability to control cell growth and apoptosis (Oberley and Steinert 1983; Almeida, Ilic et al. 2000; Danen and Yamada 2001). To determine if the failure of lens placode formation in *Fn1* deficient head explants was due to decreased proliferation or increased cell death, we performed TUNEL and EdU analyses. Cell death increased in the *Fn1*-deficient embryos (Fig. 7C), although to a level that was still consistent with placode formation and lens invagination (Rajagopal, Huang et al. 2009). The percentage of cells in S-phase, as detected with EdU staining, was not significantly altered in *Fn1*-deficient head explants (Fig. 7D).

Previous studies showed that the ECM might play a role in sequestering morphogens involved in inductive tissue interactions. For example, FGF ligands bind to heparan sulfate in order to function in target cells (Allen and Rapraeger 2003; Smith, West et al. 2007; Pan, Carbe et al. 2008) and the association of BMPs with the ECM have been suggested to be important in inducing the differentiation of resident mesenchymal stem cells into osteoblasts (Gregory, Ono et al. 2005; Seib, Lanfer et al. 2009). Without intact

ECM, morphogens might diffuse more readily, reducing their concentration and their inductive ability. BMPs are produced by the lens-forming ectoderm and the optic vesicle and BMP signaling is required in the ectoderm for lens formation (Furuta and Hogan 1998; Wawersik, Purcell et al. 1999; Rajagopal, Huang et al. 2009). We, therefore, stained for BMP-activated Smads (phosphorylated Smad1/5/8) in the surface ectoderm. Phosphorylated Smad1/5/8 staining was strong in heterozygous and *Fn1*-deficient head explants (Fig. 7G, H), suggesting that the loss of *Fn1* did not affect BMP signaling. The level of Pax6 protein, a marker lens induction, was also not affected in *Fn1*-deficient head explants (Fig.7E, F).

The extracellular matrix is disrupted in both *Pax6*^{CKO} embryos and *Fn1*-deficient explants. To examine if the extracelluar matrix is disrupted in the *Fn1*-deficient head explants and Pax6 conditional knockout embryos, we performed an electron microscopy (EM) experiment. EM results showed that the fibrillar like matrix in the contrl embryos (Fig.S3A-B) is reduced and fragmented in both knockout embryos (Fig.S3C-D), suggesting that the failure of lens placode formation in these knockout embryos is due to the malfunction of the extracellular matrix.

The cytoskeletal reorganization that accompanies lens invagination occurs in the absence of placode formation. Although placode thickening and invagination are distinct morphogenetic events, they have rarely been studied as separate processes. Therefore, it is not clear whether placode formation is required for subsequent invagination. Invagination of the lens placode involves the BMP-dependent re-localization of actin microfilaments from the periphery to the apical ends of the placode cells, accompanied by the apical localization of myosin II (Rajagopal, Huang et al. 2009; Plageman, Chung et al. 2010). These events are followed by constriction of the cell apices, which appears to drive placode bending to initiate invagination. We stained embryos and cultured heads with fluorescent phalloidin to determine whether the apical redistribution of the actin cytoskeleton, which occurs just prior to invagination, occurred in the absence of placode formation (Rajagopal, Huang et al. 2009). We confirmed that in wild type placodes, F-actin was uniformly distributed around the cell periphery before invagination and localized to the apical ends of the placode cells during invagination (Fig. 8A, B). In *Fn1*-deficient head explants, F-actin also localized to the apical ends of the surface ectoderm cells, although these cells did not invaginate (Fig. 8C). As in placode cells lacking BMP receptors, F-actin did not redistribute to the apical ends of cells in the prospective lens-forming ectoderm of $Pax6^{CKO}$ embryos (Rajagopal, Huang et al. 2009)

(Fig. 8D).

Discussion

How to make a placode. Lens placode formation in the mouse embryo was accompanied by a doubling of cell density, while the contact area between the optic vesicle and the surface ectoderm did not change. At the same time, the surface area of the adjacent head ectoderm outside the placode was increasing as a result of the normal growth of the head. During placode formation, average cell volume and the rate of cell proliferation did not change. These results are consistent with previous studies in chicken embryos, which also found that the contact area between the optic vesicle and surface ectoderm remained constant and the mitotic and tritiated thymidine labeling indices were not different in the cells of the placode and the surrounding, non-placodal ectoderm (McKeehan 1951; Zwaan and Hendrix 1973). Zwaan and Hendrix estimated that the increase in cell number in the fixed area of the placode was sufficient to account for the increase in cell density and cell length seen during placode formation. Based on these observations, Zwaan and co-workers proposed what we have termed the "restricted expansion" model: adhesion between the surface ectoderm and the underlying ECM prevents the expansion of the prospective lens ectoderm; continued cell proliferation within this restricted area results in thickening of the head ectoderm to form the lens placode (Zwaan and Hendrix 1973;

Hendrix and Zwaan 1975).

While these data are sufficient to explain the formation of the lens placode in birds and mammals, it is worth considering whether alternative mechanisms might be involved. Cells might elongate if cell-cell adhesion increased. Since cell volume remains constant, this could increase the area of cell-cell contact at the expense of contact with the basal lamina. Supporting this possibility, increases in cadherin levels have been described during lens placode formation, (van Raamsdonk and Tilghman 2000; Xu, Overbeek et al. 2002; Pontoriero, Deschamps et al. 2008). Conditional deletion of N- and E-cadherin from the lens placode did not prevent placode formation, but this could be due to the perdurance of cadherins after gene disruption (Pontoriero, Smith et al. 2009). Cytoskeletal reorganization and function has also been suggested as a possible explanation for cell elongation during lens placode and neural plate formation (Byers and Porter 1964; Burnside 1971). However, if cell volume remained constant, either of these changes would make cells longer and thinner, decreasing the surface area of the placode. Since the area of the placode was constant during its formation, it seems more likely that proliferation within a restricted area, not cell elongation, provides the driving force for placode formation.

Deletion of Pax6 in the prospective lens ectoderm provides clues to the mechanism of placode formation. Deletion of *Pax6* in the surface ectoderm prevented placode formation and the increase in cell density that occurs during placode formation without altering the BrdU labeling index, average cell volume, or decreasing cell death. This result differs from a previous report, which found thinner placodes and a modest decrease in the BrdU labeling index in embryos with reduced *Pax6* expression due to deletion of the *Pax6* ectoderm enhancer (Dimanlig, Faber et al. 2001). However, our data agree with measurements performed in *Pax6* germline heterozygous embryos (van Raamsdonk and Tilghman 2000), which found thinner placodes, fewer cells in the placode, but no change in the percentage of phospho-histoneH3-labeled cells, a measure of cell proliferation. Importantly, we observed that the contact area between the optic vesicle and the surface ectoderm increased in the $Pax6^{CKO}$ embryos, showing that these cell layers were not prevented from expanding and providing an explanation for the inability of $Pax6^{CKO}$ ectoderm to form a placode.

Since deletion of *Pax6* prevented placode formation, the genes that are regulated by Pax6 must be required for placode formation. Comparison of gene expression in wild type placodes and ectoderm from which *Pax6* had been conditionally deleted revealed

decreased levels of well known targets of *Pax6* and a number of ECM components. Given the importance of the ECM in the restricted expansion model, we tested whether disrupting the assembly of the ECM would prevent placode formation.

We focused these experiments on *Fn1*, which was significantly decreased in $Pax6^{CKO}$ embryos in our microarray and in situ hybridization analyses. Fibronectin is both a component of the ECM and required for its assembly (Leiss, Beckmann et al. 2008). Fibronectin binds to cell-surface integrins, which promotes the assembly of a fibrillar fibronectin matrix. The fibronectin matrix then acts as a template for the assembly other components of the ECM. We reasoned that absence of fibronectin might disrupt the assembly of a functional matrix between the optic vesicle and surface ectoderm. If the restricted expansion hypothesis were correct, failure of matrix assembly should prevent placode formation.

Deletion of *Fn1* from the lens placode, the optic vesicle, or both tissues did not prevent placode formation or lens invagination. This appeared to be due to the perdurance of fibronectin in the ECM after deletion or, possibly, to fibronectin derived from adjacent head mesenchyme cells, since the lens vesicles formed in these knockouts had substantial

fibronectin at their basal surfaces. Deletion of *Fn1* using ubiquitously-expressed, tamoxifen-inducible Cre recombinase resulted in a more extensive reduction in fibronectin in the ECM between the optic vesicle and the surface ectoderm, absence of a lens placode and failure of lens formation. As in the $Pax6^{CKO}$ ectoderm, the area of contact between the optic vesicle and the surface ectoderm was larger in $Fn1^{CKO}$ embryos than in embryos heterozygous for *Fn1*. As suggested in the "restricted expansion model" (Fig. 9A), adhesion between the surface ectoderm and the underlying ECM is required for lens placode formation. Adhesion to the ECM prevents the lens ectoderm from expanding while the ectoderm cells continue to proliferate within the zone of adhesion. As they become crowded in this area, the cells have no choice but to elongate, thereby forming the lens placode. When the matrix between the optic vesicle and the overlying head ectoderm was disrupted by deleting *Pax6* or *Fn1*, the contact area between the lens ectoderm and optic vesicle expanded and the lens placode did not form (Fig.9B)

Differences between deletion of *Pax6* and *Fn1* in the surface ectoderm. Removal of one *Pax6* allele with the Le-Cre transgene reduced the thickness of the lens placode. However, deletion of *Fn1* in the lens placode did not inhibit placode formation or prevent invagination. Therefore, other *Pax6* target genes contribute to placode formation. These

may include genes encoding other components of the ECM that are reduced in *Pax6*^{CKO} placodes, like *Has2* and *Tnc*, or genes required to maintain the adhesion of placode cells with the ECM. Further studies are required to identify the *Pax6*-regulated genes that are required in the ectoderm for placode formation.

Prevention of placode formation by defects in the ECM or contact with the ECM are consistent with previous studies on chimeric embryos derived from *Pax6*$^{+/+}$ and *Pax6*$^{-/-}$ cells, which showed that most *Pax6*$^{-/-}$ cells were eliminated from the lens placode (Collinson, Hill et al. 2000). Presumably, this occurred because the *Pax6*$^{-/-}$ cells had decreased adhesion to the basal lamina and were excluded by adjacent *Pax6*$^{+/+}$ cells. This study also showed that contact between the optic vesicle and the prospective lens placode was not robust when either or both layers had a high proportion of *Pax6*$^{-/-}$ cells. Data from this work and the present study argue that cells lacking *Pax6* have lower adhesion to the ECM.

Implications for the formation of other placodes. We are aware of few studies, other than those conducted on the lens and otic placodes, in which mechanism of placode formation has been examined in a quantitative manner. Like the lens placode, the area of

the otic placode does not change during placode thickening (Meier 1978). The mitotic index is also similar in otic placode cells and in the surrounding, non-placode ectoderm. Electron microscopic examination of the ECM beneath the otic placode showed that it had a fibrillar structure, while the ECM underlying the ectoderm outside the placode had a granular appearance (Meier 1978). This raises the possibility that, like the lens, a specialized ECM is secreted or assembled to restrict epithelial spreading and promote otic placode formation (Meier 1978; Legan and Richardson 1997). The otic vesicle was present in the *Fn1*-deficient embryos generated in the present study (data not shown). However, the otic vesicle forms about one day earlier than the lens placode. Earlier exposure to tamoxifen would be required to test whether fibronectin is required to assemble a specialized ECM beneath the otic placode.

Like most placodes and unlike the lens, the otic placode is adjacent to mesenchyme during its formation. This raises the question of whether its close contact with the optic vesicle makes the lens placode a special case. However, it appears that a lens placode may form without contact with the optic vesicle (McKeehan 1958; Muthukkaruppan 1965). Although lens induction normally requires BMP4 from the optic vesicle (Furuta and Hogan 1998), rudimentary lens formation can occur when the optic vesicle is

genetically ablated; for example, if *β-catenin* is deleted from the ectoderm (Smith, Miller et al. 2005; Swindell, Liu et al. 2008). In one of these studies, the prospective lens-forming ectoderm appeared to thicken to form a placode in the absence of the optic vesicle, although ectodermal thickening and ECM accumulation were not measured (Swindell, Liu et al. 2008). In addition, the ventral extent of the lens placode is in contact with mesenchyme, not with the optic vesicle, yet it thickens and invaginates. Thus, like the otic placode, the lens placode cells may be able to secrete a specialized matrix and form over mesenchyme, as long as the appropriate inductive signals are provided.

Why make a placode? Placodes form prior to the invagination or involution of many tissues, but an explanation of the need for placode formation has not been provided and, to our knowledge, the requirement of placode formation for subsequent invagination has not been tested. In the present study, although the lens placode did not form, response to a lens-inducing stimulus, as indicated by phosphorylated Smad1/5/8 staining and lens induction, as indicated by Pax6 accumulation, occurred normally. Just before the invagination of the lens placode, actin filaments decrease at the lateral surfaces of the placode cells and increase at their apical ends (Rajagopal, Huang et al. 2009; Plageman, Chung et al. 2010). Actin redistribution is accompanied by increased apical localization

of myosin II (Plageman, Chung et al. 2010). In the present study, deletion of *Pax6* from the prospective lens ectoderm or *Fn1* from the entire embryo prevented placode formation. However, unlike deletion of *Pax6*, loss of fibronectin from the lens ECM did not prevent the reorganization and apical localization of the actin cytoskeleton. Although we cannot be certain that all of the subcellular components required for invagination were properly localized in the $Fn1^{CKO}$ embryos, it appears that the lens-forming ectoderm cells were prepared for invagination, but that invagination failed. These observations raise the possibility that placode formation might be a mechanical precondition for invagination.

From a mechanical perspective, the formation of a placode would seem to make its deformation (invagination) more difficult, since more force is required to bend a thicker tissue. However, if it is correct that the contractile apparatus assembled at the apical ends of each placode cell provides the force required to bend the placode during invagination, having a larger number of longer, thinner cells could decrease the force required from each cell to bend the tissue (Fig. 10). Doubling the length of a cell while maintaining its volume, as occurs during lens placode formation, increases the number of cell apices per area by a factor of four. This process also decreases by a factor of four the average area of the apical ends of the placode cells. Together with the apical localization of actin

filaments that occurs prior to invagination (Rajagopal, Huang et al. 2009; Plageman, Chung et al. 2010), reducing the apical area of the cells would increase the density of actin filaments in the apical actin web (Fig. 10). Since actin filaments of opposite polarity interact with myosin II to drive contraction (Ivanov 2008; Plageman, Chung et al. 2010), increasing the density of actin filaments could increase the interaction between actin filaments and myosin II. Together, these changes should increase the force available to reduce the apical surface area of the tissue and drive invagination. Therefore, placode formation may be required to establish the minimal mechanical and biochemical conditions necessary for invagination. If correct, this perspective could explain why placode formation precedes invagination in most tissues throughout embryogenesis.

References

Akiyama, S. K., S. S. Yamada, et al. (1989). "Analysis of fibronectin receptor function with monoclonal antibodies: roles in cell adhesion, migration, matrix assembly, and cytoskeletal organization." J Cell Biol **109**(2): 863-875.

Allen, B. L. and A. C. Rapraeger (2003). "Spatial and temporal expression of heparan sulfate in mouse development regulates FGF and FGF receptor assembly." J Cell Biol **163**(3): 637-648.

Almeida, E. A., D. Ilic, et al. (2000). "Matrix survival signaling: from fibronectin via focal adhesion kinase to c-Jun NH(2)-terminal kinase." J Cell Biol **149**(3): 741-754.

Ashery-Padan, R., T. Marquardt, et al. (2000). "Pax6 activity in the lens primordium is required for lens formation and for correct placement of a single retina in the eye." Genes Dev **14**(21): 2701-2711.

Burnside, B. (1971). "Microtubules and microfilaments in newt neuralation." Dev Biol **26**(3): 416-441.

Byers, B. and K. R. Porter (1964). "Oriented Microtubules in Elongating Cells of the Developing Lens Rudiment after Induction." Proc Natl Acad Sci U S A **52**: 1091-1099.

Collinson, J. M., R. E. Hill, et al. (2000). "Different roles for Pax6 in the optic vesicle and facial

epithelium mediate early morphogenesis of the murine eye." Development **127**(5): 945-956.

Corbett, S. A., L. Lee, et al. (1997). "Covalent cross-linking of fibronectin to fibrin is required for maximal cell adhesion to a fibronectin-fibrin matrix." J Biol Chem **272**(40): 24999-25005.

Cvekl, A. and M. K. Duncan (2007). "Genetic and epigenetic mechanisms of gene regulation during lens development." Prog Retin Eye Res **26**(6): 555-597.

Danen, E. H. and K. M. Yamada (2001). "Fibronectin, integrins, and growth control." J Cell Physiol **189**(1): 1-13.

Dimanlig, P. V., S. C. Faber, et al. (2001). "The upstream ectoderm enhancer in Pax6 has an important role in lens induction." Development **128**(22): 4415-4424.

Furuta, Y. and B. L. Hogan (1998). "BMP4 is essential for lens induction in the mouse embryo." Genes Dev **12**(23): 3764-3775.

George, E. L., E. N. Georges-Labouesse, et al. (1993). "Defects in mesoderm, neural tube and vascular development in mouse embryos lacking fibronectin." Development **119**(4): 1079-1091.

Gregory, K. E., R. N. Ono, et al. (2005). "The prodomain of BMP-7 targets the BMP-7 complex to the extracellular matrix." J Biol Chem **280**(30): 27970-27980.

Hayashi, S. and A. P. McMahon (2002). "Efficient recombination in diverse tissues by a tamoxifen-inducible form of Cre: a tool for temporally regulated gene activation/inactivation in the mouse." Dev Biol **244**(2): 305-318.

Hendrix, R. W. and J. Zwaan (1975). "The matrix of the optic vesicle-presumptive lens interface during induction of the lens in the chicken embryo." J Embryol Exp Morphol **33**(4): 1023-1049.

Huang, S. D., X. H. Liu, et al. (2007). "Synergistic effect of fibronectin and hepatocyte growth factor on stable cell-matrix adhesion, re-endothelialization, and reconstitution in developing tissue-engineered heart valves." Heart Vessels **22**(2): 116-122.

Ivanov, A. I. (2008). "Actin motors that drive formation and disassembly of epithelial apical junctions." Front Biosci **13**: 6662-6681.

Lang, R. A. (2004). "Pathways regulating lens induction in the mouse." Int J Dev Biol **48**(8-9): 783-791.

Legan, P. K. and G. P. Richardson (1997). "Extracellular matrix and cell adhesion molecules in the developing inner ear." Semin Cell Dev Biol **8**(3): 217-224.

Leiss, M., K. Beckmann, et al. (2008). "The role of integrin binding sites in fibronectin matrix assembly in vivo." Curr Opin Cell Biol **20**(5): 502-507.

Mattey, D. L. and D. R. Garrod (1984). "Organization of extracellular matrix by chick embryonic

corneal epithelial cells in culture and the role of fibronectin in adhesion." J Cell Sci **67**: 171-188.

McKeehan, M. S. (1951). "Cytological aspects of embryonic lens induction in the chick." J. Exp. Zool. **117**: 31-64.

McKeehan, M. S. (1958). "Induction of portions of the chick lens without contact with the optic cup. ." Anat. Rec. **132**: 297-305.

Meier, S. (1978). "Development of the embryonic chick otic placode. I. Light microscopic analysis." Anat Rec **191**(4): 447-458.

Meier, S. (1978). "Development of the embryonic chick otic placode. II. Electron microscopic analysis." Anat Rec **191**(4): 459-477.

Muthukkaruppan, V. (1965). "Inductive tissue interaction in the development of the mouse lens in vitro." J. Exp. Zool. **159**: 269-288.

Naiche, L. A. and V. E. Papaioannou (2007). "Cre activity causes widespread apoptosis and lethal anemia during embryonic development." Genesis **45**(12): 768-775.

Oberley, T. D. and B. W. Steinert (1983). "Effect of the extracellular matrix molecules fibronectin and laminin on the adhesion and growth of primary renal cortical epithelial cells." Virchows Arch B Cell Pathol Incl Mol Pathol **44**(3): 337-354.

Pan, Y., C. Carbe, et al. (2008). "Bud specific N-sulfation of heparan sulfate regulates

Shp2-dependent FGF signaling during lacrimal gland induction." Development **135**(2): 301-310.

Plageman, T. F., Jr., M. I. Chung, et al. (2010). "Pax6-dependent Shroom3 expression regulates apical constriction during lens placode invagination." Development **137**(3): 405-415.

Pontoriero, G. F., P. Deschamps, et al. (2008). "Cell autonomous roles for AP-2alpha in lens vesicle separation and maintenance of the lens epithelial cell phenotype." Dev Dyn **237**(3): 602-617.

Pontoriero, G. F., A. N. Smith, et al. (2009). "Co-operative roles for E-cadherin and N-cadherin during lens vesicle separation and lens epithelial cell survival." Dev Biol **326**(2): 403-417.

Rajagopal, R., J. Huang, et al. (2009). "The type I BMP receptors, Bmpr1a and Acvr1, activate multiple signaling pathways to regulate lens formation." Dev Biol **335**(2): 305-316.

Reza, H. M., H. Ogino, et al. (2002). "L-Maf, a downstream target of Pax6, is essential for chick lens development." Mech Dev **116**(1-2): 61-73.

Sakai, T., K. J. Johnson, et al. (2001). "Plasma fibronectin supports neuronal survival and reduces brain injury following transient focal cerebral ischemia but is not essential for skin-wound healing and hemostasis." Nat Med **7**(3): 324-330.

Seib, F. P., B. Lanfer, et al. (2009). "Biological activity of extracellular matrix-associated

BMP-2." J Tissue Eng Regen Med.

Smith, A. N., L. A. Miller, et al. (2005). "The duality of beta-catenin function: a requirement in lens morphogenesis and signaling suppression of lens fate in periocular ectoderm." Dev Biol **285**(2): 477-489.

Smith, S. M., L. A. West, et al. (2007). "Heparan and chondroitin sulfate on growth plate perlecan mediate binding and delivery of FGF-2 to FGF receptors." Matrix Biol **26**(3): 175-184.

Swindell, E. C., T. J. Bailey, et al. (2006). "Rx-Cre, a tool for inactivation of gene expression in the developing retina." Genesis **44**(8): 361-363.

Swindell, E. C., C. Liu, et al. (2008). "Eye formation in the absence of retina." Dev Biol **322**(1): 56-64.

van Raamsdonk, C. D. and S. M. Tilghman (2000). "Dosage requirement and allelic expression of PAX6 during lens placode formation." Development **127**(24): 5439-5448.

Wakely, J. (1984). "Observations on the role of ectodermal spreading in the early stages of lens placode invagination in the chick embryo." Exp Eye Res **38**(6): 627-636.

Wawersik, S., P. Purcell, et al. (1999). "BMP7 acts in murine lens placode development." Dev Biol **207**(1): 176-188.

Webster, E. H., Jr., A. F. Silver, et al. (1983). "Histochemical analysis of extracellular matrix material in embryonic mouse lens morphogenesis." Dev Biol **100**(1): 147-157.

Wierzbicka-Patynowski, I. and J. E. Schwarzbauer (2003). "The ins and outs of fibronectin matrix assembly." J Cell Sci **116**(Pt 16): 3269-3276.

Xu, L., P. A. Overbeek, et al. (2002). "Systematic analysis of E-, N- and P-cadherin expression in mouse eye development." Exp Eye Res **74**(6): 753-760.

Zwaan, J. and R. W. Hendrix (1973). "Changes in Cell and Organ Shape during Early Development of the Ocular Lens." Amer. Zool. **13**: 1039-1049.

Zwaan, J. and T. L. Pearce (1971). "Cell population kinetics in the chicken lens primordium during and shortly after its contact wth the optic cup." Dev Biol **25**(1): 96-118.

Figures & Legends

Figure 1.

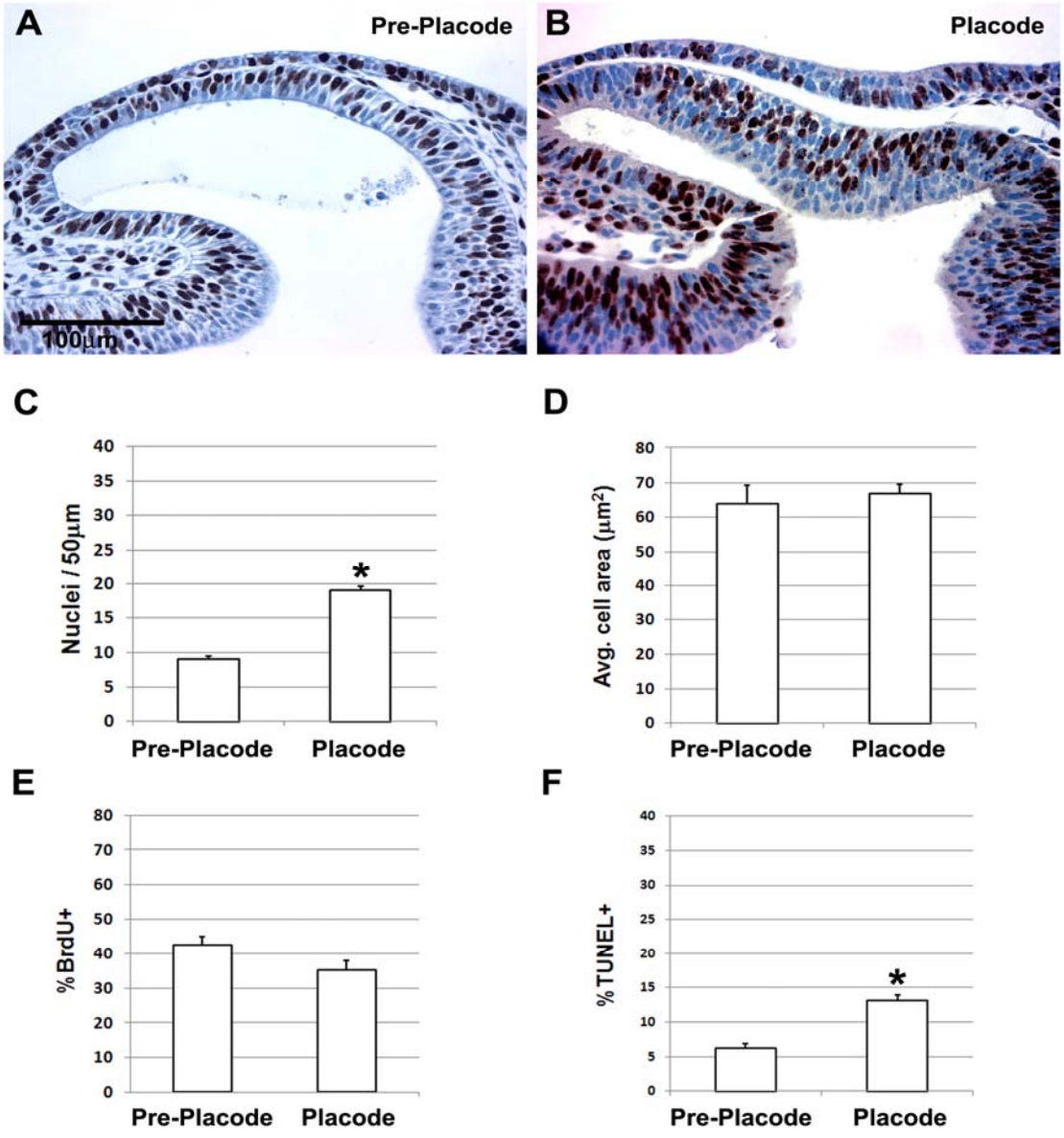

Fig. 1 Cell density, volume, proliferation and death in wild type mouse embryos during lens placode formation. Measurements were made at the pre-placode stage (**A**) and at placode stage (**B**). Embryos in **A** and **B** were BrdU-labeled. Cell density (number of nuclei/50 μm length) doubled during placode formation (**C**). Cell volume (nuclei per tissue area; **D**) and cell proliferation (BrdU labeling index; **E**) did not change during placode formation. Cell death increased during placode formation (**F**). *$p<0.05$

Figure 2.

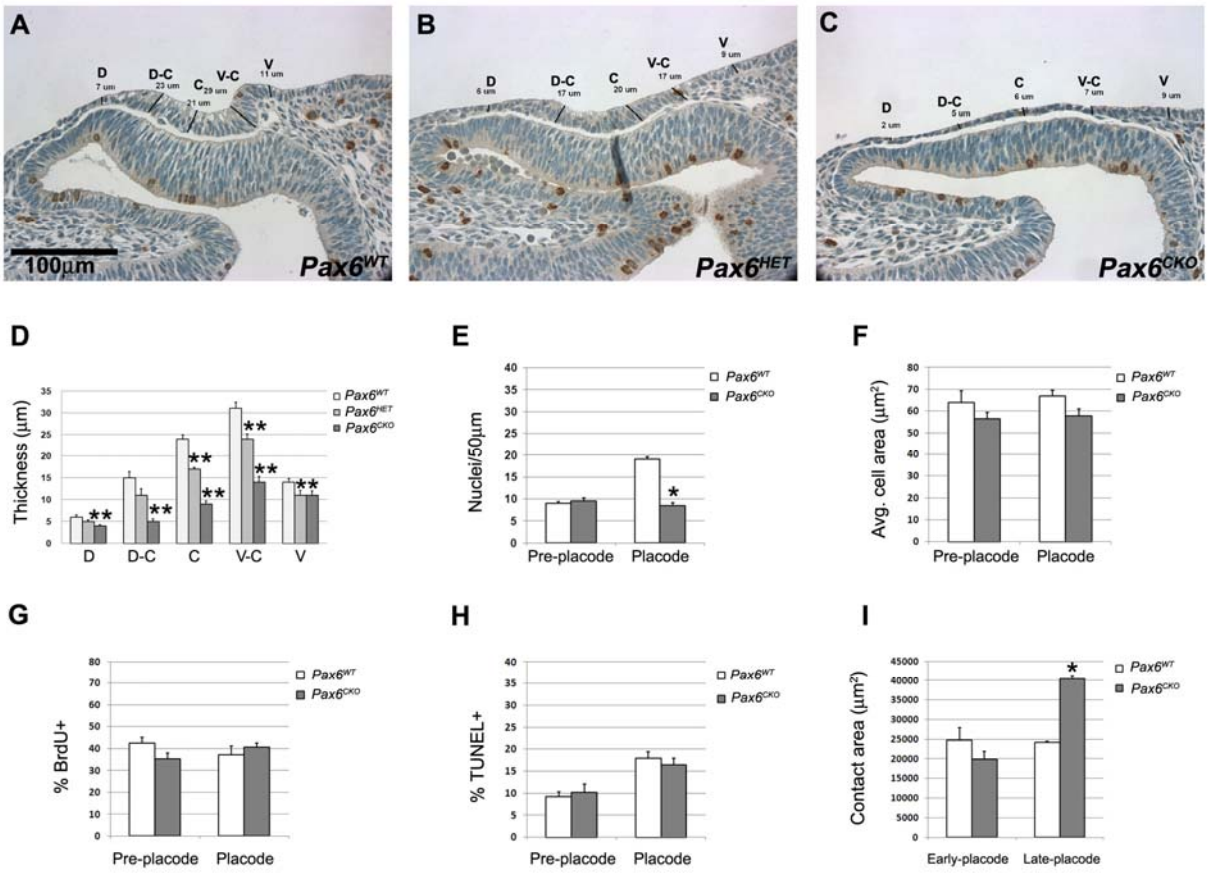

Fig. 2 Placode thickness is regulated by *Pax6* dose and correlates with cell density.

(**A**) Placode thickness of wild type (*Pax6*$^{+/+}$), (**B**) ectoderm-specific conditional heterozygote (*Pax6*^{HET}) and (**C**) ectoderm-specific conditional knockout (*Pax6*^{CKO}) embryos was measured at five positions: D (dorsal), D-C (dorsal- center), C (center), V-C (ventral- center) and V (ventral). (**D**) *Pax6*^{CKO} ectoderm was significant thinner than

wild type at all locations; heterozygous placodes were of intermediate thickness. (**E**) Unlike wild type ectoderm, average cell density did not increase in *Pax6*^{CKO} ectoderm. (**G**) Cell volume, (**F**) cell proliferation (BrdU labeling index) and (**H**) cell death (TUNEL labeling index) was not significantly different in *Pax6*$^{+/+}$ and *Pax6*^{CKO} embryos at pre-placode and placode stages. (I) contact area between the optic vesicle and the ectoderm was unchanged during lens placode formation in wild type embryos, but increased in *Pax6*^{CKO} littermate embryos. *p<0.05, ** p<0.01

Figure 3.

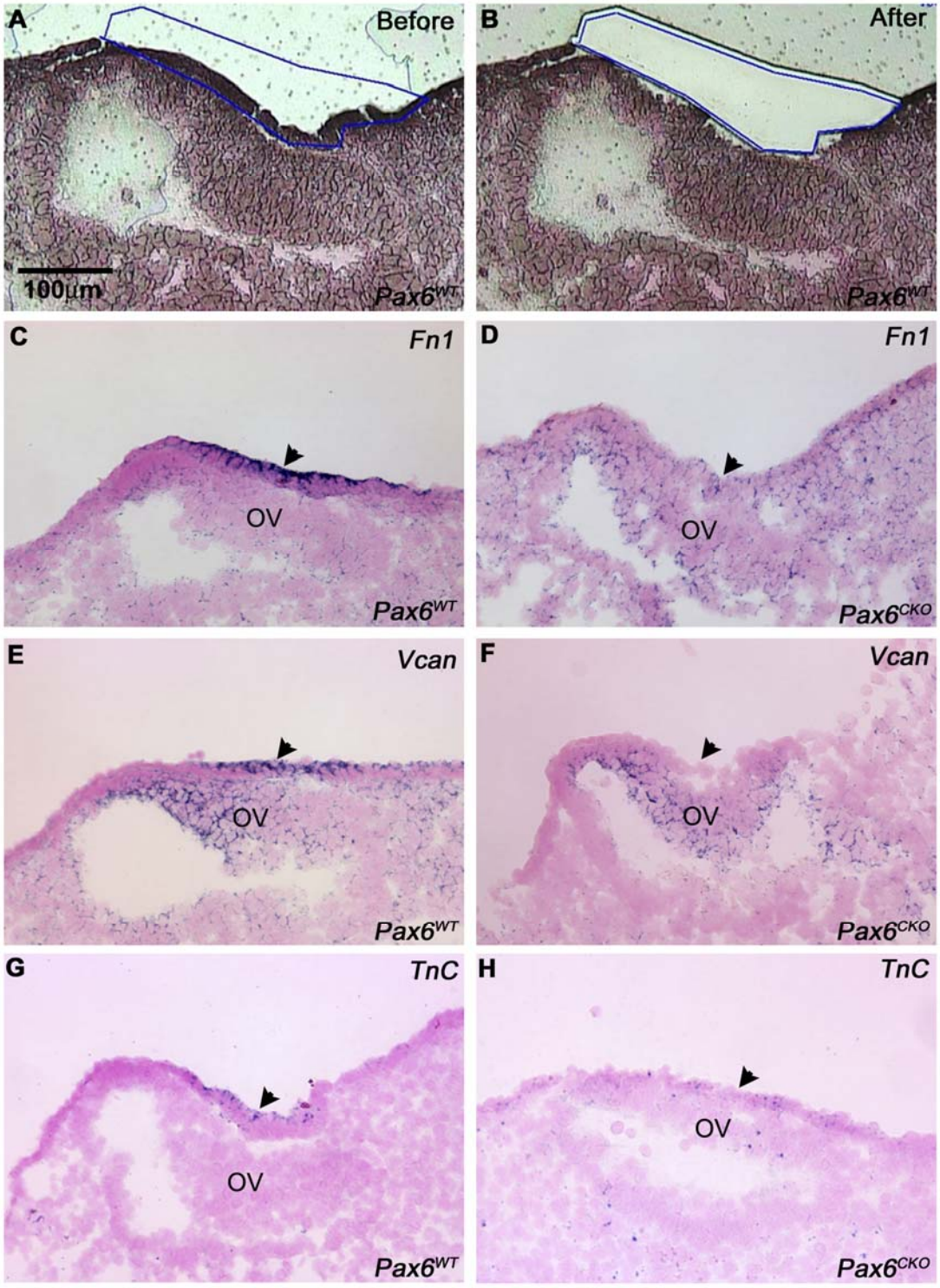
A
Before
100μm
Pax6WT
B
After
Pax6WT
C
Fn1
OV
Pax6WT
D
Fn1
OV
Pax6CKO
E
Vcan
OV
Pax6WT
F
Vcan
OV
Pax6CKO
G
TnC
OV
Pax6WT
H
TnC
OV
Pax6CKO

Fig.3 Laser microdissection and verification of microarray data by in situ hybridization. (**A**) Frontal section of a wild type embryo at the placode stage before laser microdissection. (**B**) The same section after laser microdissection. (**C, D**) In situ hybridization in $Pax6^{+/+}$ and $Pax6^{CKO}$ embryos for fibronectin (*Fn1*), (**E, F)** versican (*Vcan*) and (**G, H**) tenascin-C (*Tnc*). OV – optic vesicle; arrowheads point to the surface ectoderm forming the lens placode or where the placode would have formed.

Figure 4.

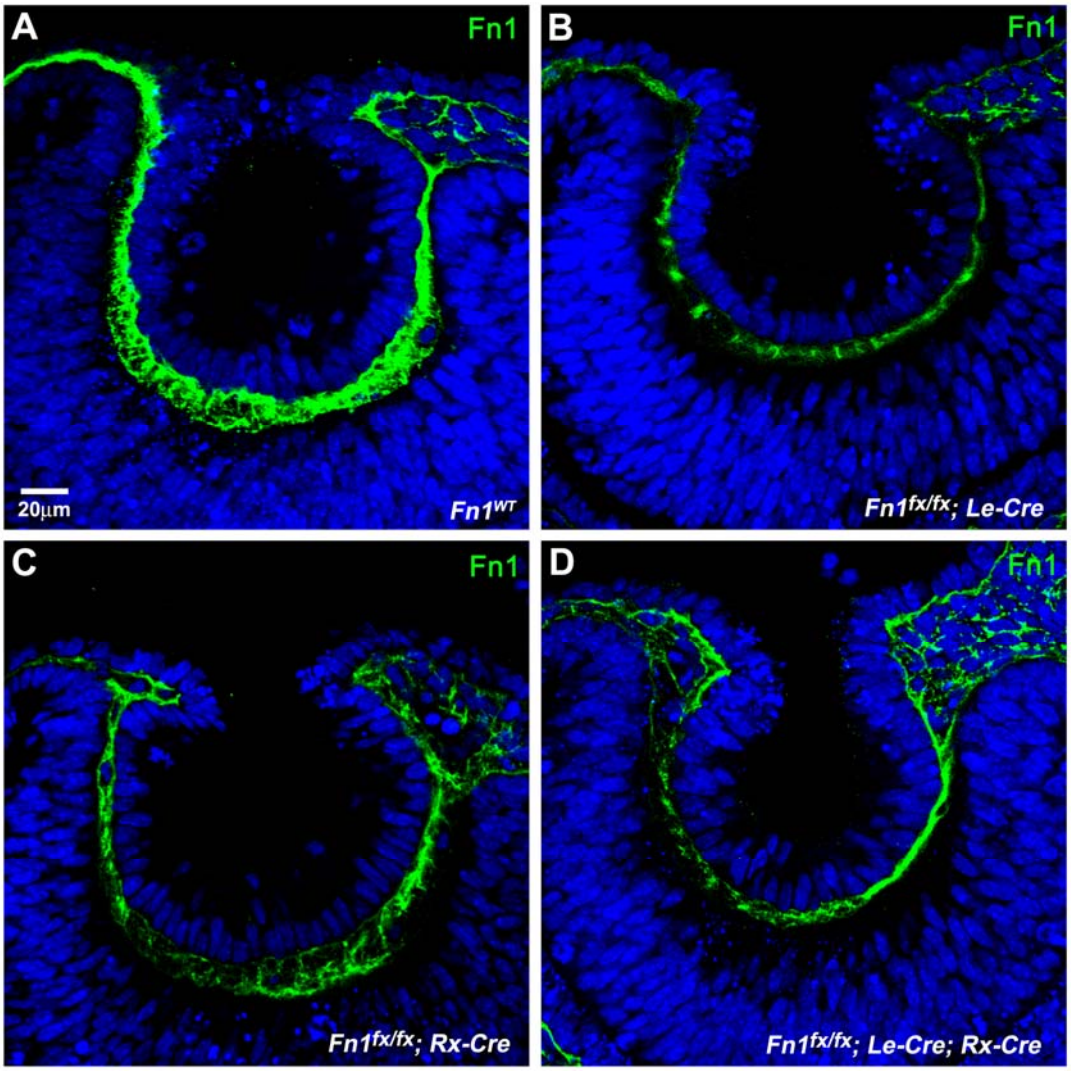

Fig.4 Lens formation and immunostaining for fibronectin in *Fn1* conditional knockouts. Genotypes are shown in the lower right corners. The lens pit formed and fibronectin immunostaining (green) was reduced, but present in the ECM in each case. Nuclei are stained blue with DRAO-5.

Figure 5.

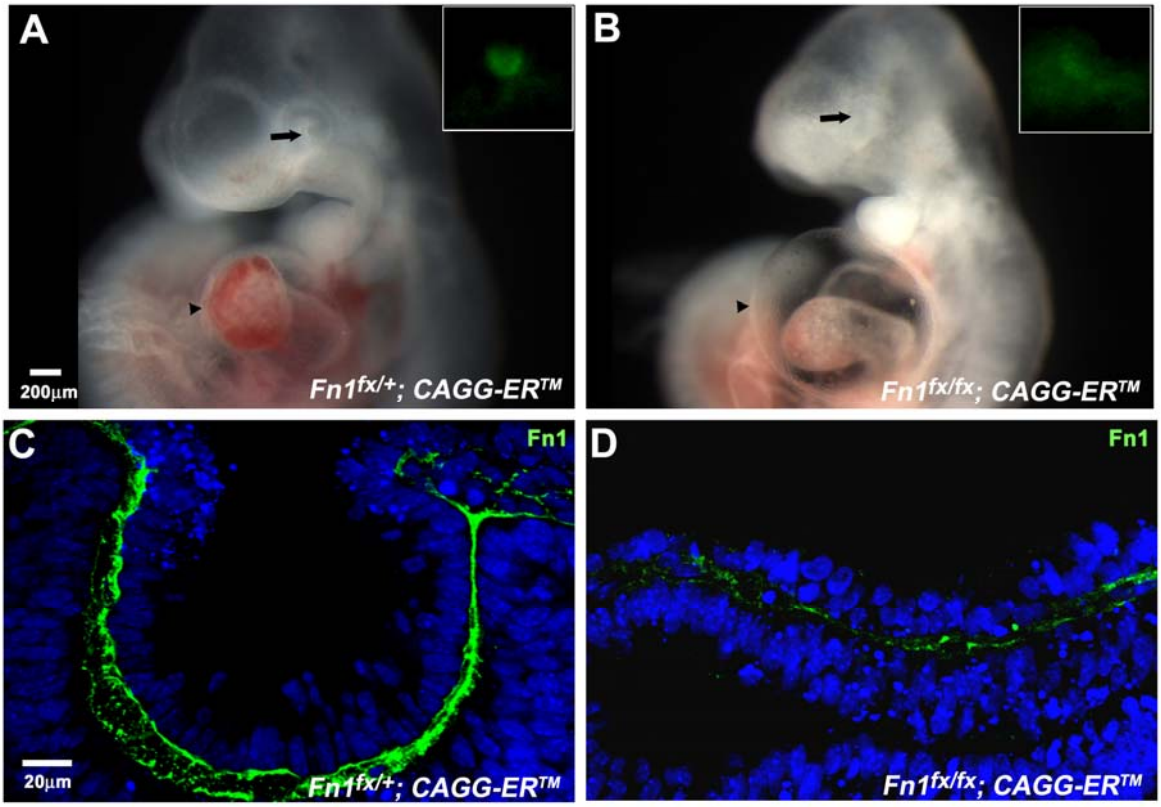

Fig. 5 Lens formation and immunostaining for fibronectin in *Fn1*-deficient embryos.

(**A**) The lens vesicle (arrow) formed in a $Fn1^{fx/+}$ embryo exposed to tamoxifen on E8. GFP fluorescence, which marks the prospective lens tissue, is strong and sharply demarcated (inset). (**B**) No lens vesicle (arrow) formed in a $Fn1^{fx/fx}$ embryo exposed to tamoxifen. GFP fluorescence in the ectoderm was weak and diffuse (inset). (**C**) Fibronectin immunostaining in a $Fn1^{fx/+}$ embryo exposed to tamoxifen on E8. (**D**) Fibronectin immunostaining decreased greatly in a $Fn1^{fx/fx}$ embryo exposed to tamoxifen on E8.

Figure 6.

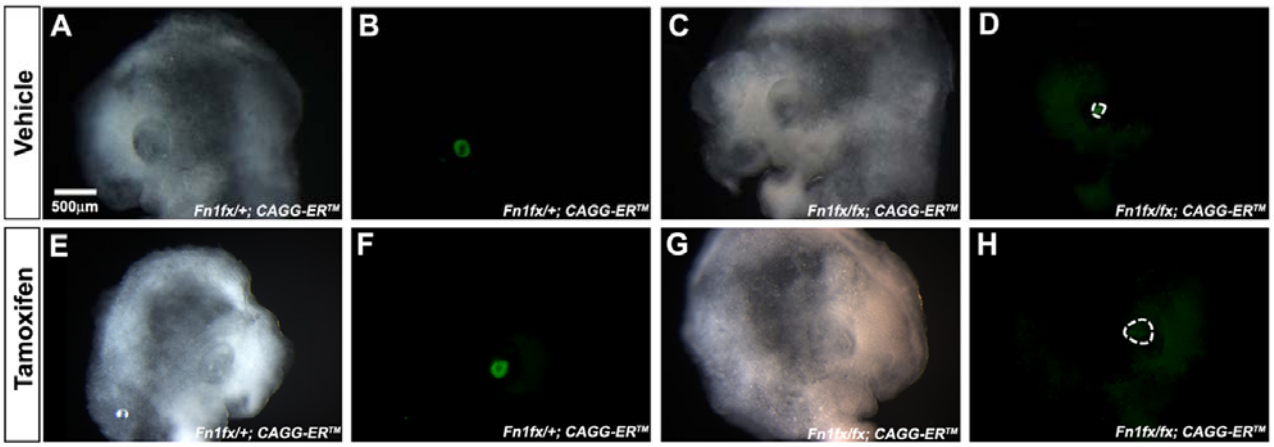

Fig. 6 Lens formation in wild type and *Fn1*-deficient head explants.

(**A, B, E, F**) Brightfield and fluorescence images showing the lens vesicles formed in $Fn^{+/fx}$; $CAGG\text{-}ER^{TM}$ head explants cultured in vehicle (**A, B**) or in tamoxifen (**E, F**). (**C, D**) Brightfield and fluorescence images showing the small aggregates of lens cells ("lentoids") that were sometimes seen in $Fn^{fx/fx}$; $CAGG\text{-}ER^{TM}$ head explants that received no supplemental tamoxifen during culture. (G, H) Brightfield and fluorescence images showing that lens vesicles were absent from cultured heads of $Fn^{fx/fx}$; $CAGG\text{-}ER^{TM}$ embryos when tamoxifen was added to the culture medium.

Figure 7.

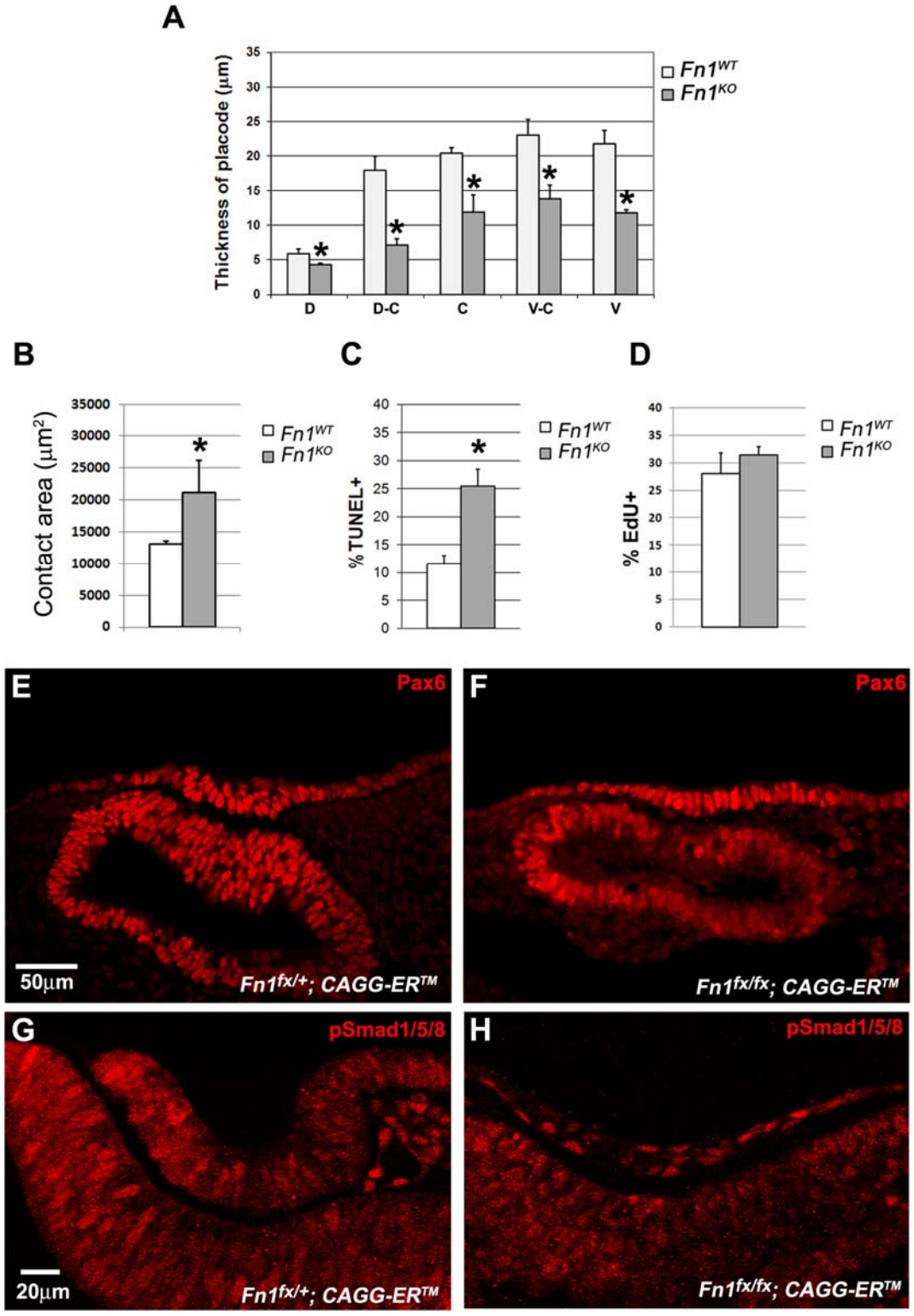
A
Thickness of placode (μm)
35
30
25
20
15
10
5
0
D
D-C
C
V-C
V
Fn1WT
Fn1KO
B
Contact area (μm2)
35000
30000
25000
20000
15000
10000
5000
0
C
% TUNEL+
40
35
30
25
20
15
10
5
0
D
% EdU+
40
35
30
25
20
15
10
5
0
E
Pax6
50μm
Fn1fx/+; CAGG-ERTM
F
Pax6
Fn1fx/fx; CAGG-ERTM
G
pSmad1/5/8
20μm
Fn1fx/+; CAGG-ERTM
H
pSmad1/5/8
Fn1fx/fx; CAGG-ERTM

Fig. 7 Deletion of *Fn1* decreased placode thickness and increased the contact area between the optic vesicle and the surface ectoderm, but did not prevent the expression of lens cell differentiation markers or BMP signaling. (**A**) Lens placode thickness was significantly decreased in *Fn1*-deficient head explants. (**B**) The contact area between the ectoderm and the optic vesicle was significantly greater in *Fn1*-deficient head explants. (**C**) The TUNEL-labeling index increased significantly in *Fn1*-deficient head explants. (**D**) Cell proliferation, as measured by the EdU-labeling index, was similar in wild type and *Fn1*-deficient head explants. (**E, F**) Pax6 protein levels were unaffected in the prospective placodal ectoderm of *Fn1*-deficient head explants. (**G, H**) BMP signaling, as measured by the nuclear localization of phosphorylated Smad1/5/8 (pSmad1/5/8), was not affected in *Fn1*-deficient head explants. *$p<0.05$

Figure 8.

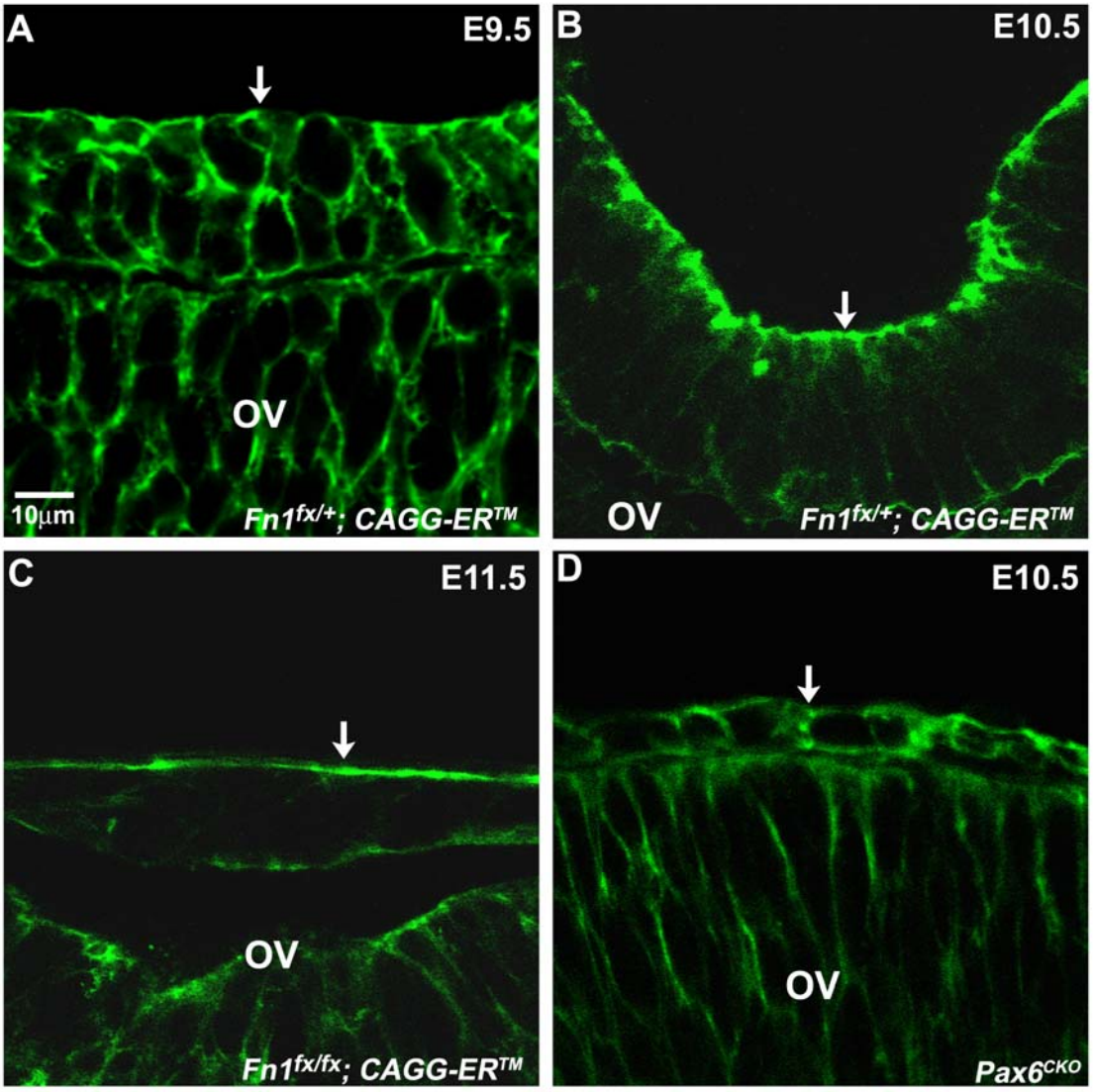

Fig. 8 Cytoskeleton reorganization in *Pax6*^{CKO} embryos and *Fn1*-deficient head explants. (A) Confocal images of phalloidin staining of a frontal section of *Fn1*$^{fx/+}$; *CAGG-ER*^{TM} that embryo showing the localization of the actin cytoskeleton at the periphery of lens placode cells on E9.5, before placode invagination. (B) A frontal section of *Fn1*$^{fx/+}$; *CAGG-ER*^{TM} embryo, showing the mainly apical localization of the F-actin

cytoskeleton during placode invagination. (C) Phalloidin staining on a frontal section of a *Fn1*$^{fxfx+}$*; CAGG-ER*^{TM} head explant that had been cultured in 4-OH tamoxifen, showing the mainly apical localization of the F-actin cytoskeleton at a stage corresponding to the lens vesicle stage in vivo. (D) Phalloidin staining in a frontal section of a *Pax6*^{CKO} embryo showing the uniform distribution of the F-actin cytoskeleton at the periphery of the surface ectoderm cells at E10.5. Arrows point to the apical surface of the ectoderm cells; OV – optic vesicle.

Figure 9.

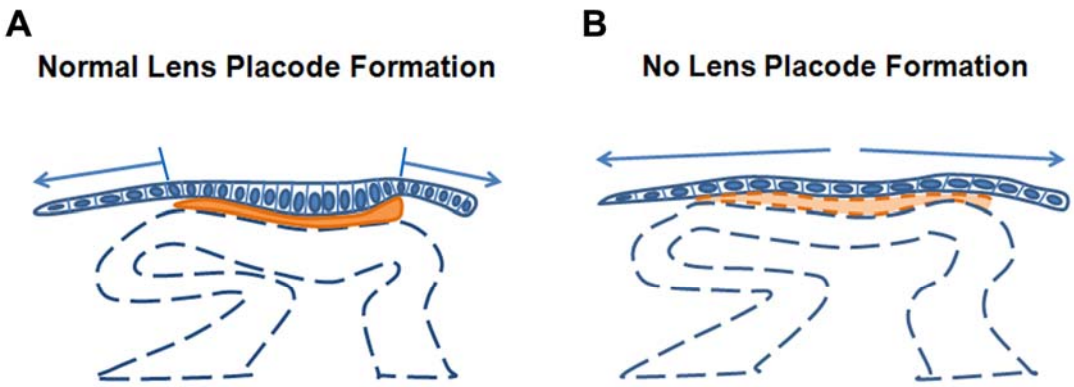

Fig. 9 The "restricted expansion model" of lens placode formation. The extracellular matrix between the optic vesicle and the surface ectoderm is colored orange.

(**A**) During normal lens placode formation, the adhesion between the head ectoderm and the extracellular matrix prevents the expansion of the prospective lens territory. Continued cell proliferation within this area of adhesion leads to cell crowding, resulting in cell elongation and placode formation (Hendrix and Zwaan 1975). (**B**) In *Pax6* ^{CKO} or *Fn1*-deficient embryos, the matrix between the optic vesicle and the overlying head ectoderm is deficient, resulting in the unrestricted expansion of the prospective lens ectoderm and impaired placode formation.

Figure 10.

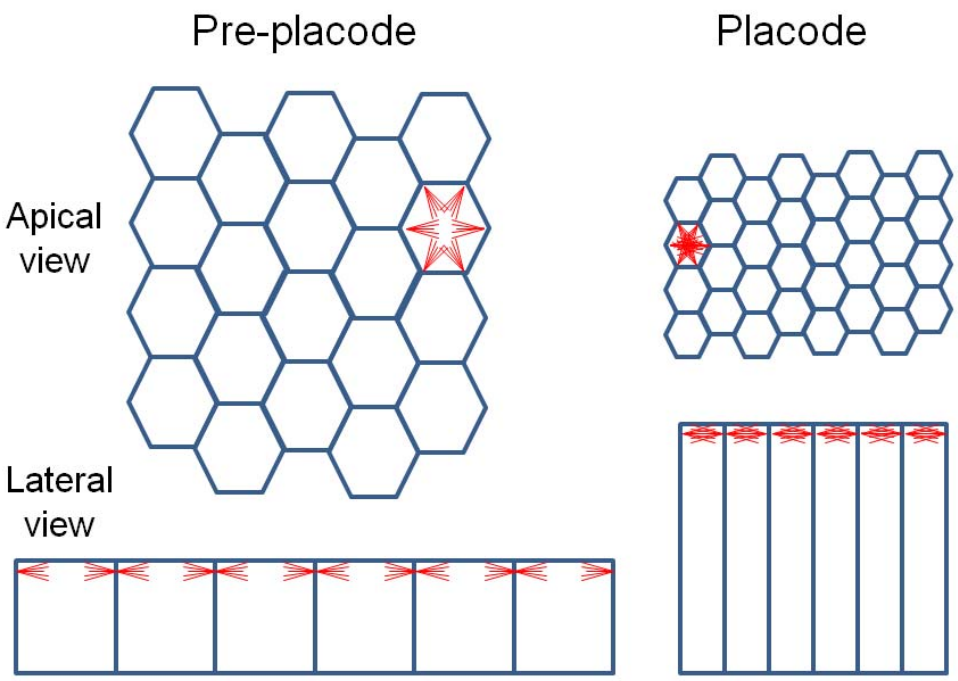

Fig.10 Illustration of the geometric consequences of doubling cell height while maintaining cell volume. During lens placode formation, crowding causes cell elongation, resulting in a fourfold decrease in area of the apical ends of the cells and a fourfold increase in the "concentration" of cell apices. If the concentration of apical actin filaments (red lines) were similar on a per-cell basis, the concentration of these filaments at the apical end of each cell would be at least four times higher after placode formation, resulting in a sixteen-fold increase in their concentration at the apical surface. Actin filaments are depicted as red lines of equal length and number in all tissues.

Supplemental Figures & Legends

Figure S1.

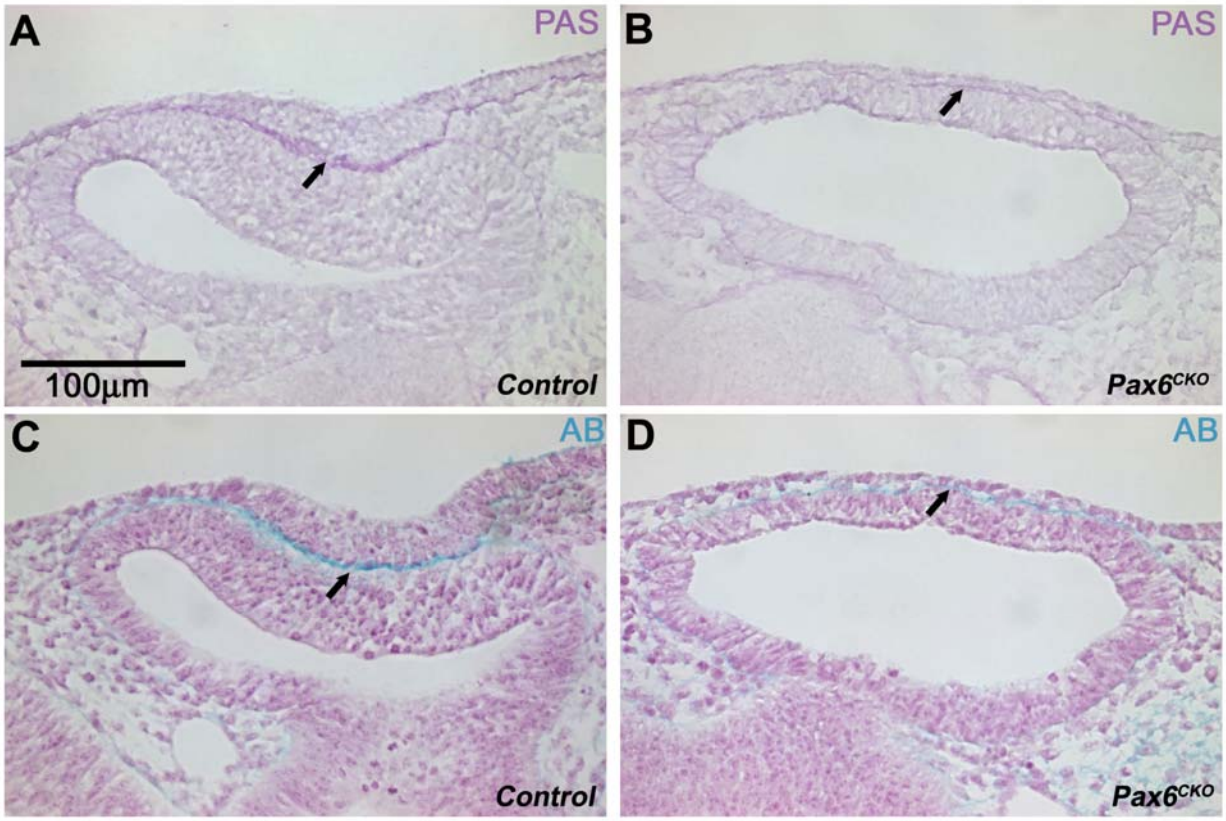

Fig. S1 Periodic acid Schiff (PAS) and Alcian Blue (AB) staining in *Pax6*^{WT} and *Pax6*^{CKO} embryos.

(A,B) Staining of the matrix between the optic vesicle and the surface ectoderm (arrows) by PAS was strong but less intense in *Pax6*^{CKO} embryos.

(C,D) Staining of the matrix between the optic vesicle and the surface ectoderm (arrows) by AB was strong but less intense in *Pax6*^{CKO} embryos.

Figure S2.

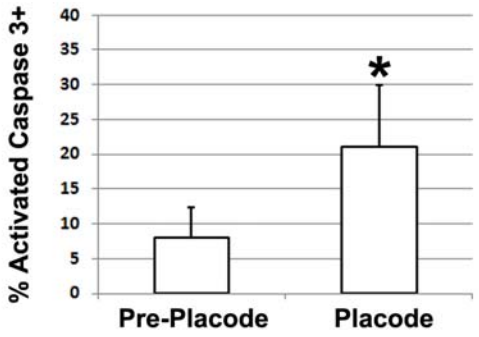

Fig. S2. Activated caspase 3 in wild type mouse embryos during lens placode formation.

The level of activated caspase 3 increased during placode formation. *$p<0.05$

Figure S3.

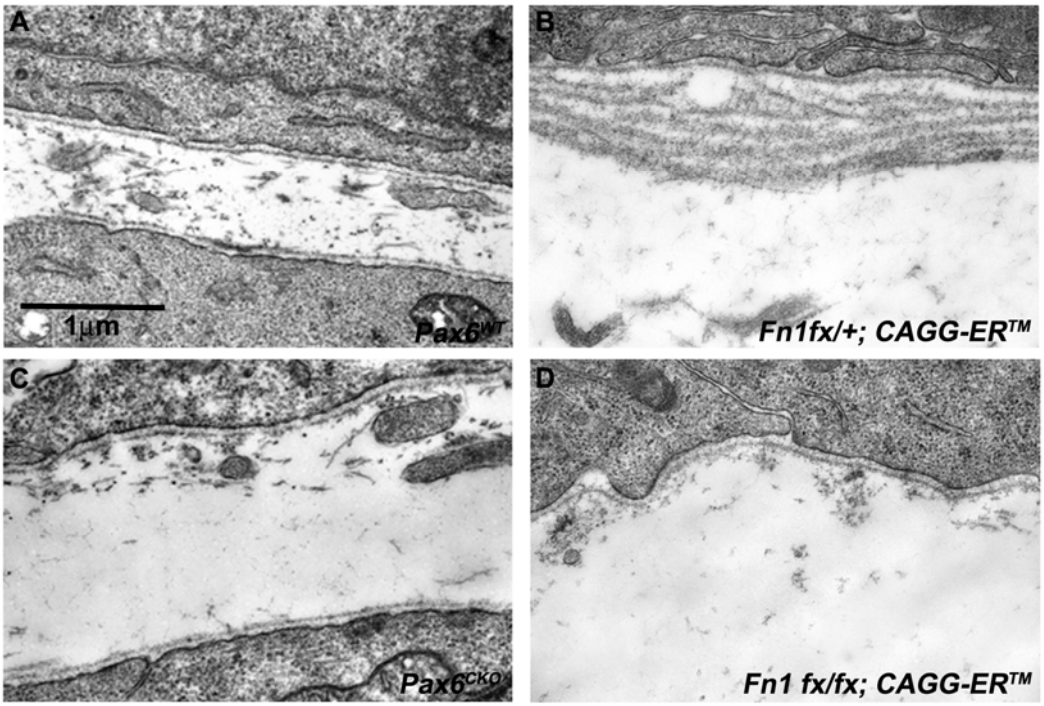

Fig. S3 The extracellular matrix is disrupted in *Pax6*^{CKO} embryos and *Fn1*-deficient explants.

(A,B) The abundant fibrillar matrix in wild type control embryos and cultured explants.

(C,D) The extracellular matrix is disrupted in *Pax6*^{CKO} embryos and *Fn1*-deficient explants.

Table 1. Transcripts significantly altered in *Pax6*^{CKO} embryos at E10.0.

Category	Gene	Fold change	P-Value
Transcription factors known to be regulated by Pax6 and/or important for lens development	*c-Maf*	-1600	<0.001
	Prox1	-197	<0.001
	Mab21l1	-3.5	<0.01
	Tcfap2a	-2.3	<0.05
	Pitx3	-12.3	<0.05
	Sox2	-4.2	<0.01
Expressed by Le-Cre transgene	*eGFP*	91	<0.001
Extracellular matrix and related transcripts	*Fn1*	-14.8	<0.05
	Vcan	-5.1	<0.001
	Leprel1 (P3h2)	-8.5	<0.001
	Has2	-6.7	<0.001
	Tnc	-95.8	<0.001
	Tgm2	-96.0	<0.001
	Col13a1	-3.3	<0.05

Chapter 2 The Role of Surface Ectoderm in Optic Vesicle Invagination

Abstract

Previous studies showed that the optic vesicle failed to invaginate to form the optic cup when the surface ectoderm was ablated at an early stage of contact, indicating the surface ectoderm plays a role in optic vesicle invagination. Our studies showed that there is a thickening of the distal optic vesicle shortly before the optic vesicle invaginates, suggesting the retina forms a retinal placode, as the lens does. We also showed that there is a correlation between the retinal placode formation and invagination, and lens placode and retinal placode formation, suggesting the lens placode is required for retinal placode formation and invagination. Finally, we showed the retinal placode invagination (optic cup formation) can occur without lens placode invagination.

Introduction

During eye morphogenesis, the lens forms from the surface ectoderm at the same time that the optic vesicle transforms into the optic cup. Experimental analysis of eye development has revealed an intimate relationship between the lens surface ectoderm and optic vesicle. When optic vesicle makes a close contact with the lens surface ectoderm, they become coherent as a result of the deposition of an abundant extracellular matrix. The intimate contact between these two tissues stimulated many studies to investigate if there are reciprocal inductive interactions taking place. This chapter will discuss the roles of lens morphogenesis in optic cup formation.

Studies in chicken and mouse embryos showed that the optic vesicle failed to invaginate to form optic cup when the surface ectoderm was ablated at an early stage of contact (Hyer, Kuhlman et al. 2003; Zhang, Burgess et al. 2008). This suggested that the surface ectoderm or signals emanating from lens surface ectoderm is required for optic vesicle invagination. Mouse embryos in which Pax6 was deleted or Wnt signaling was over-activated in the surface ectoderm failed to form a lens and the optic vesicle failed to invaginate (Ashery-Padan, Marquardt et al. 2000; Smith, Miller et al. 2005), suggesting,

again, that there may be signaling involved. On the other hand, our studies of lens placode formation showed that lens placode did not form, due to the defective extracellular matrix formation in Pax6 surface ectoderm knockout (*Pax6*^{SEKO}) embryos, suggesting that lens morphogenesis or the normal extracellular matrix may be essential for optic vesicle invagination.

To understand the mechanism of optic vesicle invagination, we analyzed the distal optic vesicle of wild type and conditional knockout embryos. This chapter will describe the effects of these knockouts on optic vesicle invagination.

Materials & Methods

Mice All animals were treated in accordance with the ARVO Statement for the Use of Animals in Ophthalmic and Vision Research and with the approval of the Animal Studies Committee of the Washington University School of Medicine. *Pax6*^{SEKO} mice are from the crosses between *Pax6*$^{fx/fx}$ mice and *Lecre* mice, as previously described (Ashery-Padan, Marquardt et al. 2000).

Laser microdissection and microarray analysis. E9.5 or E10.0 embryos were embedded in OCT and snap frozen on dry ice for 10-15min. 10 μm frozen sections were transferred to glass PEN foil slides (Leica Microsystems, #11505189). To avoid the separation of the foil and slides, slides were dipped in 70% ethanol at 4°C for 1 min, washed in RNAase-free water twice for 30 Sec, rinsed in 95% ethanol, and stained in Eosin Y. Stained samples were washed in 95% ethanol and dehydrated in 100% ethanol and xylene. The slides were dried and the lens placode or prospective lens ectoderm was microdissected using a Leica LMD 6000 laser microdissection system. Distal optic vesicles from 3 wild type control embryos or 3 *Pax6*^{CKO} embryos are pooled together, and extracted RNA respectively using a Qiagen RNeasy Microkit (Qiagen#74004). Each

RNA was then amplified into cDNA by using Nugen WT-Ovation™ Pico RNA Amplification System (NuGEN Technologies Inc, #3300-12). cDNA samples obtained from three amplification (technically triplicates) were used to probe Illumina Mouse6 bead microarrays . Microarray data were analyzed using Illumina Beadstudio 3.0 software.

Histology. Embryo heads were fixed in 4% paraformaldehyde/PBS overnight at 4°C, dehydrated through a series of ethanol concentrations, embedded in paraffin and sectioned at 4 μm. For morphological studies, sections were stained with hematoxylin and eosin (Surgipath, Richmond, IL, USA). Cell volume was determined by dividing the average cell area (μm^2) by the number of nuclei from sections of E9.5 embryo heads using the Spot camera software (Spot Diagnostic Instruments, Sterling Heights, MI). Cell density was determined by counting the number of nuclei per 50 μm length of the ectoderm. To analyze the thickness of the retinal placode, 5 equidistant points were marked along the length of the placode and the height of the tissue was measured at those positions.

Imaging. All the brightfield images of the sections were taken by an Olympus BX60

microscope (Olympus, Melville, NY) and Spot camera (Spot Diagnostic Instruments, Sterling Heights, MI). The fluorescent images were taken using an Olympus BX51 with a Spot digital camera.

Results

The optic vesicle thickens to form a retinal placode at the same time the lens placode forms. Our studies on lens placode formation in Chapter 1 showed that the lens surface ectoderm thickens to form a lens placode before it invaginates and suggest that the formation of the lens placode is required for its subsequent invagination. To examine whether the distal optic vesicle, which is going to invaginate at the same time that lens placode does, also thickens before it invaginates, we compared the thickness of the distal optic vesicle at early lens placode stage (Fig.1A) and late lens placode stage (Fig.1B). We found that the thickness of the distal optic vesicle significantly increased along with thickening of the lens placode (Fig.1C), indicating that the retina also forms a placode.

Loss of Pax6 in the surface ectoderm prevents the formation of a retinal placode and optic cup invagination. In Chapter 1 we showed that Pax6 is required for lens placode formation. Loss of Pax6 in the surface ectoderm resulted in the failure of lens placode formation. In addition, we found that Pax6 also acts non cell-autonomously on optic cup formation, since the optic vesicle failed to invaginate in the $Pax6^{SEKO}$ embryos. At E10.5, the wild type embryos and embryos heterozygous for Pax6 in the surface ectoderm

(*Pax6*^{SEHET}) have formed the lens and optic cup (Fig. 2A), although the *Pax6*^{SEHET} embryos have a smaller lens (data not shown). In contrast, in embryos homozygous for Pax6 in the surface ectoderm (*Pax6*^{SEKO}) the optic vesicle failed to invaginate (Fig. 2B). To determine if the retinal placode formed in the *Pax6*^{SEKO} embryos, we measured the thickness of distal optic vesicle at the stage when the lens placode should have already formed. We found that the thickness of distal optic vesicle failed to increase in the *Pax6*^{SEKO} embryos. The distal optic vesicle was also thinner than normal in *Pax6*^{SEHET} embryos (Fig.2C-F), showing that the formation of the retinal placode requires Pax6 in the surface ectoderm and is sensitive to the dose of Pax6. Although the retinal placode was thinner in *Pax6*^{SEHET} embryos, the optic vesicle was still able to invaginate, suggesting that a threshold activity of Pax6 is required for lens and optic cup invagination.

The retinal placode forms and invaginates independent of lens placode invagination.

Since our studies have shown that *Pax6*^{SEKO} embryos failed to form a lens placode and the lens placode failed to invaginate,we determined whether it is the absence of thickening or the absence of invagination of the lens placode that leads to failure of optic vesicle invagination. For these studies we examined the *Bmpr1a*, *Acvr1* double surface ectoderm

knockout (*Bmpr1a; Acvr1*^{DSEKO}) embryos, in which we have shown that a thinner lens placode formed, but failed to invaginate (Rajagopal, Huang et al 2009). We found that in this knockout embryo, the optic vesicle still invaginated and formed an optic cup, although the optic cup was rotated ventrally (Fig. 2A), suggesting that lens placode invagination is not necessary for the invagination of the optic vesicle to form the optic cup. We then examined retinal placode formation in *Bmpr1a;Acvr1*^{DSEKO} embryos. We found that the retinal placode in *Bmpr1a; Acvr1*^{DSEKO} embryos was not significantly thinner than in wild type embryos, suggesting that the retinal placode can form and invaginate, independent of lens invagination.

Together with the analysis on *Pax6*^{SEKO} embryos, our data suggest that lens placode formation, but not its invagination, is essential for the formation and invagination of the retinal placode.

Discussion

This study has shown correlations between, the invagination of the lens placode and optic vesicle, formation of the lens and retinal placode, and the formation of the retinal placode and optic vesicle invagination. When the lens placode formed either fully in wild type or to a lesser extent in *Pax6*^{SEHET} or in *Bmpr1a; Acvr1*^{DSEKO} embryos, the retinal placode always formed and invaginated. However, when the lens placode did not form in *Pax6*^{SEKO} embryos, the retinal placode failed to form and invaginate, suggesting that the lens placode is essential for retinal placode formation and invagination or that some other factor is required for the formation of both placodes. Our results are consistent with previous studies, which have shown optic cup malformation when the lens surface ectoderm cells were eliminated either in chicken or mouse embryos (Hyer, Kuhlman et al. 2003; Zhang, Burgess et al. 2008).

The correlation between lens placode formation and retinal placode formation and invagination is still not clear. Previous investigators suggested that there are signals coming from lens placode to direct the optic vesicle invagination. However, it is also possible that the morphogenesis of lens placode provides a non-signaling (physical or

mechanical) direction for optic vesicle invagination. For example, the secretion of extracellular matrix by the surface ectoderm may restrain the optic vesicle cells in the area of contact between the optic vesicle and the ectoderm. This may cause the crowding and elongation of optic vesicle cells, as it did for lens placode cells. However, since extracellular matrix genes are decreased in expression in the *Bmpr1a;Acvr1*^{DSEKO} embryos to a similar extent as in the *Pax6*^{SEKO} surface ectoderm (data not shown), it makes the function of extracellular matrix on the retinal placode formation more doubtful. In future studies, it will be important to quantify the extent of ECM deposition in wild type, *Pax6*^{SEKO} and *Bmpr1a;Acvr1*^{DSEKO} embryos. One possibility we cannot rule out is that Bmp signaling may function at the top of the signaling cascade that leads to lens placode formation. In this case, deletion of these receptors may not occur early enough to cause defects in extracellular matrix accumulation at the time when the retinal placode forms. Therefore, the knockout may bypass the critical time for retinal placode formation. Earlier deletion of the Bmp receptors, *Bmpr1a* and *;Acvr1* and further analysis of embryos defective in the extracellular matrix defective embryos, such as fibronectin 1 knockout embryos, may help to answer these questions. Microarray analysis on the distal optic vesicle of wild type and *Pax6*^{SEKO} embryos may also help to identify potential transcriptional pathways associated with optic vesicle invagination.

Other mechanisms we have not ruled out to explain lens placode formation, such as cell migration, may be responsible for the retinal placode formation and invagination as well. Techniques of real time recording of morphogenesis, like optical coherence tomography (OCT), will help to test these possibilities.

Although retinal placode formation only occurred when the lens placode formed, its invagination did not require lens placode invagination. The retinal placode could invaginate on its own. However, the mechanism of its invagination is not clear. When the optic vesicle makes close contact with the surface ectoderm, it adheres to the surface ectoderm on its basal side, and thus has a reversed polarity, compared to the surface ectoderm. When it invaginates, it does so in a reverse manner (expanding the apical ends of the cells, instead of contracting them). Since actin filaments are more concentrated on the apical side of the optic vesicle (Fig.4), an apical constriction mechanism, like the one explaining lens placode invagination, can not be applied to the invagination of retinal placode. The retinal placode must employ a different mechanism for its invagination. It is still not clear how this is achieved.

References

Ashery-Padan, R., T. Marquardt, et al. (2000). "Pax6 activity in the lens primordium is required for lens formation and for correct placement of a single retina in the eye." Genes Dev **14**(21): 2701-2711.

Hyer, J., J. Kuhlman, et al. (2003). "Optic cup morphogenesis requires pre-lens ectoderm but not lens differentiation." Dev Biol **259**(2): 351-363.

Rajagopal, R., J. Huang, et al. (2009). "The type I BMP receptors, Bmpr1a and Acvr1, activate multiple signaling pathways to regulate lens formation." Dev Biol **335**(2): 305-316.

Smith, A. N., L. A. Miller, et al. (2005). "The duality of beta-catenin function: a requirement in lens morphogenesis and signaling suppression of lens fate in periocular ectoderm." Dev Biol **285**(2): 477-489.

Zhang, Y., D. Burgess, et al. (2008). "Dominant inhibition of lens placode formation in mice." Dev Biol **323**(1): 53-63.

Figures & Legends

Figure 1.

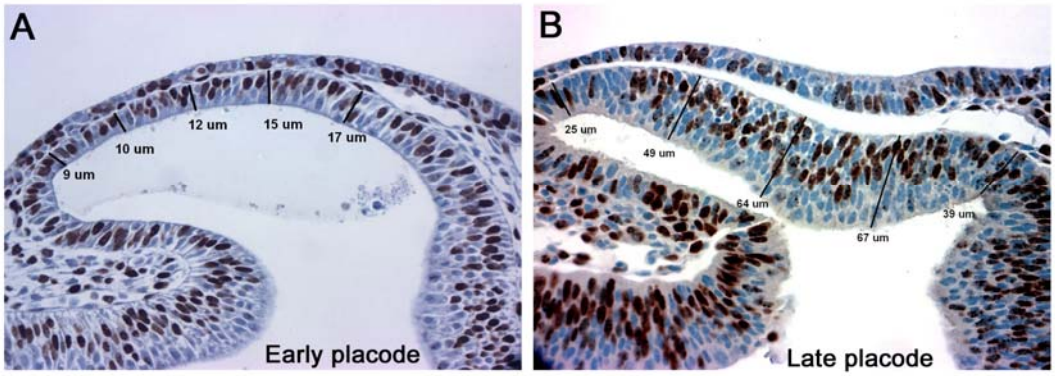

C

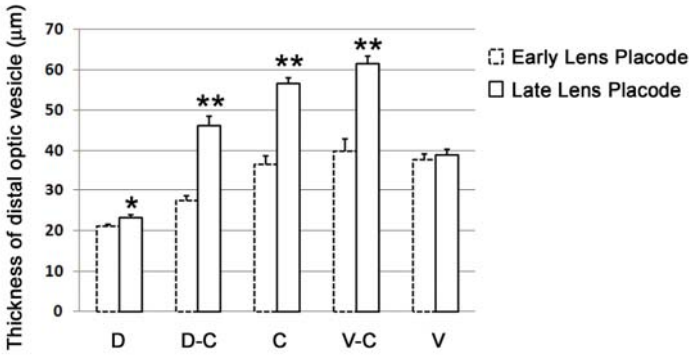

Fig.1 The thickness of the distal optic vesicle during lens placode formation

(A) A frontal section of the developing eye at the early lens placode stage.

(B) A frontal section of the developing eye at the late lens placode stage.

(C) The thickness of distal optic vesicle in wild type embryos at early lens placode stage and late lens placode stage was measured at five positions: D (dorsal), D-C (dorsal-center), C (center), V-C (ventral- center) and V (ventral). The thickness of distal optic

vesicle significantly increased at all locations, except in the ventral optic vesicle during lens placode formation.

Figure 2.

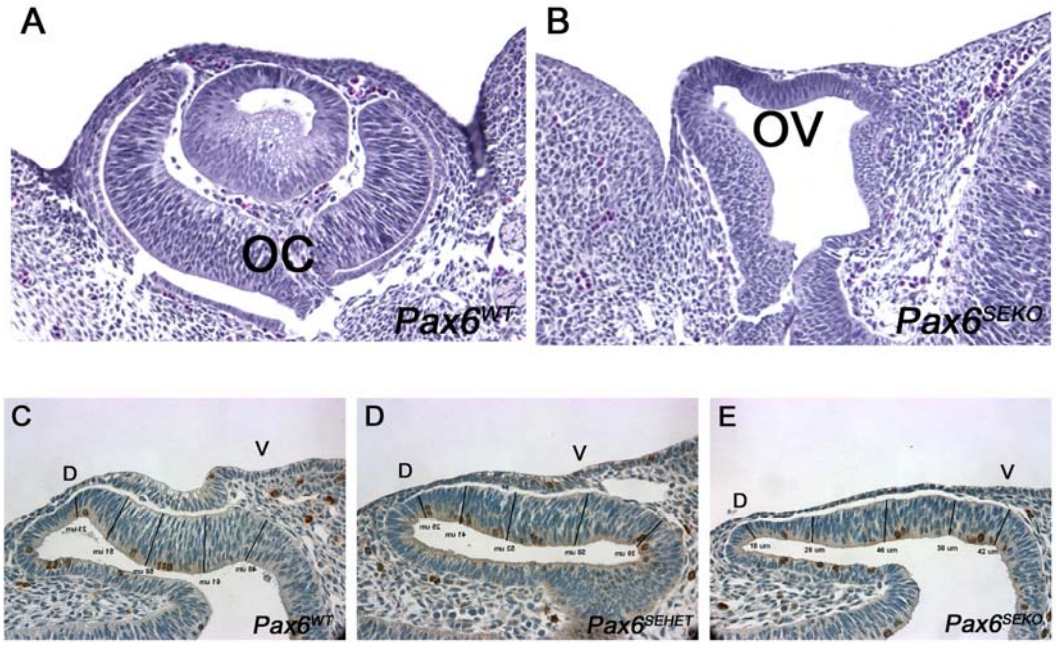

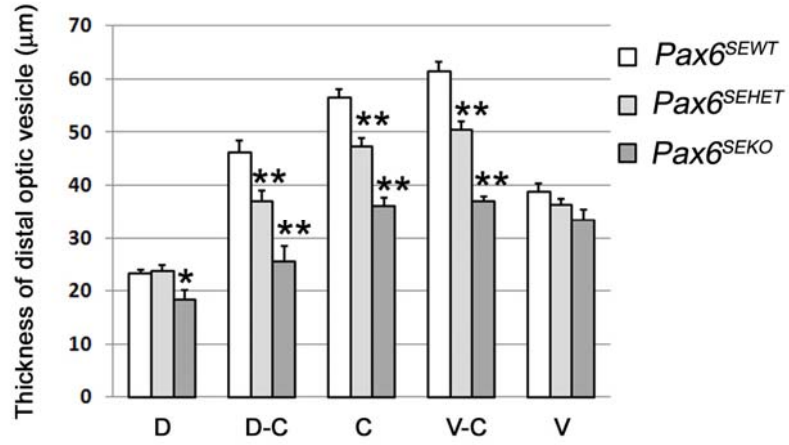

Fig.2 The optic vesicle failed to invaginate in *Pax6*^{SEKO} embryos and retinal placode thickness was regulated by the dose of Pax6 in the surface ectoderm.

(A) The optic vesicle invaginated and formed the optic cup in wild type embryos.

(B) The optic vesicle failed to invaginate, and no optic cup formed in *Pax6*^{SEKO} embryos.

The retinal placode thickness of wild type (*Pax6*^{SEWT}) (C), ectoderm-specific conditional heterozygote (*Pax6*^{SEHET}) (D) and ectoderm-specific conditional knockout (*Pax6*^{SEKO}) embryos (E) was measured at five positions: D (dorsal), D-C (dorsal- center), C (center), V-C (ventral- center) and V (ventral).

(F). In *Pax6*^{SEKO} embryos the retinal placode was significantly thinner than wild type at all locations except for the ventral point. The retinal placode in *Pax6*^{SEHET} embryos placodes was of intermediate thickness.

Figure 3.

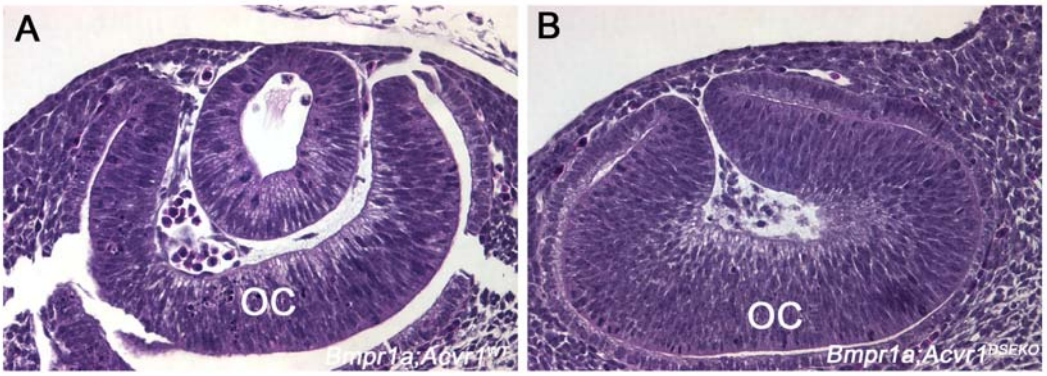

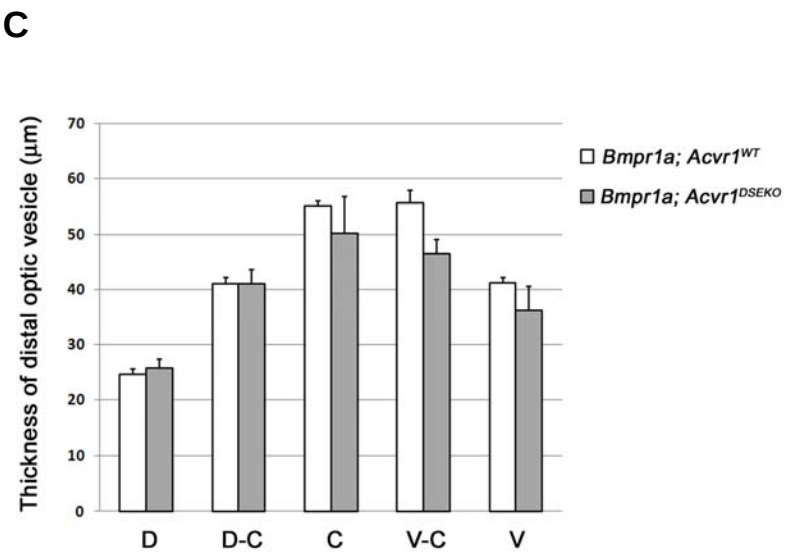

Fig.3 Optic cup formation and retinal placode thickening are independent of lens formation in *Bmpr1a;Acvr1*^{DSEKO} embryos.

(A) Lens and optic cup formation in wild type embryos.

(B) The optic cup formed without the lens in *Bmpr1a;Acvr1*^{DSEKO} embryos.

(C) The retinal placode thickness of wild type (*Bmpr1a;Acvr1*^{WT}), ectoderm-specific conditional knockout (*Bmpr1a;Acvr1*^{DSEKO}) embryos was measured at five positions:

D (dorsal), D-C (dorsal- center), C (center), V-C (ventral- center) and V (ventral). Retinal placode in *Bmpr1a;Acvr1* ^{DSEKO} embryos was not significantly thinner than in wild type embryos at all locations.

Figure 4.

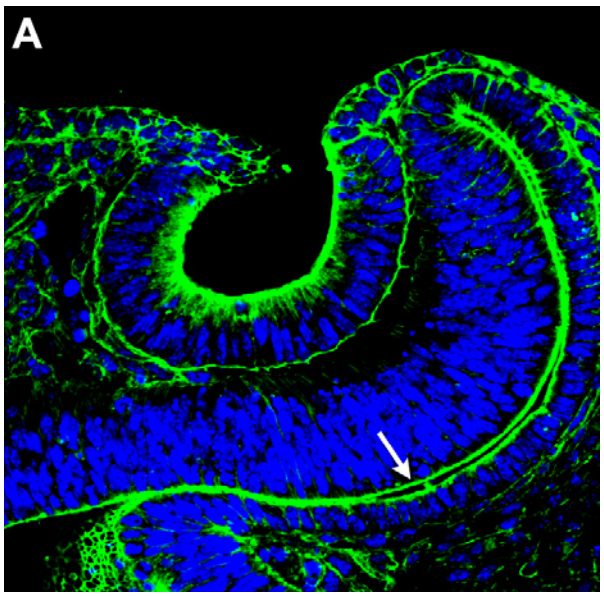

Fig.4 The actin distribution during lens placode and optic vesicle invagination.

A. The phallodin staining showing that the actin filaments are more concentrated on the apical side of the optic vesicle during invagination (white arrow).

Chapter 3 Dmrt (*doublesex* and *mab-3*-Related Transcription Factor) a2 is Required for Early Embryogenesis, and is Regulated by Pax6 in the Lens Placode.

Abstract

Dmrt family members are genes related to the *Drosophila melanogaster doublesex* (*dsx*) and *Caenorhabditis elegans mab-3* genes. They were first identified as genes controlling sexual development. However, recent stuides found out these genes have many functions in various tissues. Our studies on lens placode revealed that one of these family members, Dmrta2, is highly expressed in lens placode and its transcription is regulated by Pax6. In addition, Dmrta2 mRNA and Pax6 protein are colocalized in the olfactory placode and forebrain as well as in the lens placode, suggesting Dmrta2 is a downstream target of Pax6 in these tissues.

Introduction

Dmrt (*doublesex* and *mab-3*-related transcription factor) family is a group of genes related to the *Drosophila melanogaster doublesex* (*dsx*) and *Caenorhabditis elegans mab-3* genes. They encode transcription factors containing a DNA-binding motif known as the DM domain (Raymond, Shamu et al. 1998), and are highly conserved during evolution {reviewed in (Zarkower 2001) and (Volff, Zarkower et al. 2003)}. The Dmrt family proteins were primarily found in the indifferent gonad, and have been shown to be important in sexual development both in vertebrates and invertebrates. For example, mouse Dmrt1 is required for male gonad differentiation. Males homozygous for null mutations of *Dmrt1* are sterile and exhibit a complete loss of germ cells postnatally, disorganized seminiferous tubules, and degeneration of Leydig cells (Raymond, Murphy et al. 2000; Kim, Bardwell et al. 2007). Furthermore, mice mutant in *Dmrta1*(Dmrt4) are viable and fertile but have polyovular follicles (Balciuniene, Bardwell et al. 2006); Mice mutant in *Dmrtc2* (*Dmrt7*) showed infertility with spermatogenic arrest at pachytene stage and abnormal sex chromatin modifications. However, recent findings showed that the members of Dmrt family are also expressed and have functions in other tissues beside the gonad. For example, the Dmrt2, known as terra, is expressed in the somites and is

critical for normal development of somite and somite derivatives (Seo, Wang et al. 2006). Dmrt3 through 7, were also found in the nasal placode, otic placode and brain (Smith, Hurley et al. 2002; Kim, Kettlewell et al. 2003; Huang, Hong et al. 2005; Veith, Schafer et al. 2006). Loss of Dmrt4 impaired neurogenesis in the olfactory epithelium (Huang, Hong et al. 2005). The others have not been studied yet. Interestingly, Dmrta2 (Dmrt5) has been found to be expressed in the lens of Platyfish transiently during early development, suggesting that Dmrta2 may have function in lens development (Veith, Schafer et al. 2006). In this chapter, we will show that the Dmrta2 is expressed in the mouse lens, and is regulated by Pax6 during early lens development. Then we made a conditional knockout of Dmrta2, and will describe the knockout phenotype.

Materials and Methods

Mice. All animals were treated in accordance with the ARVO Statement for the Use of Animals in Ophthalmic and Vision Research and with the approval of the Animal Studies Committee of the Washington University School of Medicine. *Pax6*^{CKO} mice are from the crossing between the *Pax6* $^{fx/fx}$ mice and *Lecre* mice as previously described (Ashery-Padan, Marquardt et al. 2000).

Laser microdissection and microarray analysis. E9.5 or E10.0 embryos were embedded in OCT and snap frozen on dry ice for 10-15min. 10 μm frozen sections were transferred to glass PEN foil slides (Leica Microsystems, #11505189). To avoid the separation of the foil and slides, slides were dipped in 70% ethanol at 4°C for 1 min, washed in RNAase-free water twice for 30 Sec, rinsed in 95% ethanol, and stained in Eosin Y. Stained samples were washed in 95% ethanol and dehydrated in 100% ethanol and xylene. The slides were dried and the lens placode or prospective lens ectoderm was microdissected using a Leica LMD 6000 laser microdissection system. Lens placodes or surface ectoderms from 3 wild type control embryos or 3 *Pax6*^{CKO} embryos are either pooled together or separate as individual samples. RNA was either isolated from pooled sample or from 3 separate samples respectively using a Qiagen RNeasy Microkit

(Qiagen#74004). Each RNA was then amplified into cDNA by using Nugen WT-Ovation™ Pico RNA Amplification System (NuGEN Technologies Inc, #3300-12). cDNA samples obtained from three amplification (either biologically or technically triplicates) were used to probe Illumina Mouse6 bead microarrays . Microarray data were analyzed using Illumina Beadstudio 3.0 software.

Dmrta2 conditional knockout. A full-length construct was retrieved from the BAC vector, bQM 354M19. A neomycin resistance gene flanked by two loxP sites was inserted 487bp downstream of exon1, and another loxP site was inserted at 448bp downstream of Exon2. This construct was introduced into embryonic stem (ES) cells through homologous recombination. The targeted ES clones were initially screened by a probe located 770bp downstream of the construct, the 3'Probe (a 582bp PCR fragment). The ES clones were digested with SpeI, which was added during the construction to the LoxP site downstream of the conditional arm. The resulting hybridization gave a WT fragment of 16.3kb and a correctly targeted fragment of 7.6kb. The positive ES clone was then screened with a probe located 481bp upstream of the 5' homology arm, the 5' Probe (a 399bp PCR fragment). The ES clones were digested with HindIII and the resulting hybridization yielded a WT fragment of 6.8kb and a correctly targeted fragment of 8.0kb.

The targeted ES cells were then injected into blastocysts, which were then injected into the uterus of a pregnant female. The chimeric offspring were screened by PCR.

Primers for genotyping are:

Forward: 5'-CATTTAGCTGGGCCTTCTCC-3'

Reverse: 5'-GAGAGA AACGGAGCCAGAGC-3'

The target allele should give a 350bp PCR product, and the wild type allele should give a 254bp PCR product.

The chimeric offspring carrying the target allele was either intercrossed, or crossed with Sox2Cre to get the animal carrying one null allele (Hayashi, Lewis et al. 2002). The animal having one null allele and one wild type allele are then intercorssed to make double null allele.

Immunostaining on paraffin sections. Embryos were fixed as described above, embedded in 5 % agarose, processed and embedded in paraffin and sectioned 4 μm. For morphological studies, sections were stained with hematoxylin and eosin (Surgipath,

Richmond, IL). For antibody staining, the slices were deparaffinized and rehydrated. Endogenous peroxidase activity was inactivated with 3% H_2O_2 in methanol for 30 min at room temperature for those samples that would be treated for horseradish peroxidase (HRP). Epitope retrieval was performed in 0.01 M citrate buffer (pH 6.0) by placing the slides in a pressure cooker for 3 min. Slides were then incubated in blocking solution containing 20% inactivated normal donkey serum for 30 min at room temperature followed by incubation in primary antibodies overnight at 4° C. Slides were then incubated for 1 hr at room temperature either with Alexa-Fluor-labeled secondary antibodies (Molecular Probes, Eugene, OR) or biotinylated secondary antibodies (Vector Laboratories, Burlingame, CA). Slides incubated with biotinylated secondary antibodies were treated with the ABC-peroxidase reagent from Vectastain Elite ABC Kit (Vector Laboratories, Burlingame, CA) followed by treatment with diaminobenzidine (Dabrowski and Alwine) (Sigma, St. Louis, MO) and H_20_2. The slides were washed with PBS, and counterstained with hematoxylin (Surgipath, Richmond, IL).

In situ hybridization on frozen sections. Frozen sections were fixed in 4% paraformaldehyde/PBS, treated with proteinase K (10 μg/ml), post-fixed in 4% paraformaldehyde/PBS and acetylated in triethanolamine-acetic anhydride solution.

Samples were pre-hybridized in 50% formamide, 5×SSC, 5 mM EDTA, 1×Denhardt's, 100 ug/ml heparin, 0.3 mg/ml yeast tRNA and 0.1% Tween-20, incubated in the same solution with riboprobes overnight, washed with 0.2×SSC, blocked in 10% lamb serum and incubated with anti-digoxigenin antibody overnight. The color reaction was developed using NBT and BCIP in the dark. After the reaction was completed, the slides were washed in PBS, fixed in 4% paraformaldehyde/PBS and mounted in 100% glycerol. Digoxigenin-labeled riboprobes were synthesized from cDNA generated from RNA isolated from wild-type E9.5 embryos using the following PCR primer pairs:

Dmrta2: 5’-gttgcggtatttgtcgctctc-3’

5’-cactcacccgacgctctattc-3’

Results

Dmrta2 co-localized with Pax6, and was regulated by Pax6. Previous studies have shown that Dmrt family members are expressed in brain, olfactory placode and otic placode, in addition to the gonad (Smith, Hurley et al. 2002; Kim, Kettlewell et al. 2003; Huang, Hong et al. 2005; Veith, Schafer et al. 2006). Our microarray data found that Dmrta2 is also expressed in the lens placode. Microarray analysis suggested that Dmrta2 (Dmrt5) gene expression is high in lens placode, compared with other Dmrt family members, such as Dmrt3, a1, c1a (Table 1). Other members of the Dmrt family are not detectable in lens placode. Interestingly, Dmrta2 expression in the lens placode was significantly decreased in $Pax6^{CKO}$ surface ectoderm suggesting that Pax6 regulates Dmrta2 in the lens placode.

To confirm the microarray data, we performed double staining for Dmrta2 mRNA and Pax6 protein. The results showed that, in the eye area, the lens expresses Dmrta2 at relatively high level, while the optic cup shows a lower level of Dmrta2 expression (Fig.1A). Outside the eye area, Dmrta2 expression was found in the olfactory placode and forebrain (Fig. 1C). In all of these area, the Pax6 protein co-localized with Dmrta2

(Fig.1B,D). Furthermore, in *Pax6*^{CKO} embryos, the expression of Dmrta2 decreased in the presumptive lens surface ectoderm (Fig.1E, F), confirming that Pax6 regulates Dmrta2 expression in lens placode.

Loss of Dmrta2 causes early embryonic lethality. To study the function of Dmrta2, we generated a conditional allele of *Dmrta2*, in which a neomycin resistance gene flanked by two loxP sites 487bp downstream of exon1. Another loxP site was inserted at 448bp downstream of exon2 (Fig.2). One of the chimeric mice successfully gave germline transmission. However, animals homozygous for the conditional allele have not been found, either in the offspring or in embryos after E7.5, while animals heterozygous for the conditional allele are viable. This result suggested that insertion of neomycin cassette into Dmrta2 locus disrupted the function of Dmrta2, and animals that are homozygous for the insertion are functionally null, resulting in early embryonic lethality or implantation defects (although "empty" implantation sites were present at E7.5. However, the early embryonic lethality or implantation defects could result from the disruption of other genes close to Dmrta2 locus by the insertion of neomycin cassette. Therefore, to examine whether the insertion of neomycin cassette disrupted Dmrta2 gene or other genes, we crossed the chimeric offspring with Sox2Cre animals to get a Dmrta2 null animals. Again

the animals homozygous for the null allele have not been found in the offspring, suggesting that loss of Dmrta2 lead to embryonic lethality.

Discussion

This study found that Dmrt family members are expressed in the lens placode. One of the family members, Dmrta2 is highly expressed, and its expression in the lens placode is consistently regulated by Pax6 in four microarray analyses and by in situ hybridization. Although it is strange that a gene related to the sexual development is expressed in the lens placode, this is not the first such case. Mab21l1, another gene related to this family ("mab" stands for "male abnormal," was discovered in lens placode, where its expression is regulated by Pax6, as well. In *Mab21l1* mutant embryos, the lens placode thickened less and was narrower than in the *Mab21l1* hemizygous embryos, and the cell proliferation was reduced, suggesting that Mab21l1 has a cell-autonomous role in lens placode formation (Yamada, Mizutani-Koseki et al. 2003) .

To examine the role of Dmrta2, we generated a targeted allele of Dmrta2. However, it seems that the insertion of neo cassette into Dmrta2 locus inactivated Dmrta2, since homozygosity for the mutation resulted in early embryonic lethality, or an implantation defect. In the future studies, the neo cassette will be removed from ES cell by Cre transfection, and we will screen for the new targeted allele in chimeric mice. Once we

have successfully transmitted the target allele to germline, we will start to look at the function of Dmrta2 in both early and late lens development.

Reference

Ashery-Padan, R., T. Marquardt, et al. (2000). "Pax6 activity in the lens primordium is required for lens formation and for correct placement of a single retina in the eye." Genes Dev **14**(21): 2701-2711.

Balciuniene, J., V. J. Bardwell, et al. (2006). "Mice mutant in the DM domain gene Dmrt4 are viable and fertile but have polyovular follicles." Mol Cell Biol **26**(23): 8984-8991.

Hayashi, S., P. Lewis, et al. (2002). "Efficient gene modulation in mouse epiblast using a Sox2Cre transgenic mouse strain." Gene Expr Patterns **2**(1-2): 93-97.

Huang, X., C. S. Hong, et al. (2005). "The doublesex-related gene, XDmrt4, is required for neurogenesis in the olfactory system." Proc Natl Acad Sci U S A **102**(32): 11349-11354.

Kim, S., J. R. Kettlewell, et al. (2003). "Sexually dimorphic expression of multiple doublesex-related genes in the embryonic mouse gonad." Gene Expr Patterns **3**(1): 77-82.

Raymond, C. S., M. W. Murphy, et al. (2000). "Dmrt1, a gene related to worm and fly sexual regulators, is required for mammalian testis differentiation." Genes Dev

14(20): 2587-2595.

Raymond, C. S., C. E. Shamu, et al. (1998). "Evidence for evolutionary conservation of sex-determining genes." Nature **391**(6668): 691-695.

Seo, K. W., Y. Wang, et al. (2006). "Targeted disruption of the DM domain containing transcription factor Dmrt2 reveals an essential role in somite patterning." Dev Biol **290**(1): 200-210.

Smith, C. A., T. M. Hurley, et al. (2002). "Restricted expression of DMRT3 in chicken and mouse embryos." Gene Expr Patterns **2**(1-2): 69-72.

Veith, A. M., M. Schafer, et al. (2006). "Tissue-specific expression of dmrt genes in embryos and adults of the platyfish Xiphophorus maculatus." Zebrafish **3**(3): 325-337.

Volff, J. N., D. Zarkower, et al. (2003). "Evolutionary dynamics of the DM domain gene family in metazoans." J Mol Evol **57 Suppl 1**: S241-249.

Yamada, R., Y. Mizutani-Koseki, et al. (2003). "Cell-autonomous involvement of Mab2l1 is essential for lens placode development." Development **130**(9): 1759-1770.

Zarkower, D. (2001). "Establishing sexual dimorphism: conservation amidst diversity?" Nat Rev Genet **2**(3): 175-185.

Table

Table 1. Gene expression of Dmrt family members in lens placode

Gene*	WT avg.	KO avg.	Fold change	**P value
Dmrt3	37.35	55.75	1.49	>0.5
Dmrta1	65.25	124.89	1.91	>0.5
Dmrta2	**2932.12**	**1094.72**	**0.37**	**<0.001**
Dmrtc1a	11.74	-3.42	-0.29	>0.5

*Genes that have the detection p values of 2out of 3 samples more than 0.05 are not listed.

**P value is calculated from a t-test with tails number=2, and types number=3.

Figures & Legends

Figure 1.

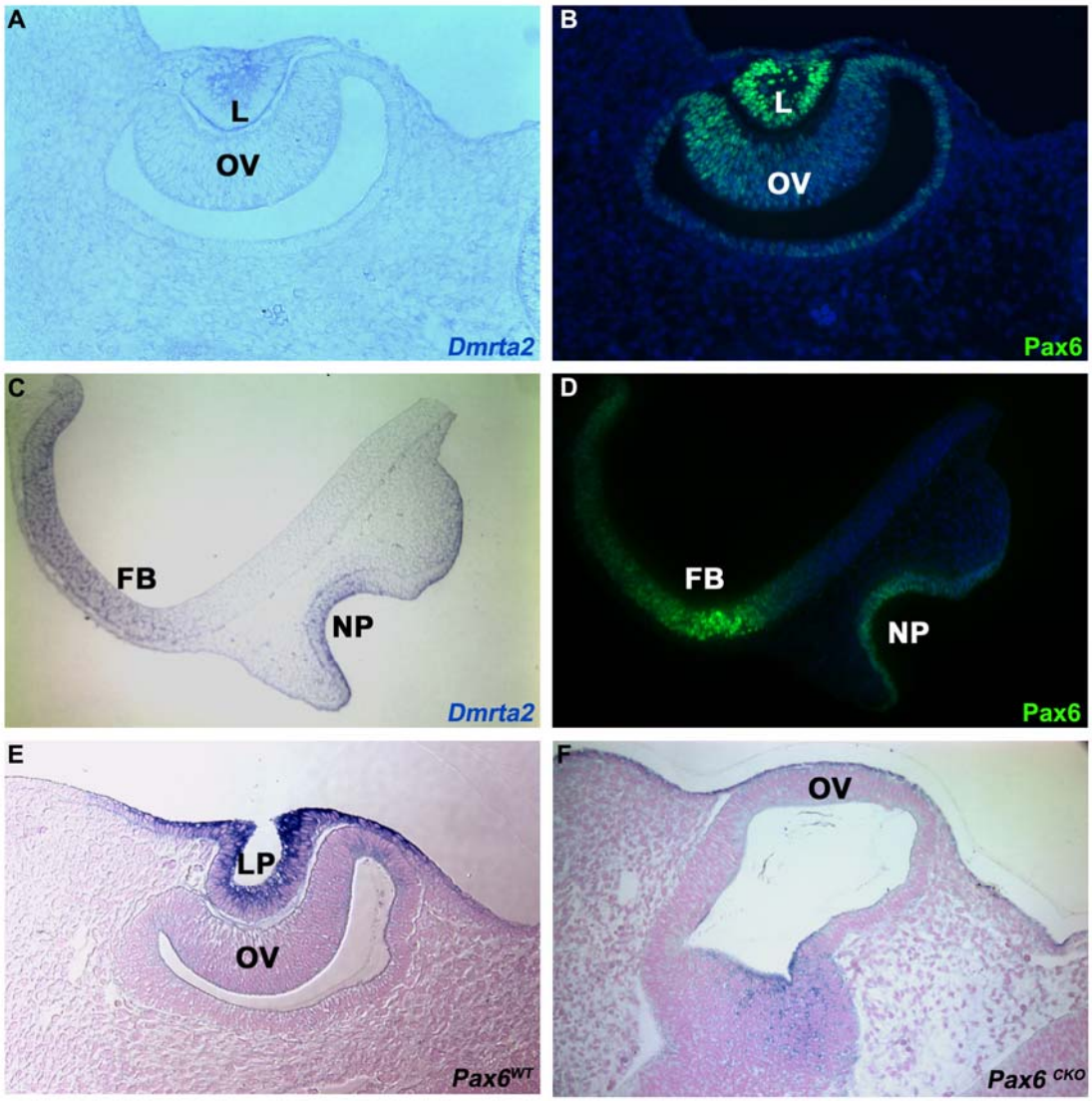

Fig.1 The expression of Dmrta2 is co-localized with Pax6 and is regulated by Pax6 in the lens.

A. Dmrta2 expression was found in the lens pit and optic cup at early developmental stage.

B. Pax6 expression was co-localized with Dmrta2 in the lens pit and optic cup.

C. Dmrta2 expression was found in the olfactory placode and forebrain at early developmental stage.

D. Pax6 expression was co-localized with Dmrta2 in the olfactory placode and forebrain.

E, F. Dmrta2 expression was regulated by Pax6 in the lens-forming ectoderm.

Figure 2.

A

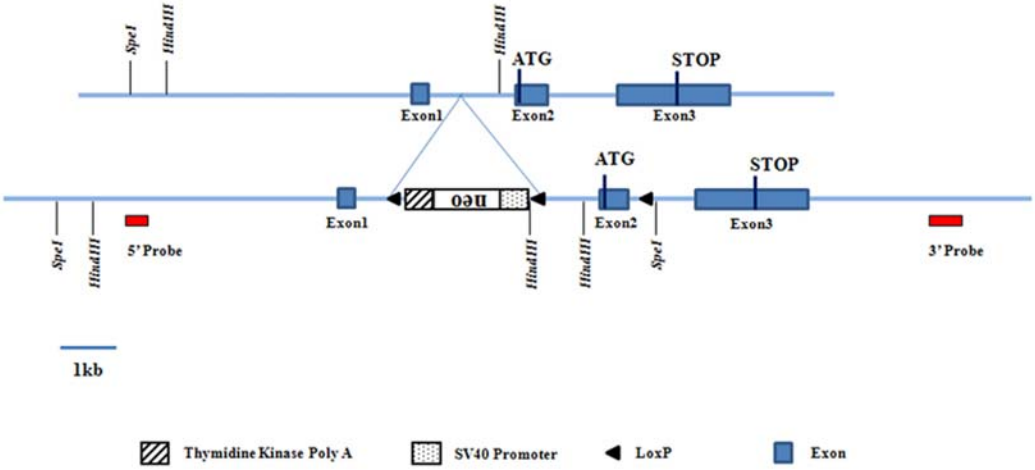

B

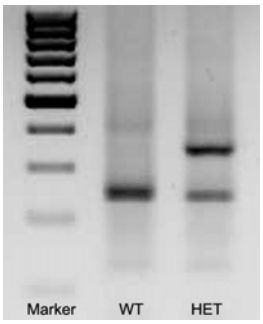

Fig.2 The construct to make a conditional knockout of Dmrta2 and Dmrta2 genotyping.

A. To knockout the essential exon 2 containing the start codon of Dmrta2, one neo cassette flanked by two LoxP sites were inserted into the site that is ~ 1kb upstream of

the exon2, another loxP site inserted into the site that is ~1kb downstream of the exon2.

B. Genotyping of Dmrta2 wild type and heterozygous mice

Chapter 4 Pax6 Selectively Regulated Crystallin Expression in Lens Placode

Abstract

Crystallins are water-soluble structural proteins in the lens of the eye. Their main function was believed to increase the refractive index while not obstructing light. Previous studies showed that most crystallins were not expressed until the lens fiber cells differentiated. However, our studies on lens placode revealed that the crystallins, such as Cryba1, Crybb3, Crygc, Crygd, Cryge and Crygn were transcribed in lens placode and their transcriptions were regulated by Pax6.

Introduction

Crystallins are the major water soluble proteins of the lens and contribute to the transparency and refractive properties by a uniform concentration gradient in lens. There are ubiquitous crystallins (α, β and γ-crystallins) that are found in all vertebrate lens and taxon-specific crystallins that are present in selected species. The function of crystallins was first considered to be a structrual protein of the lens. However, recent studies showed that crystallins are more than inanimate building blocks of the transparent lens fiber cells. They also have non-refractive functions as they do in other tissues. For example, α crystallins (Cryaa and Cryab crystallin) are small heat shock proteins, and act as molecular chaperones to prevent protein misfolding and inhibit the denaturation and aggregation of lens proteins (Bhat 2003; Horwitz 2003). They can also bind to β and γ crystallins (Cryba1-4, Crybb1-3 and Cryga-f, n, s), and make the complex soluble and stable (Bours 1996; Goishi, Shimizu et al. 2006). Interestingly, α crystallin has also been shown to have a role in the nucleus, which was supported by the finding that a subset of lens epithelial in *Cryab* knockout mice showed hyperproliferation and genomic instability. Cryab also prevent stress and provide thermotolerance in numerous tissues.

Taxon-specific soluble proteins that are more related to metabolic enzymes such as

glutathione S-transferase and aldehyde dehydrogenase (Wistow 1993; Tomarev and Piatigorsky 1996). In contrast, β and γ crystallins appear to have a distant relationship to other proteins (Wistow 1993), and their function is still not clear. Because most if not all crystallins appear to be multifunctional proteins, mutations in these proteins have been shown to result in cataracts both in humans and in animals (Russell, Smith et al. 1979; Garner, Garner et al. 1981; Lubsen, Renwick et al. 1987; Litt, Carrero-Valenzuela et al. 1997; Berry, Francis et al. 2001; Bateman, von-Bischhoffshaunsen et al. 2007; Richter, Flodman et al. 2008).

Although crystallins are highly diversified, they have been derived from duplication(s). For example, the α crystallin gene duplication occurred at least 500 million years ago (de Jong, Leunissen et al. 1993). β and γ crystallins are related and clustered by multiple duplication of a common ancestral sequence (Inana, Piatigorsky et al. 1983; Breitman, Lok et al. 1984; Aarts, Den Dunnen et al. 1987; Aarts, Jacobs et al. 1989). However, in spite of their clustering, crystallins either within or between the same classes have distinct expression both spatially and temporally. Previous studies showed that, in mouse embryos, the *Cryab* were the first to be expressed in lens placode, followed by *Cryaa* at the transition from lens pit to lens vesicle (Robinson and Overbeek

1996). β and γ crystallins were only found in the subsequent developing lens (Goring, Breitman et al. 1992; Xiao, Liu et al. 2006). However, the approaches in the early studies, such as the northern blot might be not sensitive enough to detect the small amount of transcription of crystallins, and the lack of specific antibodies for the highly homologous crystallins make it unclear whether the specific type of crystallins are translated. Therefore the expression of crystallin genes need to be examined carefully.

Recent studies on crystallin expression revealed many signaling pathways and transcription factors responsible for the spatial and temporal pattern of crystallin genes expression. Fgf and Bmp signaling pathways are essential for crystalline expression (Faber, Robinson et al. 2002; Zhao, Yang et al. 2008; Rajagopal, Huang et al. 2009). Transcription factors, such as Pax6, Maf, Prox1 and Sox1, are well known regulators of crystalline genes expression. These transcription factors can be either synergistic or antagonistic (Nishiguchi, Wood et al. 1998; Ring, Cordes et al. 2000; Yang, Chauhan et al. 2004; Yang and Cvekl 2005; Yang, Stopka et al. 2006). Some of these transcription factors even have a dual role, acting as both an activator and a repressor of crystallin expression (Duncan et al., 1998). For example, studies on Pax6 have shown that Pax6 activates the promoters of *Cryaa* and *Cryab*, however, represses the promoter of *Crybb1*

and *Cryge/f* in cotransfection tests (Duncan, Haynes et al. 1998; Cvekl, Yang et al. 2004; Yang, Chauhan et al. 2004). However, most of these experiments are in vitro. Therefore, more examination in vivo is required for certainty. In this study, we showed that Cryab, Cryba1, Crybb3, Crygc, Crygd, Cryge and Crygn are expressed in lens placode, and the transcription of *β*B3, γC and γE crystallins are regulated by Pax6.

Material and Methods

Mice. All animals were treated in accordance with the ARVO Statement for the Use of Animals in Ophthalmic and Vision Research and with the approval of the Animal Studies Committee of the Washington University School of Medicine. *Pax6*^{CKO} mice are from the crossing between the *Pax6*$^{fx/fx}$ mice and *Lecre* mice as previously described (Ashery-Padan, Marquardt et al. 2000).

Laser microdissection and microarray analysis. E9.5 or E10.0 embryos were embedded in OCT and snap frozen on dry ice for 10-15min. 10 μm frozen sections were transferred to glass PEN foil slides (Leica Microsystems, Cat#11505189). To avoid the separation of the foil and slides, slides were dipped in 70% ethanol at 4°C for 1 min, washed in RNAase-free water twice for 30 Sec, rinsed in 95% ethanol, and stained in Eosin Y. Stained samples were washed in 95% ethanol and dehydrated in 100% ethanol and xylene. The slides were dried and the lens placode or prospective lens ectoderm was microdissected using a Leica LMD 6000 laser microdissection system. Lens placodes or surface ectoderms from 3 wild type control embryos or 3 *Pax6*^{CKO} embryos are pooled together and extracted RNA respectively using a Qiagen RNeasy Microkit (Qiagen#74004). Each RNA was then amplified into cDNA by using Nugen WT-Ovation™ Pico

RNA Amplification System (NuGEN Technologies Inc, #3300-12). cDNA samples obtained from three amplification (technically triplicates) were used to probe Illumina Mouse6 bead microarrays . Microarray data were analyzed using Illumina Beadstudio 3.0 software.

Quantitative Real-time PCR (qRT-PCR). qRT-PCR was performed using a CFX96™ real time PCR detection system (BioRad, Hercules, CA), selected gene primers, cDNA template and SYBR Green JumpStart™ *Taq* ReadyMix™ (Sigma, St. Louis, MO) under the following conditions: 95 °C for 3 min, followed by 40 cycles of 95 °C for 10 s, 55 °C for 10 s and 72 °C for 30 s. All reactions were performed in triplicate. β-Actin and GAPDH was included in each assay as a loading control. Primer pairs were designed using Oligo Analysis software (Integrated DNA Technologies, Inc., Coraville, IA). The primer sequences and the length of the corresponding amplified products are shown in Table 2. For each gene, the qRT-PCR experiments were repeated three times with the same cDNAs. Changes (*x*-fold) in gene expression level were calculated by the $2^{\Delta\Delta ct}$ method. Statistical analysis was performed using Excel software (Microsoft, Cupertino, WA).

Results

Previous studies showed that crystallins are generally fiber cell differentiation markers, and will not express until fiber cells exit the cell cycle and receive the signal to differentiate (Goring, Breitman et al. 1992; Xiao, Liu et al. 2006). Only Cryab was found in the lens placode and was considered to be the first crystallin to be expressed (Robinson and Overbeek 1996). However, we found from microarray analysis on differential expressed genes in the lens placode of wild type and $Pax6^{CKO}$ embryos that not only Cryab is expressed in the lens placode, but Cryba1, Crybb3, Crygc, Crygd, Cryge and Crygn are expressed in lens placode at relatively high level (average signal higher than 30). In contrast, Cryba4, Crybb2, Crygc, Crygf and Crygs are expressed, if at all, at relatively low level (average signal higher than 0 but lower than 30), while the level of Cryaa, Cryba2, Crybb1, Cryga, Crygd expression are non-detectable (average signal lower than 0) (Table 1). This is the first evidence that β and γ crystallin expression preceeds fiber cell differentiation.

In addition, the mRNA level of Crybb3, Crygd and Cryge was significantly decreased in $Pax6^{CKO}$ surface ectoderm. Our previous studies of microarrays also

suggested that Crygc maybe another potential target of Pax6. In contrast, the rest of the crystallin genes expressed in lens placode are not changed, including previously proved Pax6- activated gene *Cryab*, and Pax6- repressed gene, *Crygf* (Duncan, Haynes et al. 1998; Cvekl, Yang et al. 2004; Yang, Chauhan et al. 2004) .

In order to confirm the microarray data, we performed quantitive real time PCR (qRT-PCR) for some of the crystallins. We examined the expression of *Crybb3* and *Crygc*, as they are decreased in the $Pax6^{CKO}$ surface ectoderm, and Cryab as a known target of Pax6. Our results of qRT-PCR showed that the expression of Crybb3 and Crygc were significantly decreased in $Pax6^{CKO}$ surface ectoderm to an extent much higher than we saw in microarray results, suggesting the qRT-PCR is a more sensitive way to quantify transcript levels. In addition, we found the expression of Cryba1 is not detectable at all in $Pax6^{CKO}$ surface ectoderm, while it is detectable in wild type lens placode (data not shown) suggesting that Cryba1 is another candidate genes regulated by Pax6. However, to our surprise, we could not find any change in Cryab transcription, suggesting that Pax6 did not regulate Cryab at this stage (Fig.1).

Discussion

This study showed that the lens placode expresses a variety of crystallins, including Cryba1, Crybb3, Crygc, Crygd, Cryge and Crygn, which were previously thought only expressed at later stage when lens fiber cells begin to differentiate. This result also showed that although many of the crystallin genes are clustered, their expression patterns are not always associated.

We also showed that Pax6 regulated the expression of Crybb3 and Crygc. However, we were not able to confirm that *Cryab* is activated by Pax6, or *Cryge/f* is repressed by Pax6, as suggested in previous studies. Our result is more consistent with the finding that *Cryab* expression was maintained in the lens that has *Pax6* deleted at a later stage (Shaham, Smith et al. 2009), suggesting that *Pax6* may be not required for *Cryab* expression at both stages.

Although we have shown that crystallin mRNAs are present in the lens placode, we are not able to prove these crystallins are translated, since the antibodies for crystallins are not subtype specific. In the future studies, we would like to examine if the crystallin

protein is being translated by performing experiments, such as sucrose gradient centrifugation to separate the non-translating (nonpolysomal) or potentially translating (polysomal) mRNA and look at whether the crystallin mRNA is being translated. If they are translated, it will be interesting to examine their functions in lens placodes.

Reference

Aarts, H. J., J. T. Den Dunnen, et al. (1987). "Linkage between the beta B2 and beta B3 crystallin genes in man and rat: a remnant of an ancient beta-crystallin gene cluster." Gene **59**(1): 127-135.

Aarts, H. J., E. H. Jacobs, et al. (1989). "Different evolution rates within the lens-specific beta-crystallin gene family." J Mol Evol **28**(4): 313-321.

Ashery-Padan, R., T. Marquardt, et al. (2000). "Pax6 activity in the lens primordium is required for lens formation and for correct placement of a single retina in the eye." Genes Dev **14**(21): 2701-2711.

Bateman, J. B., F. R. von-Bischhoffshaunsen, et al. (2007). "Gene conversion mutation in crystallin, beta-B2 (CRYBB2) in a Chilean family with autosomal dominant cataract." Ophthalmology **114**(3): 425-432.

Berry, V., P. Francis, et al. (2001). "Alpha-B crystallin gene (CRYAB) mutation causes dominant congenital posterior polar cataract in humans." Am J Hum Genet **69**(5): 1141-1145.

Bhat, S. P. (2003). "Crystallins, genes and cataract." Prog Drug Res **60**: 205-262.

Bours, J. (1996). "Calf lens alpha-crystallin, a molecular chaperone, builds stable

complexes with beta s- and gamma-crystallins." Ophthalmic Res **28 Suppl 1**: 23-31.

Breitman, M. L., S. Lok, et al. (1984). "Gamma-crystallin family of the mouse lens: structural and evolutionary relationships." Proc Natl Acad Sci U S A **81**(24): 7762-7766.

Cvekl, A., Y. Yang, et al. (2004). "Regulation of gene expression by Pax6 in ocular cells: a case of tissue-preferred expression of crystallins in lens." Int J Dev Biol **48**(8-9): 829-844.

de Jong, W. W., J. A. Leunissen, et al. (1993). "Evolution of the alpha-crystallin/small heat-shock protein family." Mol Biol Evol **10**(1): 103-126.

Duncan, M. K., J. I. Haynes, 2nd, et al. (1998). "Dual roles for Pax-6: a transcriptional repressor of lens fiber cell-specific beta-crystallin genes." Mol Cell Biol **18**(9): 5579-5586.

Faber, S. C., M. L. Robinson, et al. (2002). "Bmp signaling is required for development of primary lens fiber cells." Development **129**(15): 3727-3737.

Garner, W. H., M. H. Garner, et al. (1981). "Gamma-crystallin, a major cytoplasmic polypeptide disulfide linked to membrane proteins in human cataract." Biochem Biophys Res Commun **98**(2): 439-447.

Goishi, K., A. Shimizu, et al. (2006). "AlphaA-crystallin expression prevents gamma-crystallin insolubility and cataract formation in the zebrafish cloche mutant lens." Development **133**(13): 2585-2593.

Goring, D. R., M. L. Breitman, et al. (1992). "Temporal regulation of six crystallin transcripts during mouse lens development." Exp Eye Res **54**(5): 785-795.

Horwitz, J. (2003). "Alpha-crystallin." Exp Eye Res **76**(2): 145-153.

Inana, G., J. Piatigorsky, et al. (1983). "Gene and protein structure of a beta-crystallin polypeptide in murine lens: relationship of exons and structural motifs." Nature **302**(5906): 310-315.

Litt, M., R. Carrero-Valenzuela, et al. (1997). "Autosomal dominant cerulean cataract is associated with a chain termination mutation in the human beta-crystallin gene CRYBB2." Hum Mol Genet **6**(5): 665-668.

Lubsen, N. H., J. H. Renwick, et al. (1987). "A locus for a human hereditary cataract is closely linked to the gamma-crystallin gene family." Proc Natl Acad Sci U S A **84**(2): 489-492.

Nishiguchi, S., H. Wood, et al. (1998). "Sox1 directly regulates the gamma-crystallin genes and is essential for lens development in mice." Genes Dev **12**(6): 776-781.

Rajagopal, R., J. Huang, et al. (2009). "The type I BMP receptors, Bmpr1a and Acvr1,

activate multiple signaling pathways to regulate lens formation." Dev Biol **335**(2): 305-316.

Richter, L., P. Flodman, et al. (2008). "Clinical variability of autosomal dominant cataract, microcornea and corneal opacity and novel mutation in the alpha A crystallin gene (CRYAA)." Am J Med Genet A **146**(7): 833-842.

Ring, B. Z., S. P. Cordes, et al. (2000). "Regulation of mouse lens fiber cell development and differentiation by the Maf gene." Development **127**(2): 307-317.

Robinson, M. L. and P. A. Overbeek (1996). "Differential expression of alpha A- and alpha B-crystallin during murine ocular development." Invest Ophthalmol Vis Sci **37**(11): 2276-2284.

Russell, P., S. G. Smith, et al. (1979). "Age and cataract-related changes in the heavy molecular weight proteins and gamma crystallin composition of the mouse lens." Exp Eye Res **29**(3): 245-255.

Shaham, O., A. N. Smith, et al. (2009). "Pax6 is essential for lens fiber cell differentiation." Development **136**(15): 2567-2578.

Tomarev, S. I. and J. Piatigorsky (1996). "Lens crystallins of invertebrates--diversity and recruitment from detoxification enzymes and novel proteins." Eur J Biochem **235**(3): 449-465.

Wistow, G. (1993). "Lens crystallins: gene recruitment and evolutionary dynamism." Trends Biochem Sci **18**(8): 301-306.

Xiao, W., W. Liu, et al. (2006). "Gene expression profiling in embryonic mouse lenses." Mol Vis **12**: 1692-1698.

Yang, Y., B. K. Chauhan, et al. (2004). "Transcriptional regulation of mouse alphaB- and gammaF-crystallin genes in lens: opposite promoter-specific interactions between Pax6 and large Maf transcription factors." J Mol Biol **344**(2): 351-368.

Yang, Y. and A. Cvekl (2005). "Tissue-specific regulation of the mouse alphaA-crystallin gene in lens via recruitment of Pax6 and c-Maf to its promoter." J Mol Biol **351**(3): 453-469.

Yang, Y., T. Stopka, et al. (2006). "Regulation of alphaA-crystallin via Pax6, c-Maf, CREB and a broad domain of lens-specific chromatin." EMBO J **25**(10): 2107-2118.

Zhao, H., T. Yang, et al. (2008). "Fibroblast growth factor receptor signaling is essential for lens fiber cell differentiation." Dev Biol **318**(2): 276-288.

Tables

Table.1 Crystallin genes expression in lens placode

Gene	WT avg.	KO avg.	Fold change	*P value
Cryaa	N/D	N/D	N/A	N/A
Cryab	37.29	22.62	0.61	>0.05
Cryba1[1]	52.81	54.92	1.04	>0.05
Cryba1[2]	63.78	55.56	0.87	>0.05
Cryba2	ND	ND	N/A	N/A
Cryba4	24.46	21.06	0.86	>0.05
Crybb1	N/D	N/D	N/A	N/A
Crybb2	N/D	N/D	N/A	N/A
Crybb3[1]	55.88	12.73	0.23	>0.05
Crybb3[2]	**76.56**	**-6.39**	**-0.08**	**<0.01**
Crybb3[3]	**1017.68**	**708.56**	**0.70**	**<0.05**
Cryga	N/D	N/D	N/A	N/A
Crygb	66.47	25.99	0.39	>0.05
Crygc**	**111.18**	**8.66**	**0.08**	**<0.05**
Crygd[1]	85.76	16.92	0.20	<0.05
Cryge	**184.87**	**3.34**	**0.02**	**<0.01**
Crygf	N/D	N/D	N/A	N/A
Crygn[1]	N/D	N/D	N/A	N/A
Crygn[2]	N/D	N/D	N/A	N/A
Crygn[3]	206.75	98.46	0.48	>0.05
Crygs	N/D	N/D	N/A	N/A

N/D: not detectable if the detection p values of 2out of 3 samples are more than 0.05,

N/A: not available

Superscript number after each gene represents the different probe set, *p value is calculated from a t-test with tails number=2, and types number=3.

** From other microarrays

Table 2. The primer sequences for aRT-PCR

Gene	Primer sequence for qRT-PCR
Cryab	Forward:5’-TCCCTGTCATCTGATGGAGTC-3’; Reverse: 5’-CACTGATGGGAAACTTCCTTG-3’
Crybb3	Forward: 5’-GAATTCCGCCACTGGAAC-3’ Reverse:5’-GTGGGCTTTATTGAGCAGGTT-3’
Crygc	Forward : 5’-TACCAGCAGTGGATGGGTTTCAG-3’ Reverse: 5’-CTTGAGGCCTCAGCAGATACTGG-3’

Figures & Legends

Figure 1.

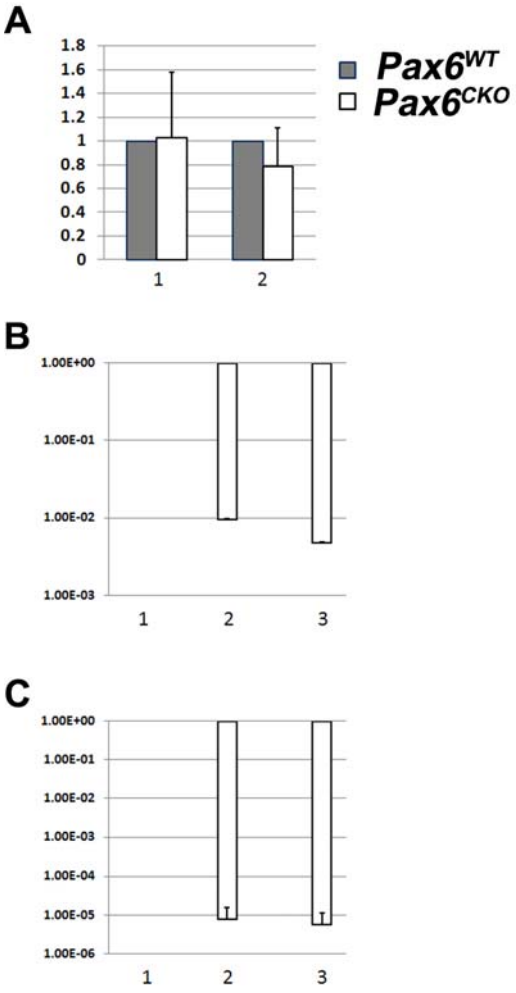

Fig.1 Quantitative real time PCR for crystallin genes expression in the lens placode.

The expression of each gene in wild type lens placode was normalized to 1.

(A) *Cryab* expression is not changed in $Pax6^{CKO}$ surface ectoderm when either normalized with *β-Actin* or *Gapdh*.

(B) *Crybb3* expression is significantly decreased in $Pax6^{CKO}$ surface ectoderm, either

normalized with *β-Actin* (2) or *Gapdh*(3).

(C) Crygc expression is significantly decreased in $Pax6^{CKO}$ surface ectoderm, either normalized with*β-Actin* (2) or *Gapdh* (3).

Chapter 5 Conclusions and Future Directions

The mechanism of lens placode formation.

As a first step toward identifying the mechanism(s) leading to lens placode formation, studies in this dissertation have determined that the lens placode thickening in wild type embryos, although accompanied by a two-fold increase in cell density and a constant contact area between the surface ectoderm and the optic vesicle, was not associated with an increase in cell proliferation, a decrease in the rate of cell death or an increase in cell volume. Then I used $Pax6^{CKO}$ embryos, in which the lens placode fails to form, as a tool to further explore the mechanism of lens placode formation. Microarray analysis revealed that many transcripts encoding extracellular matrix (ECM) components were decreased in the lens-forming surface ectoderm of $Pax6^{CKO}$ embryos. In addition, the contact area between the surface ectoderm and the optic vesicle increased in $Pax6^{CKO}$ embryos and the matrix between these tissues decreased. These observations suggested that the "Restricted Expansion" model (continued proliferation in a restricted area) proposed by Hendrix and Zwaan can explain lens placode formation. Then I tested this hypothesis genetically by decreasing the expression of *Fibronectin1* (*Fn1*), a gene crucial for ECM assembly and accumulation. This would presumably reduce the adhesion between the lens-forming

surface ectoderm and optic vesicle. The lens placode failed to form in *Fn1*-deficient embryos. However, cell proliferation, lens induction and lens differentiation were not affected, and cell death was not increased to a sufficient level to cause the failure of lens placode formation. These results suggest that the failure of lens placode formation in *Fn1*-deficient embryos was due to a reduction of the adhesion between the lens-forming surface ectoderm and optic vesicle, again supporting the "Restricted Expansion" model.

In the *Fn1* knockout embryos, blocking lens placode morphogenesis prevented the placode from invaginating, but did not affect the apical re-localization of the actin cytoskeleton. This suggested that lens placode thickening is required for invagination, possibly by increasing the density of actin filaments in the apical actin web.

Although my results are sufficient to account for lens placode formation they have not ruled out other possibilities to explain placode formation. It remains possible that non-placodal ectoderm cells migrate into the placode region, leading to a local increase in cell density and placode formation. To determine whether peri-placodal cells enter the presumptive placode region during its formation, I may use time lapse imaging in embryos mosaic for GFP to track the movement of individual cells during placode

formation in wild type embryos.

In the "Restricted Expansion" model, sustained proliferation is another key factor for lens placode formation. In future studies, I will perform experiments in which proliferation is blocked to test this hypothesis. Such experiments can be done in vitro or in vivo. Eye development proceeds when embryo heads are cultured from E9.5 to E11.5 in vitro. Proliferation can be blocked by adding aphidicolin, an inhibitor of DNA synthesis (Spadari, Pedrali-Noy et al. 1984). I predict that treatment with aphidicolin will prevent lens placode formation by blocking cell proliferation.

Proliferation may also be blocked in vivo by conditionally deleting the genes regulating proliferation in the surface ectoderm. *Cdc25a-c* phosphatases, which promote cell cycle progression by activating cyclin-dependent protein kinases, are potential targets to knockout in the surface ectoderm. Previous studies suggested that *Cdc25a-c* are required for cell proliferation in embryos and adult mice (Lee, White et al. 2009). Conditionally deleting *Cdc25s* in the lens-forming surface ectoderm should locally reduce the cell proliferation there, allowing me to test the importance of cell proliferation in lens placode formation.

These further analyses will help us better understand the mechanism of lens placode formation and may serve as a guideline for understanding the formation of the other placodes.

The mechanism of retinal placode formation.

Studies in this dissertation have discovered that the distal optic vesicle thickens along with the lens placode formation, suggesting the formation of a "retinal placode." Further analysis on *Pax6*^{SEKO} and *Bmpr1a;Acvr1*^{DSEKO} embryos suggested that the retinal placode formation correlated with optic vesicle invagination. The correlation between lens placode formation and retinal placode formation suggests that these structures may form by a similar mechanism.

To further explore the mechanism of retinal placode formation and the role of lens placode in retinal placode formation and invagination, I will further examine the cell density, proliferation, death and volume in the distal optic vesicle of wild type embryos, *Pax6*^{SEKO} embryos and *Bmpr1a;Acvr1*^{DSEKO} embryos. In addition, the cell movements and the expansion of the contact area between the optic vesicle and the ectoderm in wild type and knockout embryos will be tracked by time-lapse optical coherence microscopy

(OCT), in collaboration with Dr. Larry Taber's laboratory in the Department of Biomedical Engineering.

To determine if the ECM plays a role in retinal placode formation, as it appears to do in lens placode formation, I will further analyze the phenotypes of the *Fn1*-deficient embryos mentioned above by measuring cell density, proliferation, death and volume in the distal optic vesicle. These measurements add to our understanding of how the retinal placode forms and invaginates and the role played by the ECM in these processes.

Dmrta2 is required for early embryogenesis and is regulated by Pax6 in lens placode.

By comparing the transcripts in wild type lens placodes and $Pax6^{CKO}$ surface ectoderm, I identified downstream target genes regulated by Pax6. One of these candidate genes is Dmrta2, which belongs to a family of genes related to sexual differentiation. In situ hybridization and immunostaining showed that *Dmrta2* and Pax6 co-localize in the lens, nasal placode and forebrain, where Pax6 is required for these tissues development (Manuel, Price et. 2005; Quinn, West et al. 1996). Moreover, the expression of Dmrta2 in lens-forming surface ectoderm is reduced in $Pax6^{CKO}$ embryos. This observation

confirmed the microarray results suggesting that Pax6 directly or indirectly regulates the transcription of Dmrta2. To study the role of Dmrta2 in lens development, we made mice carrying a null allele for Dmrta2 gene. However, no homozygous germline knockout embryos have been found at E7.5, indicating that loss of Dmrta2 is early embryonic lethal. We are making a conditional knockout of *Dmrta2*, and will use it to determine the function of this gene in lens development and in the adult lens.

Pax6 selectively regulates the expression of crystallin genes in the lens placode.

Our microarray analysis revealed that several crystallin genes, such as Crybb3, Crygc and Cryge, were transcribed in lens placode, where their expression was regulated by Pax6 and by BMP signaling. This observation was confirmed by in situ hybridization and qRT-PCR, indicating that the crystallin genes are already transcribed at the lens placode stage. However, the crystallin proteins were not detected until the fiber cell differentiation started, suggesting that translational control mechanisms regulate crystallin protein expression. In future studies, I will perform experiments, such as sucrose gradient centrifugation, to examine if crystallin mRNA is located primarily in the non-polysomal fraction, and, therefore, not being translated. These experiments will reveal a novel mechanism of controlling gene expression during lens development.

Reference

Lee, G., L. S. White, et al. (2009). "Response of small intestinal epithelial cells to acute disruption of cell division through CDC25 deletion." Proc Natl Acad Sci U S A **106**(12): 4701-4706.

Manuel, M. and D. J. Price (2005). "Role of Pax6 in forebrain regionalization." Brain Res Bull **66**(4-6): 387-393.

Quinn, J. C., J. D. West, et al. (1996). "Multiple functions for Pax6 in mouse eye and nasal development." Genes Dev **10**(4): 435-446.

Spadari, S., G. Pedrali-Noy, et al. (1984). "Control of DNA replication and cell proliferation in eukaryotes by aphidicolin." Toxicol Pathol **12**(2): 143-148.

Development 136, 1741-1750 (2009) doi:10.1242/dev.034082

FGF-regulated BMP signaling is required for eyelid closure and to specify conjunctival epithelial cell fate

Jie Huang[1], Lisa K. Dattilo[1], Ramya Rajagopal[1], Ying Liu[1], Vesa Kaartinen[3], Yuji Mishina[4], Chu-Xia Deng[5], Lieve Umans[6,7], An Zwijsen[6,7], Anita B. Roberts[8] and David C. Beebe[1,2,*]

There are conflicting reports about whether BMP signaling is required for eyelid closure during fetal development. This question was addressed using mice deficient in BMP or TGFβ signaling in prospective eyelid and conjunctival epithelial cells. Genes encoding two type I BMP receptors, the type II TGFβ receptor, two BMP- or two TGFβ-activated R-Smads or the co-Smad Smad4 were deleted from the ocular surface ectoderm using Cre recombinase. Only mice with deletion of components of the BMP pathway had an 'eyelid open at birth' phenotype. Mice lacking *Fgf10* or *Fgfr2* also have open eyelids at birth. To better understand the pathways that regulate BMP expression and function during eyelid development, we localized BMPs and BMP signaling intermediates in *Fgfr2* and *Smad4* conditional knockout (CKO) mice. We found that Fgfr2 was required for the expression of *Bmp4*, the normal distribution of Shh signaling and for preserving the differentiation of the conjunctival epithelium. FGF signaling also promoted the expression of the Wnt antagonist Sfrp1 and suppressed Wnt signaling in the prospective eyelid epithelial cells, independently of BMP function. Transcripts encoding Foxc1 and Foxc2, which were previously shown to be necessary for eyelid closure, were not detectable in $Smad4^{CKO}$ animals. c-Jun, another key regulator of eyelid closure, was present and phosphorylated in eyelid periderm cells at the time of fusion, but failed to translocate to the nucleus in the absence of BMP function. $Smad4^{CKO}$ mice also showed premature differentiation of the conjunctival epithelium, conjunctival hyperplasia and the acquisition of epidermal characteristics, including formation of an ectopic row of hair follicles in place of the Meibomian glands. A second row of eyelashes is a feature of human lymphedema-distichiasis syndrome, which is associated with mutations in FOXC2.

KEY WORDS: Eyelid closure, Conjunctival cell fate, c-Jun nuclear transport, BMP signaling, FGF signaling, Mouse

INTRODUCTION

Eyelid formation from the surface ectoderm and the underlying periocular mesenchyme involves four processes: eyelid specification, growth, closure and re-opening. In mice, eyelid specification begins by embryonic day (E) 9, when the expression of the transcription factor Foxl2 defines the future location of the eyelids dorsal and ventral to the globe (Swindell et al., 2008). At E11.5, invagination of the dorsal and ventral periocular ectoderm signals the beginning of the period of eyelid growth. The resulting eyelid folds grow towards each other across the surface of the eye between E11.5 and E15.5. At E15.5, a projection of the outer, peridermal layer of the ectoderm extends from the eyelid margins across the cornea until the periderm extensions meet and fuse. The two lids separate at 'eye opening' on about postnatal day 10 (P10) (Findlater et al., 1993).

[1]Department of Ophthalmology and Visual Sciences and [2]Department of Cell Biology and Physiology, Washington University, St Louis, MO 63130, USA. [3]Developmental Biology Program, Childrens Hospital Los Angeles, Departments of Pathology and Surgery, Keck School of Medicine, University of Southern California, Los Angeles, CA 90027, USA. [4]Molecular Developmental Biology Group, Laboratory of Reproductive and Developmental Toxicology, National Institute of Environmental Health Sciences, Research Triangle Park, NC 27709, USA. [5]Genetics of Development and Diseases Branch, National Institute of Diabetes and Digestive and Kidney Diseases, National Institutes of Health, Bethesda, MD 20892, USA. [6]Laboratory Molecular Biology (Celgen), Department for Molecular and Developmental Genetics, VIB, B-3000 Leuven, Belgium. [7]Laboratory Molecular Biology (Celgen), Center for Human Genetics, KU Leuven, B-3000 Leuven, Belgium. [8]Laboratory of Cell Regulation and Carcinogenesis, National Cancer Institute, National Institutes of Health, Bethesda, MD 20892, USA.

*Author for correspondence (e-mail: Beebe@vision.wustl.edu)

Accepted 9 March 2009

The closing eyelids are constituted by a loosely organized mesenchyme and the overlying epithelium. The eyelid epithelium differentiates into the palpebral epidermis (outer surface of the eyelid) and the palpebral conjunctiva (inner surface of the eyelid). The palpebral conjunctiva is continuous with the bulbar conjunctiva (the epithelium covering the anterior periphery of the globe), which is continuous with the corneal epithelium on the most anterior surface of the globe (Fig. 1).

After eyelid closure, the palpebral epidermis differentiates as part of the skin. Stratification and keratinization begin, and the regularly spaced hair follicles of the eyelashes form at the margins of the lids. However, the conjunctival epithelium does not stratify until after the eyelids re-open and it remains non-keratinized throughout life. The mature conjunctival epithelium contains abundant goblet cells, which produce mucus that is important for the properties of the tear film. Soon after birth, the Meibomian glands, which produce a lipid component of the tears, form by in growth of the conjunctival epithelial cells near the inner surface of the lid margin (Findlater et al., 1993).

Defects in eyelid growth or fusion may cause the eyelids to be open at birth (EOB). A surprising number of genes and signaling pathways are required for eyelid closure. An EOB phenotype is seen in mice with germline deletion of activin β-B (*Inhbb*), MEK kinase1 (*Map3k1*), c-Jun N-terminal kinase (*Mapk8*), c-Jun (*Jun*), the epidermal growth factor (EGF) family members HB-EGF (*Hbegf*) and transforming growth factor α (*Tgfa*), and their receptor (*Egfr*), fibroblast growth factor 10 (*Fgf10*), its receptor (*Fgfr2*), the forkhead transcription factors *Foxc1* and *Foxc2*, and the Wnt antagonist *Dkk2* (Gage et al., 2008; Kidson et al., 1999; Kume et al., 1998; Li et al., 2001; Li et al., 2003; Luetteke et al., 1994; Luetteke et al., 1993; Miettinen et al., 1995; Mine et al., 2005; Smith et al., 2000; Takatori et al., 2008; Tao et al., 2005; Vassalli et al., 1994;

Weston et al., 2004; Zenz et al., 2003; Zhang et al., 2003). Previous studies suggested that activin β-B promotes eyelid closure by activating a Smad-independent cascade involving MEK kinase1, Jun N-terminal kinase (JNK) and c-Jun (Takatori et al., 2008; Weston et al., 2004; Zhang et al., 2003). EGF family members contribute to periderm migration by activating the ERK signaling pathway (Mine et al., 2005). Upstream of the EGF cascade, c-Jun increases EGF receptor expression (Li et al., 2003; Zenz et al., 2003). FGF10 controls eyelid epithelial proliferation and periderm migration by stimulating the expression of activin β-B and TGFα, and by modulating the expression of sonic hedgehog (*Shh*) (Tao et al., 2005). The administration of a short-acting Shh antagonist at E9 results in EOB (Lipinski et al., 2008). Recently, mice lacking the Wnt antagonist *Dkk2*, showed EOB, indicating that Wnt activity must be properly tuned during eyelid development.

It has not been clear whether bone morphogenetic protein (BMP) signaling plays a role in eyelid closure. An EOB phenotype was detected in one mouse strain in which *Bmpr1a* was conditionally deleted in the ectoderm by using a keratin 14-driven Cre-recombinase transgene (Andl et al., 2004). However, mice overexpressing the BMP antagonist noggin under the control of the human K14 or K5 promoters had eyelid defects, but no EOB phenotype (Plikus et al., 2004; Sharov et al., 2003). Mice overexpressing the inhibitory Smad Smad7, driven by the bovine K5 promoter, did have an EOB phenotype (He et al., 2002). However, whether this phenotype was attributable to blocking TGFβ, activin, or BMP signaling has not been clarified. In addition, overexpression of BMP signaling antagonists or deficiencies in the BMP signaling pathway cause other epithelial defects that may indirectly result in EOB. For example, in some of these cases, the epidermal, conjunctival and corneal epithelia were hyperplastic, and sweat glands transdifferentiated into hair follicles (He et al., 2002; Plikus et al., 2004).

To clarify the possible function of BMP signaling in eyelid development, we conditionally deleted two type I BMP receptors, two of the BMP-activated R-Smads or the co-Smad Smad4 in the prospective eyelid epithelium beginning on E9. In each case, the mice showed normal eyelid formation and adequate growth, but the eyelid epithelia did not fuse, resulting in an EOB phenotype. Deletion of the sole type II TGFβ receptor or the two activin- and TGFβ-activated R-Smads did not interfere with eyelid closure. Further analysis suggested that Fgf10 from the mesenchyme activates Fgfr2 in the lid ectoderm. Fgfr2 signaling modulates Shh levels, resulting in *Bmp4* expression in the mesenchyme. FGF signaling also inhibits Wnt signaling in the eyelid ectoderm, independently of its effects on BMP expression. BMPs are required for the expression of the transcription factors Foxc1 and Foxc2 in the ectoderm, the nuclear translocation of activated c-Jun in periderm cells, the proper timing of conjunctival epithelial differentiation and the establishment of conjunctival epithelial cell fate. In the absence of BMP signaling, ectopic hair follicles formed on the inner edges of the eyelid at the expense of the Meibomian glands, a feature of human lymphedema-distichiasis syndrome.

MATERIALS AND METHODS

Mice genotyping and mating

The following genetically modified mice were used in this study: Le-Cre (Ashery-Padan et al., 2000), *Acvr1* flox (Dudas et al., 2004), *Bmpr1a* flox (Gaussin et al., 2002), *Smad4* flox (Yang et al., 2002), *Smad1* flox (Huang et al., 2002), *Smad5* flox (Umans et al., 2003), *Smad2* flox (Piek et al., 2001), *Smad3* germline knockout (Roberts et al., 2006), *Fgfr2* floxed (Yu et al., 2003), *Tgfbr2* floxed (Chytil et al., 2002), presenilin 1 floxed (Yu et al., 2001), presenilin 2 germline knockout (Steiner et al., 1999) and TOPGAL, a Wnt reporter strain (DasGupta and Fuchs, 1999). Matings between mice that were homozygous for the floxed allele, only one of which was Cre-positive, resulted in litters in which about half of the offspring were Cre-positive (conditional knockout, CKO). The others were Cre-negative (wild type). Noon of the day when the vaginal plug was detected was considered as embryonic day (E) 0.5 of development. Embryos were collected at the desired stages (n=3 to 5 for each genotype and stage).

Histology

Embryo heads were fixed in 4% paraformaldehyde/PBS overnight at 4°C, dehydrated through a series of ethanol concentrations, embedded in paraffin and sectioned at a thickness of 4 μm. For morphological studies, sections were stained with Hematoxylin and Eosin (Surgipath, Richmond, IL, USA).

In situ hybridization

Frozen sections were fixed in 4% paraformaldehyde/PBS, treated with proteinase K (10 ug/ml), post-fixed in 4% paraformaldehyde/PBS and acetylated in triethanolamine-acetic anhydride solution. Samples were pre-hybridized in 50% formamide, 5×SSC, 5 mM EDTA, 1×Denhardt's, 100 ug/ml heparin, 0.3 mg/ml yeast tRNA and 0.1% Tween-20, incubated in the same solution with riboprobes overnight, washed with 0.2×SSC, blocked in 10% lamb serum and incubated with anti-digoxigenin antibody overnight. The color reaction was developed using NBT and BCIP in the dark. After the reaction was completed, the slides were washed in PBS, fixed in 4% paraformaldehyde/PBS and mounted in 100% glycerol.

Digoxigenin-labeled riboprobes were synthesized from cDNA generated from RNA isolated from wild-type E15.5 eyelids using the following PCR primer pairs:

Foxc1, 5′-CCAGAAAGTGTTCCAAAAGC-3′ and 5′-GAAACCACC-CCAGACTAATG-3′;

Foxc2, 5′-GCCACCTCCTGGTATCTGAAC-3′ and 5′-CTGGGCAA-GAACAAAATAGCC-3′;

BMP4, 5′-TGGTAACCGAATGCTGATGG-3′ and 5′-GGCGACGG-CAGTTCTTATTC-3′;

Sfrp1, 5′-ATCCCCCTCTTTCTGCCTTAG-3′ and 5′-GAAATACC-TCTGGGCACTTGG-3′;

Dkk2, 5′-TTTACAAAGTGGGTTCCCTTG-3′ and 5′-CTCCATTTT-CACATCACAAAGC-3′.

Probe for patched 1 was a kind gift from Dr David Ornitz (Washington University, St Louis, MO, USA). Gene expression patterns were compared between CKO and wild-type littermates and each in situ hybridization was performed at least twice.

Immunofluorescence staining

Frozen sections were warmed to room temperature and then fixed in 4% paraformaldehyde/PBS. After three washes in PBS, the samples were treated with 3% H_2O_2 in methanol to quench endogenous peroxidase activity, blocked in 5% goat serum/0.1% Triton X-100, incubated in primary antibody overnight, washed and processed with tyramide amplification. The antibodies for pSmad1/5/8 and p-c-Jun were from Cell Signaling Technology (Danvers, MA, USA). The keratin 14 and keratin 10 antibody was from Covance Research Products (Denver, PA, USA). The keratin 4 antibody was from Sigma-Aldrich (St Louis, MO, USA). The Dkk2 antibody was from Santa Cruz Biotechnology (Santa Cruz, CA, USA).

X-gal staining

Staged embryos expressing a *lacZ* reporter gene were fixed 4% in paraformaldehyde/PBS at 4°C for 30 minutes, washed twice in PBS with 2 mM $MgCl_2$, 0.02% NP-40/0.01% deoxycholate (DOC), and stained with X-gal solution [5 mM $K3Fe(CN)_6$, 5 mM $K4Fe(CN)_6$, 1 M $MgCl_2$, 0.02% NP-40/0.01% DOC NP-40, 1 mg/ml X-gal in PBS] for 5 hours at 37°C, post-fixed with 4% paraformaldehyde for 1 hour, cryoprotected and, when required, 10-μm sections were prepared.

BrdU and TUNEL staining and quantification

Pregnant female mice were injected with 50 mg/kg of a mixture of 10 mM BrdU (Roche, Indianapolis, IN, USA) and 1 mM 5-fluoro-5′-deoxyuridine (Sigma, St Louis, MO, USA) and sacrificed after 1 hour. A monoclonal anti-BrdU antibody (diluted 1:250; Dako, Carpinteria, CA, USA) was used with

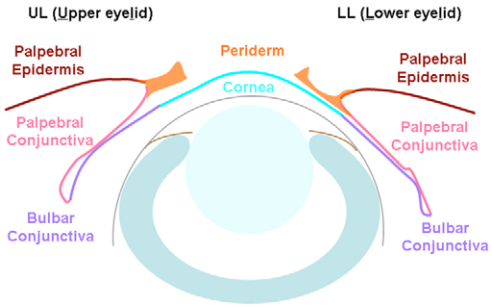

Fig. 1. Wild-type mouse eyelid anatomy at E15.5. The components of the normal ocular epithelia are color coded: bulbar conjunctiva, purple; palpebral conjunctiva, pink; palpebral epidermis, dark red; periderm, orange; cornea, blue.

a Vectastain Elite Mouse IgG ABC kit. Sections were counterstained with Hematoxylin. Terminal deoxynucleotidyl transferase (TdT)-mediated deoxyuridine triphosphate nick end-labeling (TUNEL) was done with an Apoptag kit (Chemicon, Temecula, CA, USA). The deparaffinized slides were treated with 3% H_2O_2 in methanol for 30 minutes, followed by proteinase K treatment (20 µg/ml) for 15 minutes. Slides were incubated with TdT enzyme in equilibration buffer for 1 hour at 37°C. The reaction was terminated with wash buffer provided by the manufacturer for 10 minutes at room temperature. Anti-digoxigenin-peroxidase conjugate was added for 30 minutes at room temperature, followed by DAB and H_2O_2 treatment. Slides were counterstained with Hematoxylin.

BrdU and TUNEL-positive cells were counted in the ocular surface epithelia at E14.5 in 4-5 sections from each embryo (wild type, n=6; *Smad4*^{CKO}, n=8). The means and standard error (s.e.m.) were calculated from the pooled data. Differences were considered significant if P<0.05, as determined by Student's t-test.

RESULTS

BMP signaling is required for mouse eyelid closure

To study the functions of BMPs in early eye development, we used Cre recombinase to delete floxed alleles of key components of the BMP signaling pathway. Transgenic Cre expression was driven by a promoter that is first expressed at E9 in the lens placode and in the ectoderm that later differentiates into the ocular surface epithelia (Le-Cre) (Ashery-Padan et al., 2000). The ocular surface epithelia targeted by the transgene include the palpebral epidermis, palpebral conjunctiva, bulbar conjunctiva and corneal epithelium (Ashery-Padan et al., 2000) (Fig. 1). Le-Cre mice were mated to mice with floxed alleles of two of the three type I BMP receptors (*Acvr1* and *Bmpr1a*), two of the BMP-activated R-Smads (*Smad1* and *Smad5*), the two activin/TGFβ-activated R-Smads (*Smad2* and *Smad3*), the sole type II TGFβ receptor (*Tgfbr2*) or the co-Smad *Smad4*. Matings were between Cre-positive homozygous flox and Cre-negative homozygous flox animals, assuring that about half of the offspring were Cre-positive and no animals received two copies of the transgene.

In each knockout targeting the BMP pathway (*Acvr1/Bmpr1a*, *Smad1/5* and *Smad4*), Cre-positive animals had an eyelid-open-at-birth (EOB) phenotype (Fig. 2B-D). Offspring with conditional deletion of one allele of the BMP pathway genes (*Acvr1/Bmpr1a*, *Smad1/5* and *Smad4*; not shown), both *Tgfbr2* alleles (Fig. 2G), or both *Smad2* and *Smad3* alleles (data not shown) had normal-appearing, closed eyelids at birth and normal-appearing conjunctival epithelium between E15.5 and birth. By examining embryos between E16.5 and birth, we found that eyelids from the Cre-positive embryos

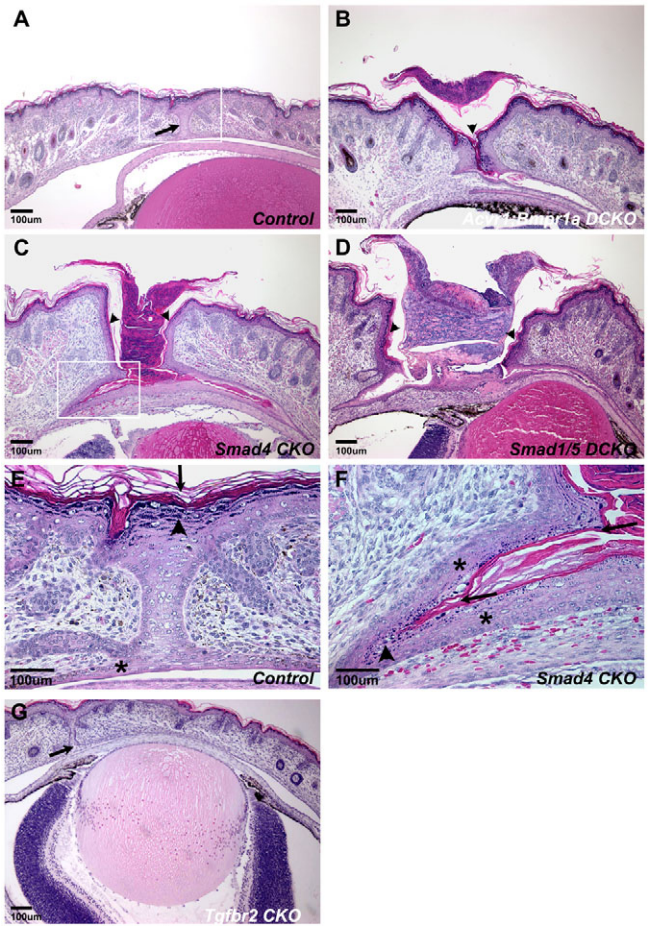

Fig. 2. Eyelid defects in mice with deficiencies in BMP signaling. (**A-G**) Hematoxylin and Eosin staining of frontal eye sections from wild-type (A,E), *Acvr1;Bmpr1a*^{DCKO} (B), *Smad4*^{CKO} (C,F), *Smad1/5*^{DCKO} (D) and *Tgfbr2*^{CKO} (G) mice at postnatal day 3 (P3). Wild-type eyelids are fused (arrow in A), whereas eyelids deficient in BMP signaling in the ectoderm are separate (arrowheads in B-D). (E,F) Higher magnification views of insets in A and C. (E) Eosin-stained keratin (arrow) and Hematoxylin-stained keratinocytes (arrowhead) in wild-type eyelid palpebral epidermis. (F) Ectopic Eosin-stained keratin-like protein (arrow) and ectopic Hematoxylin-stained keratinocyte-like cells (arrowhead) in *Smad4*^{CKO} conjunctiva. Asterisks in E and F illustrate the hyperplasia in the *Smad4*^{CKO} conjunctiva. (G) *Tgfbr2*^{CKO} neonate eyelids are fused (arrow). Scale bars: 100 µm.

with EOB never closed, indicating that the phenotype resulted from the failure of eyelid closure, not from premature eyelid opening (not shown). Because only knockouts in the canonical BMP-Smad pathway had an EOB phenotype, in the remainder of the studies described we show only the phenotype of *Smad4*^{CKO} mice to represent the function of BMP signaling in eyelid closure. The 'control' eyelids shown are all from homozygous flox, Cre-negative littermates.

Besides the EOB phenotype, eyes with BMP signaling deficiencies showed hyperplasia and what appeared to be keratinization of the conjunctival epithelium. As opposed to the two-layered epithelium seen in wild-type embryos, the conjunctival epithelium comprised several cell layers, including a stratum granulosum with dark, Hematoxylin-stained keratohyalin granules, and an eosinophilic stratum corneum, which suggested keratinization (Fig. 2E,F).

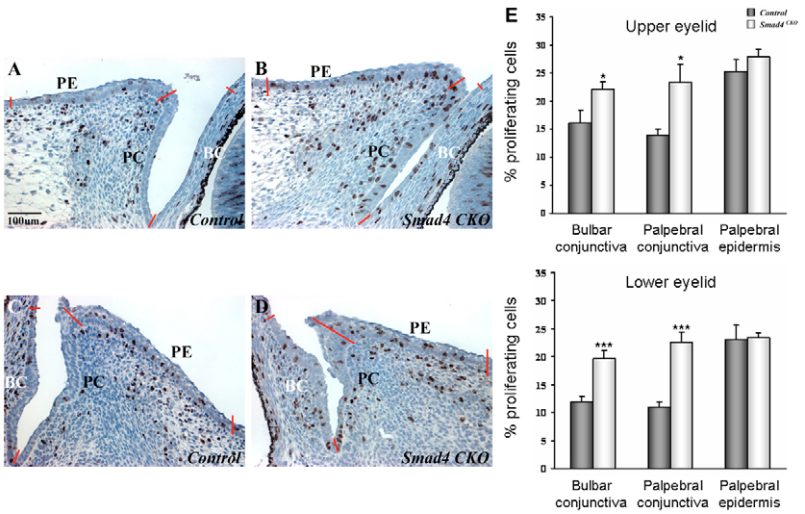

Fig. 3. Cell proliferation in *Smad4*^{CKO} eyelid epithelia at E14.5. (**A-D**) BrdU staining in frontal eye sections from wild-type upper eyelid (A), wild-type lower eyelid (C), *Smad4*^{CKO} upper eyelid (B) and *Smad4*^{CKO} lower eyelid (D). Red lines mark the approximate boundaries of the bulbar and palpebral conjunctiva and the palpebral epidermis. (**E**) Percentage of BrdU-labeled cells in each compartment. Compared with wild-type animals, the BrdU labeling index in *Smad4*^{CKO} bulbar and palpebral conjunctival epithelia was significantly increased. The *y*-axes indicate the mean percentage of BrdU incorporation in each area assayed. Error bars represent the s.e.m. **P*<0.05, ****P*<0.001. B, bulbar conjunctiva; PC, palpebral conjunctiva; PE, palpebral epidermis. Scale bar in A: 100 μm.

EOB caused by interruption of BMP signaling is not due to decreased cell proliferation or increased cell death

We investigated whether loss of BMP signaling contributed to the failure of eyelid closure by affecting cell proliferation or cell death. At E12.5, BrdU and TUNEL labeling were similar in wild-type and *Smad4*^{CKO} eyelids (not shown). However, a significant increase in BrdU labeling occurred in the conjunctival epithelia of *Smad4*^{CKO} eyes at E14.5 (Fig. 3A-E). This observation was consistent with the conjunctival hyperplasia seen at later stages. No increase in BrdU labeling was detected in the palpebral epidermis (Fig. 3A-E) and no change was seen in programmed cell death in any of the ocular surface epithelia (not shown).

BMP signaling activates the expression of transcription factors that are required for eyelid closure

Expression of the forkhead transcription factors Foxc1 and Foxc2 is required for eyelid closure (Kidson et al., 1999; Kume et al., 1998; Smith et al., 2000). *Foxc1* mRNA was present in wild-type upper and lower eyelid epithelia (Fig. 4A), but undetectable in *Smad4*^{CKO} eyelids (Fig. 4C). Similarly, in wild-type embryos, *Foxc2* mRNA was expressed in palpebral conjunctival epithelial cells (Fig. 4D), but could not be detected in *Smad4*^{CKO} palpebral conjunctiva (Fig. 4F).

BMP signaling is required to promote the translocation of c-Jun into the nuclei of migrating periderm cells

c-Jun and the signaling cascade that leads to its phosphorylation are required for eyelid closure (Li et al., 2003; Zenz et al., 2003). In wild-type mice, a shelf of periderm cells begins to extend from the margin of the eyelids at E15.0 (Fig. 5A), covering much of the cornea by E15.5 (Fig. 5B). The nuclei of these periderm cells were strongly stained by an antibody to phosphorylated c-Jun (Fig. 5A,B, insets). In the *Smad4*^{CKO} eyelid epithelium, the appearance of the lid margin was comparable to that of wild type at E15.0 (Fig. 5C), although, by E15.5, fewer migrating periderm cells were present than in control eyes (Fig. 5D). In the *Smad4*^{CKO} embryos, the levels of phosphorylated c-Jun appeared to be lower than in wild-type periderm cells and p-c-Jun staining was present in the perinuclear cytoplasm, but not in the nuclei (Fig. 5C,D, insets). Thus, BMP signaling is required for the full activation of c-Jun and for its translocation into the nucleus to exert its function as a transcription factor.

BMP expression and function is regulated by FGF signaling during eyelid closure

Fgf10 signaling via Fgfr2 is essential for eyelid growth and closure (Li et al., 2001; Tao et al., 2005). To determine whether there is a relationship between FGF and BMP signaling, we deleted *Fgfr2* in the prospective eyelid epithelium using Le-Cre. Mice deficient in *Fgfr2* in the ectoderm showed an EOB phenotype, as described previously (Garcia et al., 2005), and deficiencies in BMP expression and function. In wild-type lower eyelids at E15.5, *Bmp4* mRNA was expressed in a cluster of mesenchymal cells underlying the palpebral conjunctival epithelium (Fig. 6A, arrows), but *Bmp4* transcripts were undetectable in the lower eyelids of *Fgfr2*^{CKO} mice (Fig. 6C). *Bmp4* mRNA was expressed in two groups of mesenchymal cells in the wild-type upper eyelid: in a cluster corresponding to those found in the lower eyelid (Fig. 6A, arrows) and in a cluster underlying the palpebral epidermis (Fig. 6A, arrowheads). In the *Fgfr2*^{CKO} upper eyelid, *Bmp4* mRNA accumulation in the mesenchyme underlying the palpebral conjunctiva was not affected, but *Bmp4* transcripts were not detectable in the mesenchyme underlying the palpebral epidermis (Fig. 6B).

A previous study found that Fgf10 maintains *Shh* expression in the eyelid mesenchyme (Tao et al., 2005). We found that hedgehog function in the mesenchyme, as measured by the expression of the hedgehog receptor patched 1 (*Ptch1*), a direct target of Shh signaling, was remarkably similar to the distribution of *Bmp4* transcripts (Fig. 6D). Moreover, the pattern of residual *Ptch1* expression in the *Fgfr2*^{CKO} eyelid was similar to the pattern of residual *Bmp4* expression. Although *Ptch1* expression was preserved in the upper lid ectoderm and mesenchyme, it diminished greatly in the lower lid ectoderm and mesenchyme of *Fgfr2*^{CKO} mice (Fig. 6E). *Ptch1* expression was not affected in *Smad4*^{CKO} mice (Fig. 6F).

In agreement with the dependence of *Bmp4* expression on Fgfr2, nuclear staining for phosphorylated Smad1/5/8, the receptor-activated Smads that transduce BMP signals, was strong in wild-type epithelial cells (Fig. 6G,H), but greatly diminished in the upper and lower eyelids of *Fgfr2*^{CKO} mice (Fig. 6I,J). As in the *Smad4*^{CKO} eyelids, *Foxc1* and *Foxc2* mRNA was not detectable in *Fgfr2*^{CKO}

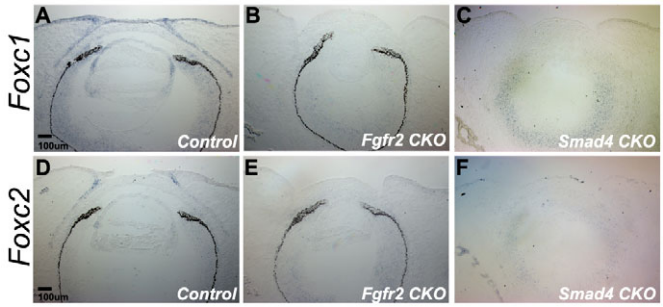

Fig. 4. *Foxc1* and *Foxc2* transcripts are greatly reduced in *Fgfr2*^{CKO} and *Smad4*^{CKO} eyelids. (**A-C**) In situ hybridization for *Foxc1* mRNA on frontal eye sections from wild-type (A), *Fgfr2*^{CKO} (B) and *Smad4*^{CKO} (C) eyelids at E15.5. In wild-type eyelid (A), *Foxc1* mRNA was detected in the palpebral epithelium, palpebral conjunctiva, bulbar conjunctiva, periderm and retina. In *Fgfr2*^{CKO} (B) and *Smad4*^{CKO} (C) eyelids, *Foxc1* mRNA was detectable only in the retina. (**D-F**) In situ hybridization of *Foxc2* mRNA on frontal eye sections from wild-type (D), *Fgfr2*^{CKO} (E) and *Smad4*^{CKO} (F) eyelids. In wild type eyelids (D), *Foxc2* mRNA was detected in the palpebral conjunctiva and retina at E15.5. In *Fgfr2*^{CKO} (E) and *Smad4*^{CKO} (F) eyelids, *Foxc2* mRNA was detectable only in the retina. Scale bars: 100 μm.

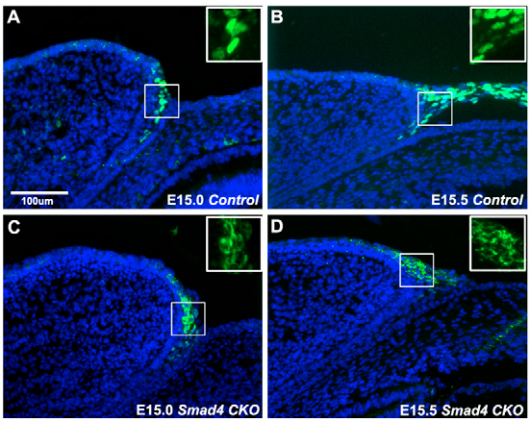

Fig. 5. The nuclear localization of phosphorylated c-Jun requires *Smad4*. Immunostaining for phosphorylated c-Jun (p-c-Jun, green) on frontal eye sections from wild-type E15.0 (A), wild-type E15.5 (B), *Smad4*^{CKO} E15.0 (C) and *Smad4*^{CKO} E15.5 (D) embryos. (**A**) In wild-type eyelids, a small number of migrating periderm cells are present at E15.0. Staining for p-c-Jun is present in the nuclei of these cells (inset). (**B**) By E15.5, the number of periderm cells has increased and they have begun to migrate over the cornea. Staining for p-c-Jun is present in the nuclei of these cells (inset). (**C**) At E15.0, periderm cells in *Smad4*^{CKO} eyelids appeared similar in number to wild type. However, p-c-Jun staining was restricted to the cytoplasm around the nuclei (inset). (**D**) At E15.5, fewer periderm cells were present in *Smad4*^{CKO} eyelids than in wild type. Staining for p-c-Jun was weaker than in wild-type periderm cells and was still restricted to the perinuclear cytoplasm (inset). Insets show p-c-Jun staining without the nuclear counterstain (blue). Scale bar in A: 100 μm.

conjunctival epithelia (Fig. 4B,E). Thus, FGF signaling controls eyelid closure, at least in part, through the activation of BMP signaling.

Activation of Fgfr2 suppresses Wnt signaling and promotes the expression of *Sfrp1* in a BMP-independent manner

Loss of Dkk2, a Wnt signaling antagonist, causes EOB, revealing that excessive Wnt signaling can prevent eyelid closure (Gage et al., 2008). To further assess the regulation of Wnt pathway signaling in the ocular surface epithelia, we produced *Fgfr2* and *Smad4* conditional knockouts in the ectoderm in a TOPGAL background, in which canonical Wnt signaling activates a β-galactosidase reporter transgene (DasGupta and Fuchs, 1999). In wild-type (Cre-negative) eyelids at E15.5, β-galactosidase staining was abundant in hair follicles of the epidermis and in the conjunctival epithelium in a band near the edge of the upper eyelid. Weaker staining was present in a band along the edge of the lower eyelid (Fig. 7A,D). In *Fgfr2*^{CKO} eyes, TOPGAL reporter activity increased in intensity and spread over the conjunctival epithelium of the upper and lower eyelids (Fig. 7B,E). In *Smad4*^{CKO} eyelids, β-galactosidase expression was not increased, but had a different distribution from wild type. Instead of localizing in a continuous band in the peripheral conjunctival epithelium, staining was present in an extra row of ectopic hair follicles in the upper and lower eyelids (Fig. 7C,F). A double row of eyelashes is called distichiasis. Because distichiasis occurs in humans and mice haploinsufficient for FOXC2 (Fang et al., 2000; Kriederman et al., 2003), this finding is consistent with our observation that BMP signaling was required for *Foxc2* expression.

Although loss of *Dkk2* expression causes EOB (Gage et al., 2008), *Dkk2* mRNA or protein expression was not affected in *Fgfr2*^{CKO} or in *Smad4*^{CKO} eyelid epithelial cells (Fig. 8A-F). FGF signaling modulates *Shh* expression in the eyelid and, in other tissues, hedgehog signaling induces the expression of the Wnt antagonist, secreted frizzle-related protein 1 (Sfrp1) (He et al., 2006; Katoh and Katoh, 2006). We examined the levels of *Sfrp1* mRNA in wild-type, *Fgfr2*^{CKO} and *Smad4*^{CKO} eyelids. In wild-type eyelids, *Sfrp1* mRNA was expressed in the entire eyelid epithelium, with strongest expression in the conjunctival epithelia (Fig. 8G). Consistent with the effects of FGF and BMP signaling on TOPGAL activity, *Sfrp1* transcripts were undetectable in *Fgfr2*^{CKO} eyelids (Fig. 8H), but were present at normal levels in *Smad4*^{CKO} eyelids (Fig. 8I). Thus, FGF signaling suppresses Wnt signaling, at least in part, through the activation of *Sfrp1*. However, the control of *Sfrp1* expression by Fgfr2 is independent of BMP signaling.

Although the BMP-Smad pathway is not involved in suppressing Wnt signaling, it appears to be required to suppress ectopic hair follicle formation from the conjunctival epithelial cells at the inner margin of the eyelid (Fig. 7C). In its absence, the uniform band of Wnt signaling near the eyelid margin was replaced by a row of eyelash follicles (Fig. 7C,F). These observations suggest that BMP signaling maintains the pattern of Wnt pathway activity required for the differentiation of the Meibomian gland progenitor cells at the inner margins of the eyelids.

BMP signaling suppresses the differentiation of conjunctival epithelial cells prior to eyelid closure and specifies conjunctival epithelial cell fate

The conjunctival epithelium in mice deficient in BMP signaling developed features that were reminiscent of epidermis, including keratinization and ectopic hair follicles. We, therefore, examined the levels of the epithelial cell differentiation marker keratin 14 (K14) at E15.0, before eyelid closure, and at E15.5, during closure. We also stained for a specific epidermal differentiation marker, keratin 10 (K10), and a conjunctival epithelial differentiation marker, keratin 4 (K4), at E17.5, after eyelid closure. In wild-type mice, the conjunctival

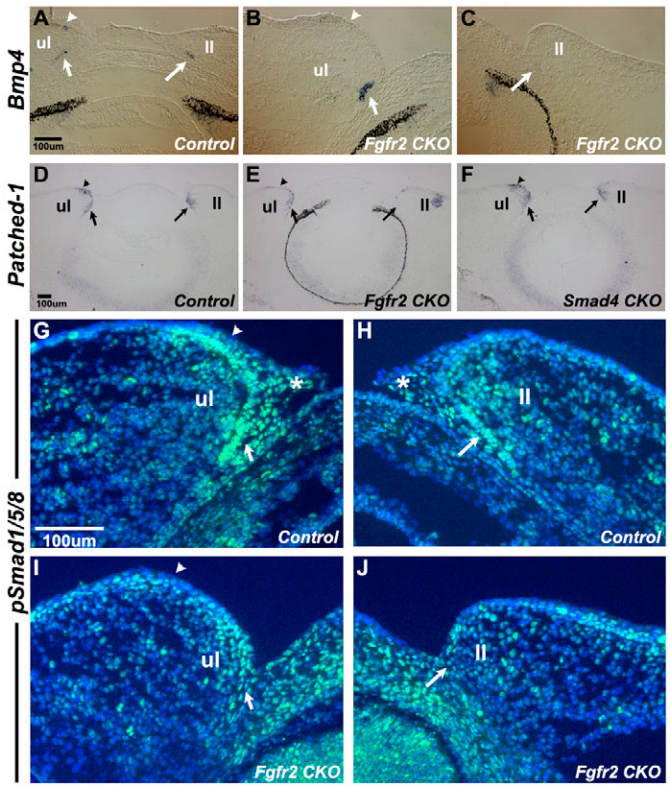

Fig. 6. Signaling from Fgfr2 promotes Bmp4, patched 1 expression and BMP signaling in the eyelid. (**A-C**) In situ hybridization for *Bmp4* transcripts at E15.5 in frontal eye sections from wild-type upper and lower eyelids (A) and $Fgfr2^{CKO}$ upper (B) and lower (C) eyelids. (A) In the wild-type eyelids, *Bmp4* transcripts were present in a cluster of mesenchyme cells underlying the palpebral conjunctiva (arrows) and the palpebral epidermis (arrowhead). (B) In the upper eyelids of $Fgfr2^{CKO}$ mice, *Bmp4* transcripts were detected in the mesenchyme underlying the palpebral conjunctiva (arrow), but not in the mesenchyme underlying the palpebral epidermis (arrowhead). (C) In the lower eyelids of $Fgfr2^{CKO}$ mice, *Bmp4* transcripts were not detected in the mesenchyme underlying the palpebral conjunctiva (arrow). (**D-F**) In situ hybridization for *Ptch1* transcripts in frontal eye sections from wild-type (D), $Fgfr2^{CKO}$ (E) and $Smad4^{CKO}$ (F) eyelids. In wild-type (D) and $Smad4^{CKO}$ eyelids (F), *Ptch1* transcripts were present in clusters of mesenchyme cells and the overlying palpebral conjunctiva (arrows) and palpebral epidermis (arrowhead). (E) In the upper eyelids of $Fgfr2^{CKO}$ mice, *Ptch1* transcripts were decreased in the mesenchyme and the overlying palpebral conjunctiva (arrow), and were barely detectable in the mesenchyme and the overlying palpebral epidermis (arrowhead). In the lower eyelids of $Fgfr2^{CKO}$ mice, *Ptch1* transcripts were undetectable in the mesenchyme and the overlying palpebral conjunctiva (arrow). (**G-J**) Immunostaining for phosphorylated Smad1/5/8 (pSmad1/5/8) in frontal eye sections from wild-type upper (G), wild-type lower (H), $Fgfr2^{CKO}$ upper (I) and $Fgfr2^{CKO}$ lower (J) eyelids. (G) In the wild-type upper eyelid, nuclear pSmad1/5/8 staining was seen in the eyelid mesenchyme, the overlying palpebral conjunctiva (arrow), the palpebral epidermis (arrowhead) and the periderm (asterisk). (H) In the wild-type lower eyelid, pSmad1/5/8 staining was seen in the eyelid mesenchyme, the overlying palpebral conjunctiva (arrow) and the periderm (asterisk). (I) In the upper eyelid of $Fgfr2^{CKO}$ embryos, pSmad1/5/8 staining was reduced in the palpebral conjunctiva (arrow) and greatly reduced in the palpebral epidermis (arrowhead). (J) In the $Fgfr2^{CKO}$ lower eyelid, pSmad1/5/8 staining was greatly reduced in the palpebral conjunctiva (arrow). ul, upper eyelid; ll, lower eyelid. Scale bars: 100 μm.

epithelium first expressed K14 at about the time of eyelid closure (Fig. 9A). However, in conjunctival epithelial cells deficient in BMP signaling, expression of K14 was precocious (Fig. 9C), with the mutant conjunctiva differentiating at the same time as the epidermis. In wild-type E17.5 eyes, K10 is expressed by epidermis, and K4 is expressed by conjunctiva (Fig. 9D,G). However, in $Smad4^{CKO}$ conjunctival epithelium, we found ectopic K10 expression, with K4 staining detected only in a few residual cells (Fig. 9F,I), suggesting that most mutant conjunctival cells transdifferentiated into epidermal cells. Although conjunctival differentiation in $Fgfr2^{CKO}$ eyes was premature, as determined by K14 expression (Fig. 9B), the transdifferentiation of conjunctiva to epidermis was not evident, because $Fgfr2^{CKO}$ conjunctiva did not express K10 (Fig. 9E,H). It seems possible that residual BMP signaling in the $Fgfr2^{CKO}$ conjunctiva maintained conjunctival cell fate, but was unable to suppress the premature differentiation of this tissue.

DISCUSSION

Smad-dependent BMP signaling is required for eyelid closure

Conditional deletion of the genes encoding two of the three type I BMP receptors, two of the three BMP-associated R-Smads or the co-Smad Smad4 in the eyelid epithelia resulted in an EOB phenotype, precocious conjunctival epithelial differentiation and the transdifferentiation of conjunctiva to epidermis, including ectopic eyelash follicle formation and epidermis-specific keratin expression. Although activin signaling is important for eyelid closure, a previous investigation indicated that activin β-B signals are transduced to c-Jun by MEKK1 and JNK, not through the canonical Smad pathway (Zhang et al., 2003). Our results are consistent with this interpretation, as deletion of the activin/TGFβ-stimulated R-Smads Smad2 and Smad3 did not cause an EOB phenotype. Deletion of the TGFβ type II receptor also did not show an eyelid phenotype, indicating that the Smad4 phenotype was due to defects in signaling through the canonical BMP pathway, and not in another of the TGFβ superfamily pathways that share Smad4 function.

The EOB phenotype in eyelids lacking epithelial BMP receptors and BMP-activated R-Smads is consistent with the results of *Bmpr1a* deletion using a K14-Cre transgene (Andl et al., 2004) and the overexpression of the inhibitory Smad Smad7 using the bovine K5 promoter (He et al., 2002). The inability of K14-driven noggin overexpression to cause EOB may be due to the late expression of K14 in the conjunctiva, just as eyelid closure is occurring, giving insufficient time for noggin to prevent the activation of BMP receptors. EOB in mice deficient in BMP signaling was not due to decreased cell proliferation or increased cell death in the palpebral epithelia. On the contrary, increased cell proliferation was found in the conjunctival epithelia, consistent with the hyperplasia observed in the BMP receptor knockouts or when Smad7 is driven by the K14 promoter (Andl et al., 2004; He et al., 2002). Thus, BMPs normally inhibit the proliferation and differentiation of the conjunctival epithelium, and specify conjunctival epithelial cell fate.

FGF-regulated BMP signaling is required for the nuclear localization of phosphorylated c-Jun and the transcription of *Foxc1* and *Foxc2*

The phosphorylation and function of c-Jun in the eyelid epithelium depends, at least in part, on Smad-independent signaling by activin β-B (Zhang et al., 2003). However, in $Acvr1;Bmpr1a^{DCKO}$, $Smad1/5^{DCKO}$ and $Smad4^{CKO}$ eyelids, c-Jun appeared to be more weakly phosphorylated than in wild type and failed to translocate into the nuclei of periderm cells. Previous studies showed that

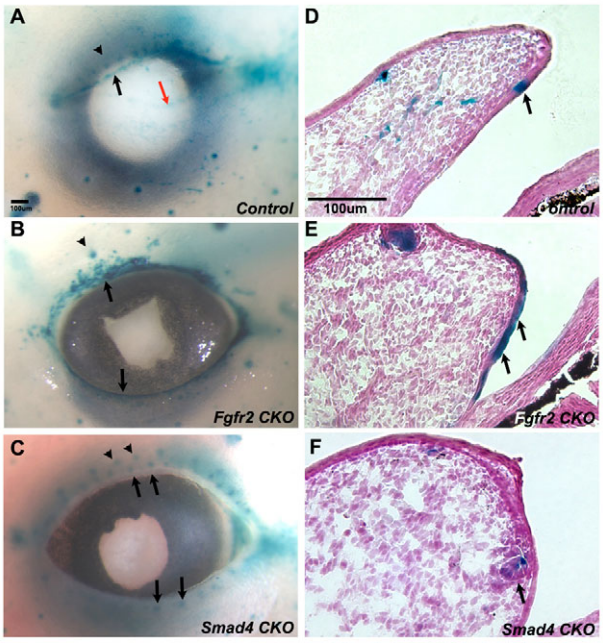

Fig. 7. The activity of the canonical Wnt pathway in the eyelid is modified in different ways by FGF and BMP signaling. (**A-C**) Whole-mount X-gal staining from the TOPGAL reporter in wild-type (A), *Fgfr2*^{CKO} (B) and *Smad4*^{CKO} (C) eyelids at E15.5. (**D-F**) Frontal sections of the eyes shown in A-C. (A) A prominent band of Wnt activity is present in the upper (black arrow) and a weaker band in the lower eyelid margins (red arrow) of wild-type eyes. Wnt activity is also present in eyelash follicles (arrowhead) and in epidermal hair follicles. (B) Wnt activity is uniformly increased in the upper and lower eyelids of *Fgfr2*^{CKO} mice (black arrows) and is present in epidermal hair follicles (arrowhead). (C) Wnt activity is present in the epidermal hair follicles (arrowhead) and in ectopic patches in the upper and lower eyelids of *Smad4*^{CKO} mice (black arrows). (D) Frontal sections reveal that Wnt activity is located near the anterior edge of the palpebral conjunctiva of wild-type eyelids (arrow). (E) In *Fgfr2*^{CKO} eyelids, Wnt activity expands into the palpebral conjunctiva (arrows). (F) In *Smad4*^{CKO} eyelids, Wnt activity is present in ectopic hair follicles (arrow), corresponding to the location of the band of cells with high Wnt activity in the wild-type palpebral conjunctiva. Scale bars: 100 μm.

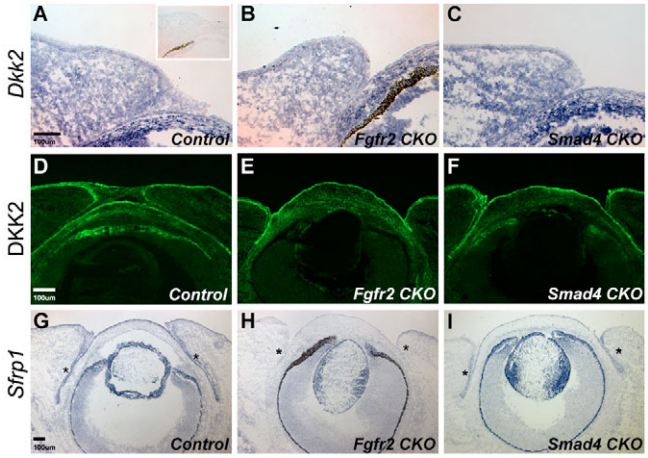

Fig. 8. The effects of FGF and BMP signaling on *Dkk2* and *Sfrp1* expression in the eyelid. (**A-C**) In situ hybridization for *Dkk2* transcripts in frontal sections from wild-type (A), *Fgfr2*^{CKO} (B) and *Smad4*^{CKO} (C) embryos at E15.5. (A) *Dkk2* transcript levels (blue) were strong in the eyelid epidermis, bulbar conjunctiva and corneal stroma, with weaker staining in the palpebral conjunctiva, periderm and mesenchyme in wild type. A sense probe control is shown in the inset. (B,C) No significant change in *Dkk2* mRNA level was detected in *Fgfr2*^{CKO} (B) and *Smad4*^{CKO} (C) embryos at E15.5. (**D-F**) Immunostaining for DKK2 protein in frontal eye sections from wild-type (D), *Fgfr2*^{CKO} (E) and *Smad4*^{CKO} (F) embryos at E15.5. DKK2 protein in wild-type and CKO embryos was similar to the in situ hybridization results. (**G-I**) In situ hybridization for *Sfrp1* transcripts in frontal sections from wild-type (G), *Fgfr2*^{CKO} (H) and *Smad4*^{CKO} (I) eyelids. In wild-type (G) and *Smad4*^{CKO} (I) eyelids, *Sfrp1* transcripts were present in the conjunctiva (asterisks), retina, retinal pigment epithelium and lens. In *Fgfr2*^{CKO} embryos (H), *Sfrp1* transcripts were readily detected in the retina, retinal pigment epithelium and lens, with low levels in the conjunctiva and palpebral epithelium. Scale bars: 100 μm.

Smads can bind to c-Jun when it is not associated with DNA, that c-Jun is phosphorylated after treatment of cells with TGFβ and that Smad-c-Jun complexes promote AP-1-dependent transcription (Liberati et al., 1999; Qing et al., 2000; Verrecchia et al., 2001; Zhang et al., 1998). Our data suggest that BMPs, acting through the canonical R-Smad/Smad4 pathway, cooperate with activin β-B to promote maximal phosphorylation of c-Jun, and that association with the R-Smad/Smad4 complex mediates the translocation of phosphorylated c-Jun to the nucleus. To our knowledge, this is the first report suggesting that activated Smads are required for the nuclear translocation of c-Jun. Further studies are required to determine whether this function of BMP signaling is important in other examples of epithelial fusion, such as closure of the neural tube and ventral closure of the optic cup, for which proper function of the JNK pathway is essential (Xia and Karin, 2004).

BMP signaling was required for the accumulation of Foxc1 and Foxc2, transcription factors shown in previous studies to be required for eyelid closure (Kidson et al., 1999; Kume et al., 1998; Smith et al., 2000). Foxc1 and Foxc2 are also expressed in periocular mesenchyme (Gage et al., 2005) and limb bud mesenchyme (Nifuji et al., 2001), and treatment with Bmp4 and Bmp7 increases the transcription of Foxc2 in limb bud mesenchyme in organ culture (Nifuji et al., 2001). The function of Foxc1 and Foxc2 in eyelid closure is not clear. However, it has been shown that Foxc1 and Foxc2 control somitogenesis by regulating Notch signaling (Kume et al., 2001). Foxc transcription factors also directly stimulate the production of the Notch ligand Dll4, to activate Hey2 accumulation in vascular endothelial cells (Hayashi and Kume, 2008). In experiments undertaken for another study, we found that deletion in the surface ectoderm of the presenilins *Psen1* and *Psen2* resulted in an EOB phenotype (see Fig. S1 in the supplementary material). Because, in most tissues, presenilin activity is required for Notch activation, Foxc1 and Foxc2 might promote Notch signaling during eyelid closure. However, the presenilins are also required for the activity of other transmembrane proteins. For this reason, the function of Notch signaling in eyelid closure requires further exploration.

BMPs do not mediate all effects of FGF signaling in eyelid development

Although the functions of BMPs that were identified in this study were dependent on Fgfr2, BMPs do not mediate all effects of FGF signaling in eyelid development. *Fgfr2* is required in the palpebral ectoderm to suppress Wnt signaling, at least in part by inducing the Wnt antagonist Sfrp1. Loss of BMP signaling does not affect the expression of *Sfrp1*.

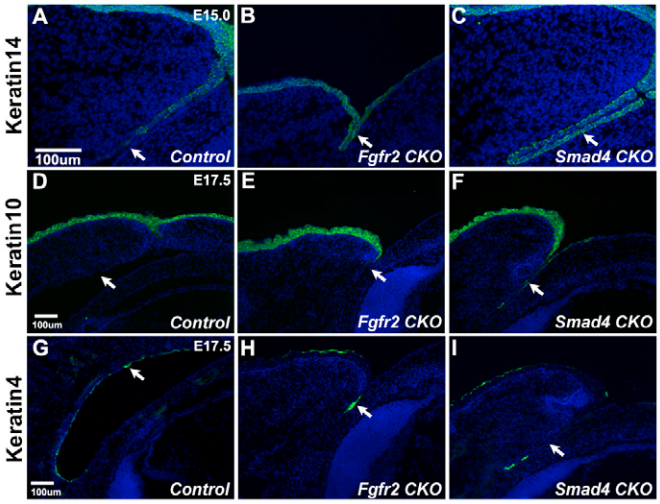

Fig. 9. Abnormal eyelid epithelial differentiation in *Fgfr2*^{CKO} and *Smad4*^{CKO} mice. (**A-C**) Immunostaining for keratin 14 (K14) in frontal sections from wild-type (A), *Fgfr2*^{CKO} (B) and *Smad4*^{CKO} (C) embryos at E15.0. In wild-type eyelids (A), K14 staining was weak in the palpebral conjunctiva and was not detected in the bulbar conjunctiva (arrows). In *Fgfr2*^{CKO} (B) and *Smad4*^{CKO} (C) eyelids, K14 staining was strong and uniform in the palpebral and bulbar conjunctiva (arrows). (**D-F**) Immunostaining for keratin 10 (K10) in frontal sections from wild type (D), *Fgfr2*^{CKO} (E) and *Smad4*^{CKO} (F) embryos at E17.5. In wild-type eyelids (D), K10 staining is observed only in the epidermis; it is negative in the conjunctiva (arrow). In *Fgfr2*^{CKO} (E), K10 is found in epidermis and a few cells of the palpebral conjunctiva, although the majority of conjunctival cells do not express K10 (arrow). In *Smad4*^{CKO} (F), K10 is detected in the epidermis and in the majority of conjunctival cells (arrow). (**G-I**) Immunostaining for keratin 4 (K4) in frontal sections from wild-type (G), *Fgfr2*^{CKO} (H) and *Smad4*^{CKO} (I) embryos at E17.5. In wild-type eyelids (G), expression of K4 is continuous in the conjunctiva (arrow). In *Fgfr2*^{CKO} (H), K4 is found in most conjunctival cells (arrow). In *Smad4*^{CKO} (I), K4 is only detected in a few conjunctival cells; most conjunctival cells do not express K4 (arrow). Scale bars: 100 μm.

This arm of the FGF signaling pathway might involve Shh, as expression of *Shh* in the eyelid is modulated by Fgf10 (Tao et al., 2005), and the expression of *Ptch1*, an Shh receptor that is a direct target of Shh signaling, was greatly decreased in the lid ectoderm and the underlying mesenchyme in eyelids lacking *Fgfr2* in the ectoderm.

Wnt signaling must be suppressed in the palpebral epithelia to effect eyelid closure (Gage et al., 2008) (this study). However, a band of Wnt signaling activity is normally present in the palpebral conjunctiva near the margins of the upper and lower eyelids. These cells appear to include the precursors of the Meibomian glands. BMP signaling is required to maintain this domain of Wnt signaling and Meibomian gland cell fate (Plikus et al., 2004) (this study). Thus, FGF signaling is required to suppress Wnt signaling and promote BMP signaling, yet BMPs maintain local Wnt signaling in the Meibomian gland precursor cells. The factors that specify the location and extent of BMP and Wnt signaling in Meibomian gland formation remain to be studied.

Mice deficient in BMP signaling provide a model for the human disease distichiasis

In mice deficient in BMP signaling, conjunctival epithelial cells in both eyelids formed an extra row of eyelashes, a characteristic called distichiasis. This phenotype is similar to that of mice that overexpress noggin in the ectoderm, in which ectopic eyelashes are formed at the expense of the Meibomian glands (Plikus et al., 2004). Human distichiasis syndrome is characterized by the presence of an aberrant second row of eyelashes in place of the Meibomian glands (Fox, 1962). As a consequence, patients have Meibomian gland dysfunction, corneal irritation, conjunctivitis and photophobia. Most families presenting with distichiasis have lymphedema in common, or lymphedema-distichiasis (LD) syndrome (OMIM 153400). LD syndrome is an autosomal dominant disease caused by mutations in *FOXC2*. *Foxc2* heterozygous mice mimic LD syndrome, demonstrating distichiasis and hyperplasia of lymphatic vessels and lymph nodes (Kriederman et al., 2003). The distichiasis seen in our studies is consistent with a dependence of Foxc2 expression on BMP signaling.

Dkk2-null mice also develop distichiasis, with decreased *Foxc2* expression in the eyelids (Gage et al., 2008). *Dkk2* expression is promoted by the transcription factor Pitx2, which functions in the neural crest-derived eyelid mesenchyme. Surprisingly, we detected *Dkk2* mRNA and protein in the eyelid epithelia and in the mesenchyme. This observation suggests that another pathway regulates *Dkk2* expression in the ectoderm. Excessive Wnt signaling, whether resulting from defects in the Pitx2→Dkk2 pathway (Gage et al., 2008), or the Fgf10→Fgfr2→Sfrp1 pathway, appears to be sufficient to suppress *Foxc2* expression, prevent eyelid closure and cause distichiasis. Because loss of BMP signaling also leads to distichiasis, it seems possible that excessive Wnt pathway activity inhibits *Bmp4* expression in the eyelid mesenchyme or the function of the BMP pathway in the conjunctival epithelium. These possibilities remain to be tested.

BMP signaling is required for normal conjunctival epithelial cell fate

Different temporal and spatial expression of keratin intermediate filaments is an important aspect of the differentiation and function of many epithelia (Kurpakus et al., 1994). In wild-type eyelids, the palpebral epidermis expresses K14 before eyelid closure, whereas the conjunctival epithelia begin expressing K14 as the eyelids close. However, in mice deficient in BMP signaling, the conjunctival epithelium expressed K14 at the same time as the epidermis. In addition, conjunctival cells expressed K10, which is normally restricted to the epidermis, and K4 expression was reduced. Together with the transdifferentiation of the Meibomian gland precursor cells to hair follicles, these observations suggest that BMP signaling normally prevents conjunctival cells from adopting the epidermal cell fate (Fig. 10A).

The cross-talk between FGF and BMP signaling may be mediated by Shh

Previous studies and the results described here reveal complex epithelial-mesenchymal interactions in eyelid development. Activation of Fgfr2 in the surface ectoderm by Fgf10 from the underlying mesenchyme (Tao et al., 2005) is required for the localized expression of *Bmp4* in the palpebral mesenchyme. The signal from the epithelium that promotes *Bmp4* expression in the mesenchyme is likely to be Shh, as *Shh* is expressed in the eyelid margin from E13.5 and active Shh signaling (indicated by *Ptch1* expression) has an expression pattern similar to that of *Bmp4* in the wild-type eyelid. Moreover, the pattern of residual Shh signaling in the *Fgfr2*^{CKO} eyelid is similar to the pattern of residual *Bmp4* expression. These observations, together with the fact that preventing BMP signaling did not alter Shh function, suggested that Shh mediates the Fgfr2-dependent cross-talk between epithelium and mesenchyme.

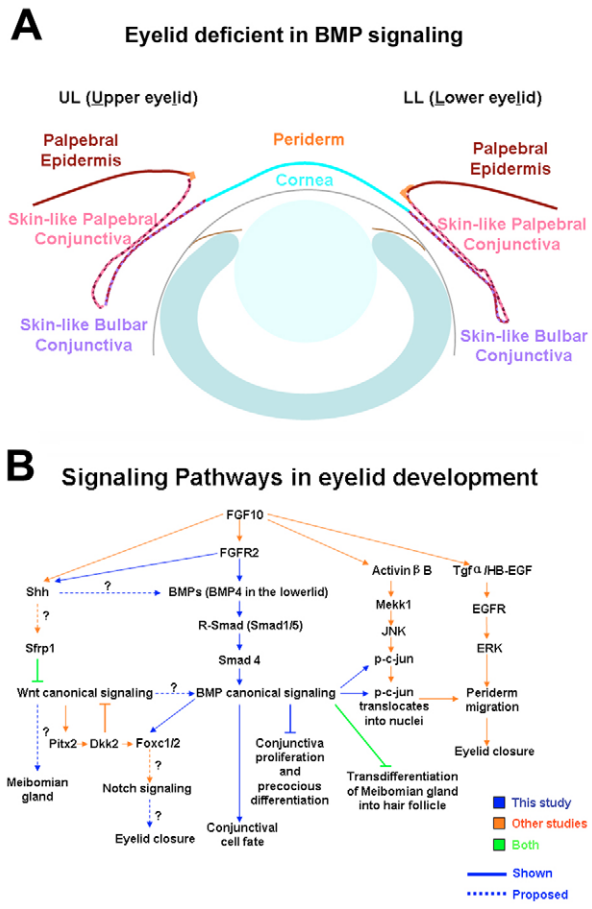

Fig. 10. Summary of the role of BMP signaling and its interaction with the other signaling pathways known or proposed to function in mouse eyelid development. (**A**) In eyelids that are deficient in BMP signaling, the conjunctival epithelial cells express epidermis-specific keratin 10 and form hair follicles near that lid margin. (**B**) The network of known or proposed signaling pathways controlling eyelid development. Observations made in this study are indicated by blue arrows, previous findings by orange arrows and findings confirmed in this study by green arrows. Our model suggests that epidermal cell fate is the default pathway and that BMP signaling is required for prospective conjunctival epithelial cells to suppress the epidermal differentiation pathway and become conjunctival cells. BMP signaling is not required to initiate the migration of periderm cells at the lid margins, but is required for the expansion of these cells across the corneal surface. During this process, BMP signaling is required for the expression of Foxc1 and Foxc2, and for the full activation (phosphorylation) of c-Jun. BMP-dependent formation of active R-Smad-Smad4 complexes is required for the translocation of p-c-Jun into the nuclei of periderm cells, where it has been reported to increase the expression of the epidermal growth factor receptor.

Bmp4 signals to the overlying ectoderm, as demonstrated by the phosphorylation of the BMP-dependent R-Smads in the eyelid epithelia. Phosphorylated R-Smads are also seen in the mesenchyme, suggesting that BMPs may affect additional targets there. In an additional level of complexity, the *Bmp4* and *Ptch1* expression patterns and Wnt activity were of different magnitude and location in the upper and lower eyelids, and *Bmp4* and *Ptch1* expression were differentially affected in the upper and lower eyelids by deletion of *Fgfr2*.

The signaling pathways involved in eyelid closure

In addition to the functions of the FGF, BMP, Shh and Wnt pathways examined in this study, germline deletion showed that activin β-B, TGFα, HB-EGF and the EGF receptor are each required for eyelid closure (Luetteke et al., 1994; Luetteke et al., 1993; Miettinen et al., 1995; Vassalli et al., 1994). Notch signaling might also be involved (see Fig. S1 in the supplementary material). The pathways activated by these morphogens interact in a remarkably complex web to assure the proper migration and fusion of a small population of periderm cells (Fig. 10B). Further studies are needed to fully define the functions and interactions of these pathways. Such studies will provide a more complete understanding of eyelid fusion and, perhaps, other morphogenetic events that depend on epithelial fusion, such as closure of the neural tube, the optic fissure, the lens vesicle and the palatal shelves.

The authors are indebted to Drs Zhen Mahoney and Jeff Miner for generously sharing reagents, for many suggestions on the technical aspects of this work and for assistance in editing. Belinda McMahan and Jean Jones prepared the histological sections and Dr Claudia Garcia provided guidance with the *Fgfr2* conditional knockouts, which were generously provided by Dr David Ornitz, Washington University, St Louis. The *Psen1* and *Psen2* floxed and mutant mice were generously provided by Dr J. Shen, Brigham and Women's Hospital, Boston, MA and Dr Raphael Kopan, Washington University, St Louis. Drs Peter Gruss and Ruth Ashery-Padan generated and provided the Le-Cre mice. Research was supported by NIH grant EY04853 (D.C.B.) and NIH Core Grant P30 EY02687 and an unrestricted grant from Research to Prevent Blindness to the Department of Ophthalmology and Visual Sciences. Deposited in PMC for release after 12 months.

Supplementary material

Supplementary material available online at
http://dev.biologists.org/cgi/content/full/136/10/1741/DC1

References

Andl, T., Ahn, K., Kairo, A., Chu, E. Y., Wine-Lee, L., Reddy, S. T., Croft, N. J., Cebra-Thomas, J. A., Metzger, D., Chambon, P. et al. (2004). Epithelial Bmpr1a regulates differentiation and proliferation in postnatal hair follicles and is essential for tooth development. *Development* **131**, 2257-2268.

Ashery-Padan, R., Marquardt, T., Zhou, X. and Gruss, P. (2000). Pax6 activity in the lens primordium is required for lens formation and for correct placement of a single retina in the eye. *Genes Dev.* **14**, 2701-2711.

Chytil, A., Magnuson, M. A., Wright, C. V. and Moses, H. L. (2002). Conditional inactivation of the TGF-beta type II receptor using Cre:Lox. *Genesis* **32**, 73-75.

DasGupta, R. and Fuchs, E. (1999). Multiple roles for activated LEF/TCF transcription complexes during hair follicle development and differentiation. *Development* **126**, 4557-4568.

Dudas, M., Sridurongrit, S., Nagy, A., Okazaki, K. and Kaartinen, V. (2004). Craniofacial defects in mice lacking BMP type I receptor Alk2 in neural crest cells. *Mech. Dev.* **121**, 173-182.

Fang, J., Dagenais, S. L., Erickson, R. P., Arlt, M. F., Glynn, M. W., Gorski, J. L., Seaver, L. H. and Glover, T. W. (2000). Mutations in FOXC2 (MFH-1), a forkhead family transcription factor, are responsible for the hereditary lymphedema-distichiasis syndrome. *Am. J. Hum. Genet.* **67**, 1382-1388.

Findlater, G. S., McDougall, R. D. and Kaufman, M. H. (1993). Eyelid development, fusion and subsequent reopening in the mouse. *J. Anat.* **183**, 121-129.

Fox, S. A. (1962). Distichiasis. *Am. J. Ophthalmol.* **53**, 14-18.

Gage, P. J., Rhoades, W., Prucka, S. K. and Hjalt, T. (2005). Fate maps of neural crest and mesoderm in the mammalian eye. *Invest. Ophthalmol. Vis. Sci.* **46**, 4200-4208.

Gage, P. J., Qian, M., Wu, D. and Rosenberg, K. I. (2008). The canonical Wnt signaling antagonist DKK2 is an essential effector of PITX2 function during normal eye development. *Dev. Biol.* **317**, 310-324.

Garcia, C. M., Yu, K., Zhao, H., Ashery-Padan, R., Ornitz, D. M., Robinson, M. L. and Beebe, D. C. (2005). Signaling through FGF receptor-2 is required for lens cell survival and for withdrawal from the cell cycle during lens fiber cell differentiation. *Dev. Dyn.* **233**, 516-527.

Gaussin, V., Van de Putte, T., Mishina, Y., Hanks, M. C., Zwijsen, A., Huylebroeck, D., Behringer, R. R. and Schneider, M. D. (2002). Endocardial cushion and myocardial defects after cardiac myocyte-specific conditional deletion of the bone morphogenetic protein receptor ALK3. *Proc. Natl. Acad. Sci. USA* **99**, 2878-2883.

Hayashi, H. and Kume, T. (2008). Foxc transcription factors directly regulate Dll4 and Hey2 expression by interacting with the VEGF-Notch signaling pathways in endothelial cells. *PLoS ONE* **3**, e2401.
He, J., Sheng, T., Stelter, A. A., Li, C., Zhang, X., Sinha, M., Luxon, B. A. and Xie, J. (2006). Suppressing Wnt signaling by the hedgehog pathway through sFRP-1. *J. Biol. Chem.* **281**, 35598-35602.
He, W., Li, A. G., Wang, D., Han, S., Zheng, B., Goumans, M. J., Ten Dijke, P. and Wang, X. J. (2002). Overexpression of Smad7 results in severe pathological alterations in multiple epithelial tissues. *EMBO J.* **21**, 2580-2590.
Huang, S., Tang, B., Usoskin, D., Lechleider, R. J., Jamin, S. P., Li, C., Anzano, M. A., Ebendal, T., Deng, C. and Roberts, A. B. (2002). Conditional knockout of the Smad1 gene. *Genesis* **32**, 76-79.
Katoh, Y. and Katoh, M. (2006). WNT antagonist, SFRP1, is Hedgehog signaling target. *Int. J. Mol. Med.* **17**, 171-175.
Kidson, S. H., Kume, T., Deng, K., Winfrey, V. and Hogan, B. L. (1999). The forkhead/winged-helix gene, Mf1, is necessary for the normal development of the cornea and formation of the anterior chamber in the mouse eye. *Dev. Biol.* **211**, 306-322.
Kriederman, B. M., Myloyde, T. L., Witte, M. H., Dagenais, S. L., Witte, C. L., Rennels, M., Bernas, M. J., Lynch, M. T., Erickson, R. P., Caulder, M. S. et al. (2003). FOXC2 haploinsufficient mice are a model for human autosomal dominant lymphedema-distichiasis syndrome. *Hum. Mol. Genet.* **12**, 1179-1185.
Kume, T., Deng, K. Y., Winfrey, V., Gould, D. B., Walter, M. A. and Hogan, B. L. (1998). The forkhead/winged helix gene Mf1 is disrupted in the pleiotropic mouse mutation congenital hydrocephalus. *Cell* **93**, 985-996.
Kume, T., Jiang, H., Topczewska, J. M. and Hogan, B. L. (2001). The murine winged helix transcription factors, Foxc1 and Foxc2, are both required for cardiovascular development and somitogenesis. *Genes Dev.* **15**, 2470-2482.
Kurpakus, M. A., Maniaci, M. T. and Esco, M. (1994). Expression of keratins K12, K4 and K14 during development of ocular surface epithelium. *Curr. Eye Res.* **13**, 805-814.
Li, C., Guo, H., Xu, X., Weinberg, W. and Deng, C. X. (2001). Fibroblast growth factor receptor 2 (Fgfr2) plays an important role in eyelid and skin formation and patterning. *Dev. Dyn.* **222**, 471-483.
Li, G., Gustafson-Brown, C., Hanks, S. K., Nason, K., Arbeit, J. M., Pogliano, K., Wisdom, R. M. and Johnson, R. S. (2003). c-Jun is essential for organization of the epidermal leading edge. *Dev. Cell* **4**, 865-877.
Liberati, N. T., Datto, M. B., Frederick, J. P., Shen, X., Wong, C., Rougier-Chapman, E. M. and Wang, X. F. (1999). Smads bind directly to the Jun family of AP-1 transcription factors. *Proc. Natl. Acad. Sci. USA* **96**, 4844-4849.
Lipinski, R. J., Hutson, P. R., Hannam, P. W., Nydza, R. J., Washington, I. M., Moore, R. W., Girdaukas, G. G., Peterson, R. E. and Bushman, W. (2008). Dose- and route-dependent teratogenicity, toxicity, and pharmacokinetic profiles of the hedgehog signaling antagonist cyclopamine in the mouse. *Toxicol. Sci.* **104**, 189-197.
Luetteke, N. C., Qiu, T. H., Peiffer, R. L., Oliver, P., Smithies, O. and Lee, D. C. (1993). TGF alpha deficiency results in hair follicle and eye abnormalities in targeted and waved-1 mice. *Cell* **73**, 263-278.
Luetteke, N. C., Phillips, H. K., Qiu, T. H., Copeland, N. G., Earp, H. S., Jenkins, N. A. and Lee, D. C. (1994). The mouse waved-2 phenotype results from a point mutation in the EGF receptor tyrosine kinase. *Genes Dev.* **8**, 399-413.
Miettinen, P. J., Berger, J. E., Meneses, J., Phung, Y., Pedersen, R. A., Werb, Z. and Derynck, R. (1995). Epithelial immaturity and multiorgan failure in mice lacking epidermal growth factor receptor. *Nature* **376**, 337-341.
Mine, N., Iwamoto, R. and Mekada, E. (2005). HB-EGF promotes epithelial cell migration in eyelid development. *Development* **132**, 4317-4326.
Nifuji, A., Miura, N., Kato, N., Kellermann, O. and Noda, M. (2001). Bone morphogenetic protein regulation of forkhead/winged helix transcription factor Foxc2 (Mfh1) in a murine mesodermal cell line C1 and in skeletal precursor cells. *J. Bone Miner. Res.* **16**, 1765-1771.
Piek, E., Ju, W. J., Heyer, J., Escalante-Alcalde, D., Stewart, C. L., Weinstein, M., Deng, C., Kucherlapati, R., Bottinger, E. P. and Roberts, A. B. (2001). Functional characterization of transforming growth factor beta signaling in Smad2- and Smad3-deficient fibroblasts. *J. Biol. Chem.* **276**, 19945-19953.
Plikus, M., Wang, W. P., Liu, J., Wang, X., Jiang, T.-X. and Chuong, C.-M. (2004). Morpho-regulation of ectodermal organs: integument pathology and phenotypic variations in K14-noggin engineered mice through modulation of bone morphogenic protein pathway. *Am. J. Pathol.* **164**, 1099-1114.
Qing, J., Zhang, Y. and Derynck, R. (2000). Structural and functional characterization of the transforming growth factor-beta -induced Smad3/c-Jun transcriptional cooperativity. *J. Biol. Chem.* **275**, 38802-38812.
Roberts, A. B., Tian, F., Byfield, S. D., Stuelten, C., Ooshima, A., Saika, S. and Flanders, K. C. (2006). Smad3 is key to TGF-beta-mediated epithelial-to-mesenchymal transition, fibrosis, tumor suppression and metastasis. *Cytokine Growth Factor Rev.* **17**, 19-27.
Sharov, A. A., Weiner, L., Sharova, T. Y., Siebenhaar, F., Atoyan, R., Reginato, A. M., McNamara, C. A., Funa, K., Gilchrest, B. A., Brissette, J. L. et al. (2003). Noggin overexpression inhibits eyelid opening by altering epidermal apoptosis and differentiation. *EMBO J.* **22**, 2992-3003.
Smith, R. S., Zabaleta, A., Kume, T., Savinova, O. V., Kidson, S. H., Martin, J. E., Nishimura, D. Y., Alward, W. L., Hogan, B. L. and John, S. W. (2000). Haploinsufficiency of the transcription factors FOXC1 and FOXC2 results in aberrant ocular development. *Hum. Mol. Genet.* **9**, 1021-1032.
Steiner, H., Duff, K., Capell, A., Romig, H., Grim, M. G., Lincoln, S., Hardy, J., Yu, X., Picciano, M., Fechteler, K. et al. (1999). A loss of function mutation of presenilin-2 interferes with amyloid beta-peptide production and notch signaling. *J. Biol. Chem.* **274**, 28669-28673.
Swindell, E. C., Liu, C., Shah, R., Smith, A. N., Lang, R. A. and Jamrich, M. (2008). Eye formation in the absence of retina. *Dev. Biol.* **322**, 56-64.
Takatori, A., Geh, E., Chen, L., Zhang, L., Meller, J. and Xia, Y. (2008). Differential transmission of MEKK1 morphogenetic signals by JNK1 and JNK2. *Development* **135**, 23-32.
Tao, H., Shimizu, M., Kusumoto, R., Ono, K., Noji, S. and Ohuchi, H. (2005). A dual role of FGF10 in proliferation and coordinated migration of epithelial leading edge cells during mouse eyelid development. *Development* **132**, 3217-3230.
Umans, L., Vermeire, L., Francis, A., Chang, H., Huylebroeck, D. and Zwijsen, A. (2003). Generation of a floxed allele of Smad5 for cre-mediated conditional knockout in the mouse. *Genesis* **37**, 5-11.
Vassalli, A., Matzuk, M. M., Gardner, H. A., Lee, K. F. and Jaenisch, R. (1994). Activin/inhibin beta B subunit gene disruption leads to defects in eyelid development and female reproduction. *Genes Dev.* **8**, 414-427.
Verrecchia, F., Vindevoghel, L., Lechleider, R. J., Uitto, J., Roberts, A. B. and Mauviel, A. (2001). Smad3/AP-1 interactions control transcriptional responses to TGF-beta in a promoter-specific manner. *Oncogene* **20**, 3332-3340.
Weston, C. R., Wong, A., Hall, J. P., Goad, M. E., Flavell, R. A. and Davis, R. J. (2004). The c-Jun NH2-terminal kinase is essential for epidermal growth factor expression during epidermal morphogenesis. *Proc. Natl. Acad. Sci. USA* **101**, 14114-14119.
Xia, Y. and Karin, M. (2004). The control of cell motility and epithelial morphogenesis by Jun kinases. *Trends Cell Biol.* **14**, 94-101.
Yang, X., Li, C., Herrera, P. L. and Deng, C. X. (2002). Generation of Smad4/Dpc4 conditional knockout mice. *Genesis* **32**, 80-81.
Yu, H., Saura, C. A., Choi, S. Y., Sun, L. D., Yang, X., Handler, M., Kawarabayashi, T., Younkin, L., Fedeles, B., Wilson, M. A. et al. (2001). APP processing and synaptic plasticity in presenilin-1 conditional knockout mice. *Neuron* **31**, 713-726.
Yu, K., Xu, J., Liu, Z., Sosic, D., Shao, J., Olson, E. N., Towler, D. A. and Ornitz, D. M. (2003). Conditional inactivation of FGF receptor 2 reveals an essential role for FGF signaling in the regulation of osteoblast function and bone growth. *Development* **130**, 3063-3074.
Zenz, R., Scheuch, H., Martin, P., Frank, C., Eferl, R., Kenner, L., Sibilia, M. and Wagner, E. F. (2003). c-Jun regulates eyelid closure and skin tumor development through EGFR signaling. *Dev. Cell* **4**, 879-889.
Zhang, L., Wang, W., Hayashi, Y., Jester, J. V., Birk, D. E., Gao, M., Liu, C. Y., Kao, W. W., Karin, M. and Xia, Y. (2003). A role for MEK kinase 1 in TGF-beta/activin-induced epithelium movement and embryonic eyelid closure. *EMBO J.* **22**, 4443-4454.
Zhang, Y., Feng, X. H. and Derynck, R. (1998). Smad3 and Smad4 cooperate with c-Jun/c-Fos to mediate TGF-beta-induced transcription. *Nature* **394**, 909-913.